CHARACTERIZATION OF ALLOSTERIC INTERPLAY BETWEEN THE SPECIALIZED-SENSORY MODULES IN BK CHANNEL BY CALCIUM-DRIVEN REGULATION OF VOLTAGE-SENSING DOMAINS

Tesis entregada a

LA UNIVERSIDAD DE VALPARAÍSO

en Cumplimiento Parcial de los requisitos para optar al grado de

Doctorado en Ciencias con Mención en Neurociencia

Facultad De Ciencias

Por

Yenisleidy Lorenzo Ceballos

Marzo, 2019

Dirigida por: Ramón Latorre de la Cruz

Co-Dirigida por: Carlos Gonzalez Leon

FACULTAD DE CIENCIAS

UNIVERSIDAD DE VALPARAÍSO

INFORME DE APROBACIÓN

TESIS DE DOCTORADO

Se informa a la Facultad de Ciencias que la Tesis de Doctorado presentada por:

YENISLEIDY LORENZO CEBALLOS

Ha sido aprobada por la comisión de Evaluación de la tesis como requisito para optar al grado de Doctor en Ciencias con mención en Neurociencia, en el examen de Defensa de Tesis rendido el día 18 del Mes de Marzo del 2019

Director de Tesis:

Dr. Ramon Latorre ……

Co-Director de Tesis:

Dr. Carlos González ……

Comisión de Evaluación de la Tesis

Dr. David Naranjo ……

Dr. Alan Nelly ……

Dr. Daniel Basilio ……

AGRADECIMIENTOS

Agradezco infinitamente a cada una de las personas que de alguna forma hicieron posible el desarrollo de esta tesis. Partiendo por mis directores de tesis y profesores; le doy gracias:

Al profesor Ramón Latorre por su guía, enseñanzas y la oportunidad de realizar este trabajo bajo su tutela y al profesor Carlos González quien me mostró el camino hasta Chile.

A los profesores de la comisión David Naranjo, Daniel Basilio y Alan Neely por sus comentarios siempre constructivos que ayudaron a mejorar la calidad de esta tesis.

A todos los profesores del programa que con sus conocimientos aportaron a mi formación profesional.

Este trabajo en particular no hubiese sido posible sin el significativo aporte experimental y teórico de Karen Castillo, Willy Carrasquel, Gustavo Contreras, y el profesor Osvaldo Alvarez; y el especial apoyo de Luisa Soto con sus mágicas manos.

A mis compañeros de lab, las que quedan conmigo, Luisita (Soto) y Karencilla (Castillo), y los que se marcharon pero están en mis recuerdos, JJ (Hans), Will, Javi, Berna, el Animal (Karel), Pupo (Amaury), JP (Juan Pablo), Felipe, Estercita, David, quiero darle las gracias por su amistad, consejos, apoyo y compañía entre experimentos, cafés y chelas.

A mi familia por estar siempre. Todo el camino recorrido es por y para ellos. A Rogney por su inmensa paciencia y su incondicionalidad para seguirme a este lado del mundo.

CONTENTS

FIGURES

ABBREVIATIONS

BK	Large conductance Ca^{2+}- and voltage-activated K^+ channel.
C	Allosteric factor that accounts for the interaction between the Ca^{2+}-binding sites and the channel gate.
$[Ca^{2+}]_i$	Internal calcium ion concentration.
C-O	Closed and open configuration of the channel.
CTD	C-terminal domain.
D	Allosteric factor that accounts for the interaction between the voltage sensors and the channel gate.
E	Allosteric factor that accounts for the interaction between the voltage sensors and the Ca^{2+}-binding sites.
e0	Elementary electronic charge (1.602×10^{-9} coulomb).
F	Faraday constant.
G(*V*)	Conductance vs. Voltage.
$\Delta\Delta G_V$	Changes in Gibbs free energy of the voltage sensors activation induced by Ca^{2+}.
I_G	Gating current.
J	Equilibrium constant for the resting (R) to active (A) transition of each voltage sensor.
J_0	Equilibrium constant for the resting (R) to active (A) transition of each voltage sensor at zero voltage.
K	Equilibrium constant for the unbound (U) to Ca^{2+}-bound (B) transition for each Ca^{2+}-binding site defined.
K_D	Dissociation constant.
Kv	Voltage-dependent K^+ channels.
L	Equilibrium constant for the closed (C) to open (O) transition of the pore domain.
PD	Pore domain.

Q_C	Gating charge displaced between the closed states (C-C) of the channel.
$Q_C(V)$	Gating charge displaced between the closed states of the channel versus Voltage.
R	Gas constant.
RCK	Regulator of conductance for K^+.
R-A	Resting and active configurations of the voltage sensors.
T	Temperature.
TM	Transmembrane.
TMD	Transmembrane domain.
V	Voltage.
V_H	Half-activation voltage.
ΔV_H	Changes of the half-activation voltage relative to initial condition.
VSD	Voltage-sensing domain.
WT	Wild type.
z_J	Gating charges displacement associated with the resting to active voltage sensor transition.

ABSTRACT

A hallmark of large conductance Ca^{2+}- and voltage-activated K^+ (BK) channels is its dual regulation by two distinct physiological stimuli, intracellular Ca^{2+} and membrane potential. The specialized sensing modules responsible for detecting cytosolic Ca^{2+} elevation and membrane depolarization can act synergistically and independently allowing BK channels to operate in a wide-ranging of internal Ca^{2+} and voltage conditions. The functional contributions of the Ca^{2+} and voltage sensors to the channel opening arise from allosteric interactions propagated among three structural domains: a pore domain (PD), a voltage-sensor domain (VSD), and two Ca^{2+}-binding sites located on non-identical regulators of conductance for K^+ (RCK) domains that form a cytosolic gating ring (CTD). However, the strength of the Ca^{2+}- and voltage sensors coupling and their functional relevance on the BK channel gating mechanism is still an unresolved matter. Using gating currents analysis, we examined the allosteric coupling between Ca^{2+} and voltage sensors. Our results reveal a strong energetic interplay between the voltage- and Ca^{2+}-sensing modules through a coordinated interaction mechanism in which Ca^{2+} binding to a single α-subunit affects all VSDs equally. Interestingly, the two distinct Ca^{2+}-binding sites contained in the RCK1 and RCK2 domains appear to contribute equally to decrease the free energy necessary to activate the VSDs. Some diversity in the physiological roles of BK channels is given by co-assembly of pore-forming α-subunits with tissue-specific β-subunits. Particularly, β1-subunit affect dramatically VSD function, although the biophysical and molecular mechanisms are still under debate. Preliminary results suggest that β-subunits, specifically β1- and β3b-subunits does not affect the CTD-VSD allosteric interaction. However, the presence of β1-subunit, in addition to its known effect stabilizing the active configuration of the voltage sensor, appears to decrease the extension of VSD displacement and/or to modify the membrane electric field.

INTRODUCTION

Diverse cellular functions including synaptic transmission, muscle contraction, exocytosis, gene transcription, and cell motility involve rises in cytosolic Ca^{2+} as a primary signal in the transduction mechanisms (Ghosh and Greenberg, 1995; Berridge et al., 2000). The activation of Ca^{2+}-dependent conductances is probably some the most rapid response in the signaling pathway leading to immediate as well as long-term physiological changes (Clapham, 2007). Within the several types of Ca^{2+}-dependent ion channels (Hille, 2001), the Ca^{2+}-activated K^+ channels have widespread distribution encompassing a broad diversity of cell types (Schwarz and Passow, 1983; Latorre et al., 1984).

Increased K^+ permeability of the plasma membrane induced by elevated intracellular Ca^{2+} was initially evidenced in human erythrocytes at the end of the '50s (Gárdos, 1958). Two decades later, Ca^{2+}-mediated K^+ currents were identified by pharmacological manipulations of the internal Ca^{2+} concentration in invertebrates and vertebrates neurons (Krnjevij and Lisjewicz, 1972; Meech, 1978). Subsequently, a variety of Ca^{2+}-activated K^+ channels were described based on their molecular and pharmacological properties. At the single-channel level, the first Ca^{2+}-activated K^+ channel was identified because of its unusual large unitary conductance in cultured rat skeletal muscles (Pallotta et al., 1981), chromaffin cells (Marty, 1981) and reconstitution in bilayers from rabbit transverse tubules (Latorre et al., 1982). Under symmetric K^+ conditions (100 mM), this channel has the largest single-channel conductance within the K^+ family ranging from 200 to 300 pS, earning its name of BK (for Big K^+) (Marty, 1983) or MaxiK (Latorre and Miller, 1983). A decade later, the discovery of the *Slowpoke* (Slo) mutation in Drosophila which abolishes a Ca^{2+}-sensitive component of outward K^+ currents in muscles (Elkins et al., 1986; Singh and Wu, 1989) and neurons (Saito and Wu, 1991), eventually led to the identification of the first gene as the structural locus encoding the BK channel (Atkinson et al., 1991; Adelman et al., 1992) and its mammalian

orthologs (Butler et al., 1993; Dworetzky et al., 1994; McCobb et al., 1995), showing that the BK channel is well-conserved across the evolutionary scale and that the extensive alternative splice variants of the BK channels are the product of a single gene.

Besides its very large unitary conductance, the hallmarks of BK channels include a very high K^+ selectivity (Latorre and Miller, 1983) and a synergistic regulation by internal Ca^{2+} and membrane potential (Marty, 1981; Pallotta et al., 1981; Latorre et al., 1982). Owing to these properties, BK channels can operate over a wide dynamic range of intracellular Ca^{2+} concentration (from 0 to 10 mM) and voltage (from −200 to +300 mV) covering all possible physiological and pathological conditions (Yang and Cui, 2015). The BK channel activation leads to pore opening and a rapid efflux of K^+ ions that contribute to repolarize the membrane potential regulating the membrane excitability, intracellular ion homeostasis, Ca^{2+} signaling, and cell volume. Such roles into the cellular functionating along with its ubiquitous distribution in a variety neuronal and non-neuronal tissues make BK channels versatile players controlling several physiological processes that include smooth muscle contraction (Dopico et al., 2018), action potential duration (Vandael et al., 2010; Jaffe et al., 2011; Contet et al., 2016) and subsequently the firing frequency (Kimm et al., 2015; Contet et al., 2016) and neurotransmitter release (Griguoli et al., 2016), hearing (Pyott and Duncan, 2016), circadian rhythms (Meredith et al., 2006), and gene expression (Li et al., 2014).

Modular design of the BK channel structure.

Cloning of the Slo1 gene (also referred to as $K_{Ca}1.1$ and KCNMA1 gene in mammals) (Kaczmarek et al., 2017) and later the protein hydrophobicity profile and membrane topology analysis through several experimental approaches revealed many properties of BK channel (Adelman et al., 1992; Butler et al., 1993; Wallner et al., 1996; Meera et al., 1997). Each α-subunit is composed of a N-terminal transmembrane domain (TMD) and a cytosolic tail domain (CTD) at the C-terminus. The set of transmembrane (TM) segments define two functional domains: (1) the ion conducting part

of the channel (S5–S6), termed the pore domain (PD), and (2) the S0–S4 voltage-sensing domain (VSD) (**Figure 1A**). The S1–S6 transmembrane helices in the PD and VSD are homologous to those in the family of voltage-dependent K^+ (Kv) channels, but with an additional S0 helix in Slo1 that attaches to the VSD leaving the channel's N-terminus pointing towards the external side of the cell (Wallner et al., 1996; Meera et al., 1997).

Appended to the TMD is a large sequence that extends into the cytosol (CTD) consisting of almost two-thirds of the entire sequence (~1100 amino acids). The CTD is composed of two non-identical regulators of K^+ conductance (RCK) domains, RCK1 and RCK2 domains, each contains distinct Ca^{2+}-binding sites. Based on the full-length cryo-EM structures of *Aplysia californica* BK channel (aSlo1), it was established that the large S6-RCK1 linker creates a domain-swapped architecture of the CTD (Hite et al., 2017; Tao et al., 2017) (**Figure 1B**). Thus, the VSD of one α-subunit contact with the cytoplasmatic Ca^{2+} domain from a neighboring subunit. Also, unlike the Kv channels where the VSD is domain-swapped contacting the PD of the adjacent subunit, in BK channels the VSD interacts directly with the PD of the same subunit (**Figure 1B,C**).

Four pore-forming α-subunit assemble to form a functional BK channel (Shen et al., 1994; Quirk and Reinhart, 2001) (**Figure 1C**). Thus, the overall architecture of BK channels follows a modular design containing three distinct modules: the ion-conducting PD, the VSD, and the ligand-sensing CTD arranged into a ring-like tetrameric structure dubbed the gating ring (Wu et al., 2010; Yuan et al., 2010; Hite et al., 2017; Tao et al., 2017). The modular design suggests that each individual module may undergo relatively independent conformational changes in response to corresponding stimuli, while also enabling allosteric coupling through extensive protein-protein interactions (Zhou et al., 2017).

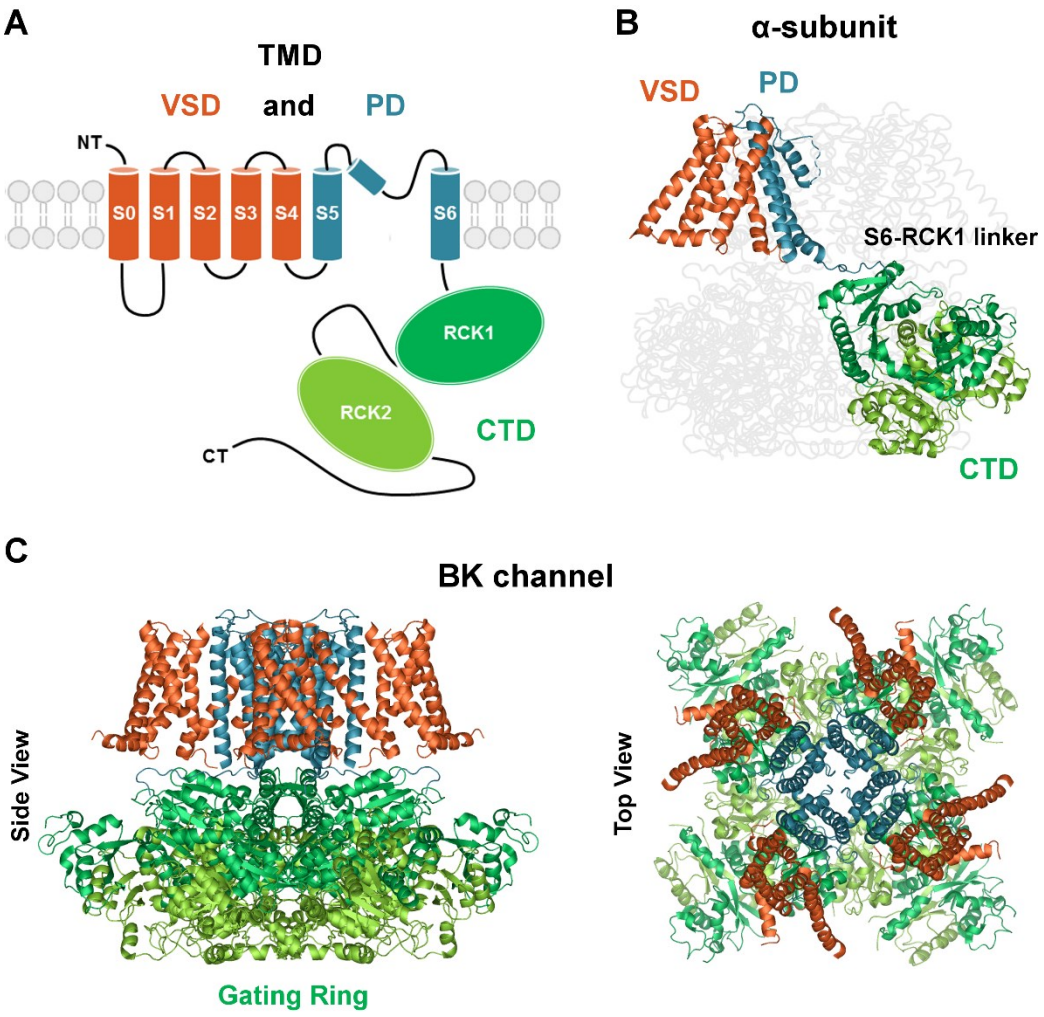

Figure 1. Structure of BK channel.

(**A**) Membrane topology of a single pore-forming α-subunit highlighting its three distinct domains: PD (S5-pore helix-S6), VSD (S0–S4), and CTD (two non-identical regulators of K^+ conductance (RCK) domains per α-subunit). (**B**) Color-coded map of PD (blue), VSD (orange), and CTD (green, RCK1; light green, RCK2) from the *Aplysia californica* Slo1 (aSlo1) structure (Protein Data Bank [PDB] ID: 5TJI) (Hite et al., 2017). Note that the VSD is not domain-swapped whereas S6–RCK1 linker creates an arrangement in which the RCKs are domain-swapped (TMD of the α-subunit resides on top of the CTD of a neighboring α-subunit). (**C**) Organization of the full homotetrameric BK channel structure showing the octameric arrangement of RCK domains in the CTD forming the gating ring (Side View) and the non-domain swapped architecture of the TMD where the VSD attachment with the PD from the same polypeptide chain (Top View).

Ion Conduction Pore Module.

The PD of the BK channel comprises the S5–S6 transmembrane segments and the pore helix (PH) from each α-subunit (**Figure 1C)** forming an aqueous pore in the center of the channel, where ion selection and permeation occur. A signature sequence, TVGYGD, which is characteristic of the selectivity filter (SF) of many K^+ channels, is located between the pore helix and S6 (**Figure 2A,B**) (Heginbotham et al., 1994). BK channel is highly selective for K^+ over Na^+ (Blatz and Magleby, 1984; Yellen, 1984; Eisenman et al., 1986), and paradoxically, it has a largest unitary conductance exceeding that of the Kv channels by an order of magnitude (Carrasquel-Ursulaez et al., 2018) despite the pore architecture similarity (Adelman et al., 1992; Butler et al., 1993; Brelidze et al., 2003). The molecular mechanism underlying to this unusually large conductance has not yet been fully resolved but is partly derived from two clusters of acidic residues that are located at the intracellular and extracellular entrances of the K^+ permeation pathway (**Figure 2C,E**). These clusters of negative charges serve as electrostatic traps to attract and concentrate local K^+ increasing the single-channel conductance (Brelidze et al., 2003; Carvacho et al., 2008). Thus, the outer negative ring of four D292 residues in the external entrance of the selectivity filter (**Figure 2B,C**) contribute to ~40% of the unitary conductance (Haug et al., 2004). Furthermore, unlike the Kv channels, an inner ring of eight negative charges (E321 and E324) (**Figure 2B,E**) surround the entrance of the internal vestibule (the aqueous region underneath the selectivity filter). Neutralization of this internal ring reduces the unitary conductance by about half (Brelidze et al., 2003; Nimigean et al., 2003). At very high symmetrical K^+ concentrations, the maximal conductance is identical in wild-type (WT) indicating that the negative charges increase the K^+ concentration in the internal vestibule through long-range electrostatic interactions. Meanwhile, interactions between the residues F315 and L312 of neighboring α-subunits (Wu et al., 2009; Carrasquel-Ursulaez et al., 2014; Hite et al., 2017) constitute a stable hydrophobic ring (**Figure 2B,D**) whose distortion of its geometry has important effects on the unitary conductance of the channel (Carrasquel-Ursulaez et al., 2014).

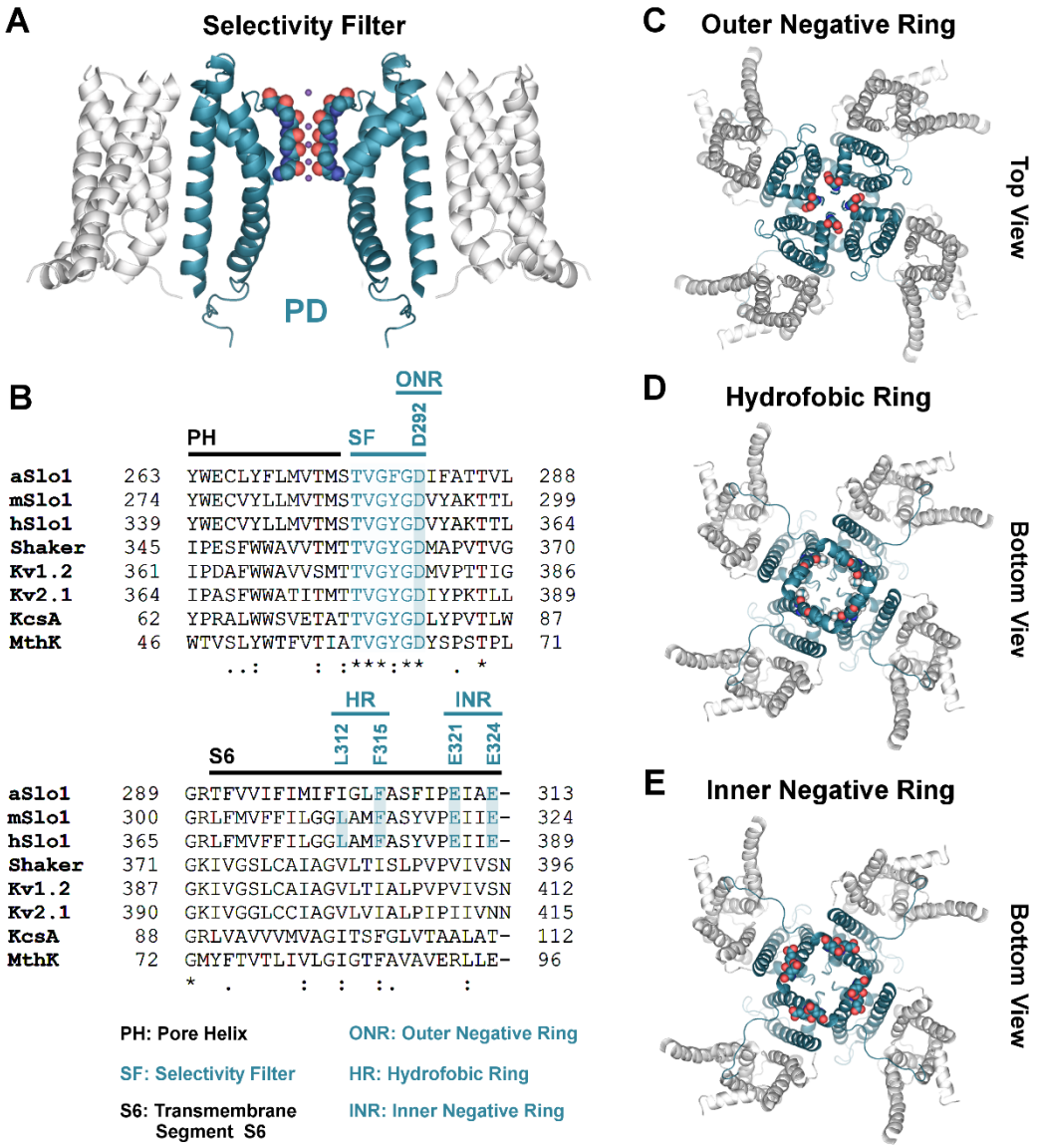

Figure 2. Structural features of the pore domain.

(**A**) Side view of secondary structure of two α-subunits of the pore domain (S5-PH-S6). Residues of selectivity filter are highlighted. (**B**) Alignment of K^+ channels pore domain including Pore Helix (PH), Selectivity Filter (SF) and S6 segment: aSlo1 (UniProt Accession Number (AC): Q5QJC5), mSlo1 (Q08460), hSlo1 (Q12791), Shaker-related (B2RU13), Kv1.2 (P16389), Kv2.1 (Q14721), KcsA (P0A334), and MthK (O27564). Signature sequence of K^+ channels SF (TVGYGD) and residues involved in determining the large single-channel conductance are highlighted and indicated with position numbers of mSlo. Outer Negative Ring (ONR) contains four D292 residues located at the PD outer entrance (**C**), eight hydrophobic residues (L312 and F315) form a Hydrophobic Ring (HR) (**D**), and eight glutamate residues (E321 and E324) located at the PD inner entrance form the Inner Negative Ring (INR) (**E**). Atomic coordinates were taken from the aSlo1 structure (PDB ID: 5TJI).

The accessibility experiments (Zhou et al., 2011) and the recent full-length structural information (Hite et al., 2017; Tao et al., 2017) revealed that the diameter of the internal entrance to the BK channel is ~20 Å which is much wider than in Kv channels (~10 Å), which has led to consider the effect of vestibule size on unitary channel conductance (Naranjo et al., 2016). Indeed, reducing the effective volume of the internal cavity of BK channel by decreasing the diffusion coefficient of K^+ using sucrose or reducing the size of the inner vestibule by increasing the side chain of the 321 and 324 residues diminishes the single channel conductance in BK channels (Brelidze and Magleby, 2005; Geng et al., 2011). Thus, most of the electric field along the pore drops in the selectivity filter and only ~7% of the total resistance of the conductive pathway lies in the inner cavity of BK channels (Brelidze and Magleby, 2005; Carvacho et al., 2008; Geng et al., 2011; Díaz-Franulic et al., 2015) (~200 pS in symmetrical 100 mM K^+) whereas in Shaker K^+ channels (~20 pS in symmetrical 100 mM K^+) this pore region entails most of the electrical resistance (Díaz-Franulic et al., 2015; Naranjo et al., 2016).

Specialized-Sensory Modules.

The opening and closing processes of the pore domain (PD) are influenced by the status of the Ca^{2+} and voltage sensors (CTD and VSD).

Voltage-Sensing Domain.

The voltage-dependence in BK channels is mainly derived from voltage-sensing residues in their intrinsic voltage-sensing domain (VSD). The S0-S4 transmembrane segments of each α-subunit form the VSD where S1-S4 structure shows a compact arrangement consistent with a role as a modular voltage-sensing (Tao et al., 2017) (**Figure 3A**). The first direct evidence that BK channels possess an intrinsic VSD came from gating current measurements in absence of Ca^{2+} by Stefani et al. (Stefani et al., 1997). The gating current is the electric current produced by the translocation

of charges or the reorientation of dipoles located on the VSD which transverse the membrane electric field upon changes in membrane potential reflecting the voltage-sensing apparatus work (Bezanilla, 2000, 2018). In the seminal paper of Stefani et al. (Stefani et al., 1997), the number of gating charges (voltage-sensing charges) per channel estimated by the Q/N method (maximum gating charge (Q) displaced during depolarization over the number of channels (N)) is about 4-5 electronic charges (e_0) (Stefani et al., 1997). However, later studies estimated that each VSD carries 0.6 voltage-sensing electronic charges or an equivalent of 2.4 e_0 per channel (Horrigan and Aldrich, 1999; Horrigan et al., 1999). These results indicate that the BK channel VSD carries about three to five-fold less voltage-sensing charges than typical Kv channel VSDs like Shaker, whose effective valence correspond to the movement per channel of ~12-14 e_0 (Aggarwal and MacKinnon, 1996; Noceti et al., 1996; Seoh et al., 1996; Schoppa and Sigworth, 1998).

The special sequence of basic residues (mainly arginines (R)) located in the S4 transmembrane segment, each separated by two uncharged residues, is a pattern that is highly conserved in the voltage-dependent channels. It has been well established that the S4 is the principal component in voltage sensing of Kv channels because it harbors nearly all charged residues involved in voltage sensitivity (R1-R4 residues) (Aggarwal and MacKinnon, 1996; Seoh et al., 1996; Islas and Sigworth, 1999; Gandhi and Isacoff, 2002; Jensen et al., 2012) which can partially or completely cross the membrane electric field and contribute practically to total gating charge (each residue account for ~1 e_0) (Aggarwal and MacKinnon, 1996; Gandhi and Isacoff, 2002). Although BK channel carries also an S4-based sensor containing regularly spaced basic residues, R207, R210, and R213, that correspond to the canonical voltage-sensing R2, R3, and R4 residues in S4 of Kv, only R213 contributes to gating charge (Ma et al., 2006) (**Figure 3B**). Neutralization of the R207 or R210 residues do not affect the total gating charge, while voltage-sensing R213 contributes about half of the total gating charge (Ma et al., 2006). In addition, E219 at the C-terminus of S4 was suggested to sense voltage (Zhang et al., 2014). Thus, the voltage-sensing residues in BK

channels are not restricted to S4. Specifically, S2 TM segment harbors two potential voltage-sensing residues, D153 and R167, and an additional voltage-sensing charge is located in S3 (D186) (**Figure 3A**) (Ma et al., 2006). The decentralized distribution of gating charges and the relatively weak voltage sensitivity suggest that the movement of the BK channel VSD undergo small movements of S2, S3, and S4 in response to voltage changes that differ from a large S4 movement during voltage sensing in Kv channels (Ma et al., 2006)

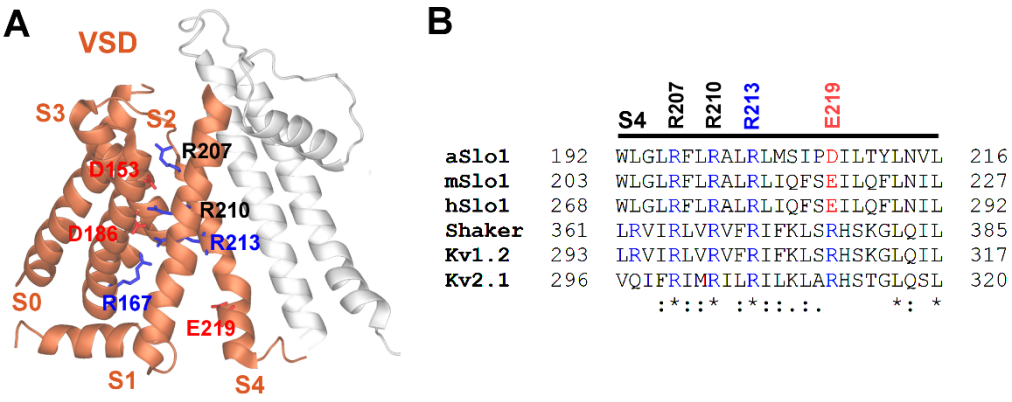

Figure 3. Structure of the voltage-sensing domain.

(**A**) Side view of secondary structure of TM region of a single α-subunit. The VSD (S0-S4) are in orange and the PD (S6-PH-S6) is in light gray. The potential voltage-sensing residues located in the S2 (D153 and R167), S3 (D186), and S4 (R213) TM segments are highlighted (positively and negatively charged residues were colored blue and red, respectively). (**B**) Alignment of S4 TM segment of Kv channels: aSlo1 (UniProt Accession Number (AC): Q5QJC5), mSlo1 (Q08460), hSlo1 (Q12791), Shaker (P08510), Kv1.2 (P16389), Kv2.1 (Q14721). Canonical voltage-sensing residues in S4 TM segment of Kv channels (R0-R4) are highlighted. The numbers indicate the charged residues in mSlo1.

Consistent with this scenario, voltage-clamp fluorometry (VCF) studies demonstrated that the relative movements of the voltage sensing S2 and S4 segments in the membrane electric field result in reciprocal and cooperative interactions between these two TM (Pantazis et al., 2010; Pantazis and Olcese, 2012). On the other hand, the aSlo1 structure shows that S4 helix is packed tightly in an antiparallel fashion with S5 in the PD of the same α-subunit (**Figure 1 B,C**), maybe restricting the S4 movement of the BK channels VSD (Tao et al., 2017; Zhou et al., 2017), whereas the Kv channel S4 is mostly separated from S5 (Long et al., 2005, 2007), appearing much freer to undergo conformational change (Tao et al., 2017). In addition, the S3–S4 paddle and charge transfer center that are important for gating charge movements in other Kv channels (Long et al., 2005) do not exist in aSlo1 structure (Tao et al., 2017; Zhou et al., 2017).

Calcium-sensing Domain.

Intracellular Ca^{2+} binds to the large cytosolic tail domain (CTD) of BK channels serving as the primary chemical sensor to respond to changes of Ca^{2+}, typically in the range of 100 nM to 300 μM, and other intracellular ligands. The main structural components of CTD are two nonidentical RCK domains (namely RCK1 and RCK2) that are linked in tandem (**Figure 1**) (Yuan et al., 2010). The overall architecture of BK channel CTD are conserved with its prokaryotic counterparts (Jiang et al., 2001; Ye et al., 2006; Lingle, 2007; Wu et al., 2010; Yuan et al., 2010, 2012; Pau et al., 2011; Giraldez and Rothberg, 2017; Hite et al., 2017; Tao et al., 2017) where the four CTDs or eight RCK domains from the tetrameric BK channel stack together and form a large gating ring structure (**Figure 4A**). Two distinct conformations of the BK channel gating ring have been detected from crystal structures solved in unliganded and Ca^{2+}-bound forms (Wu et al., 2010; Yuan et al., 2010, 2012; Hite et al., 2017; Tao et al., 2017), resembling a similar “expansion” of the gating ring induced by Ca^{2+} in the MthK gating ring. Thus, the gating ring operates as a chemo-mechanical transducer, converting the free energy of Ca^{2+} binding into structural rearrangements.

Two high-affinity Ca^{2+}-binding sites have first identified from electrophysiological and mutagenesis experiments: one located in the RCK1 domain (Bao et al., 2002; Xia et al., 2002), and the other located in the C-terminus of the RCK2 domain, known as the "Ca^{2+} bowl" (Schreiber and Salkoff, 1997). These two sites are located near the periphery of the gating ring (Figure 1B) with the Ca^{2+} bowl at the assembly interface between neighboring α-subunits and the RCK1 Ca^{2+}-site in the N-lobe of the RCK1 domain (**Figures 4A**) (Wu et al., 2010; Yuan et al., 2010, 2012; Hite et al., 2017; Tao et al., 2017).

Several residues markedly noncontiguous in the primary structure has been proposed to contribute in the formation of the RCK1 Ca^{2+}-sensor (**Figures 4B**), distinguishing the key role of D367, E535, and R514 in coordination of a Ca^{2+} (Xia et al., 2002; Zeng et al., 2005; Zhang et al., 2010; Tao et al., 2017). Other residues known to interfere with Ca^{2+}-dependent activation mediated by the RCK1 Ca^{2+}-site, such as D362 (Xia et al., 2002) and M513 (Bao et al., 2002), do not appear to be part of the Ca^{2+} binding-pocket but likely contribute indirectly to Ca^{2+} binding by stabilizing the RCK1 Ca^{2+}-site (Yang et al., 2015).

In the RCK2 domain, high-affinity Ca^{2+} sensing is attributed to a Ca^{2+}-binding region termed the "Ca^{2+} bowl", which contains consecutive aspartate residues at positions 897-901 (hD894-hD898) within RCK2 domain (Wei and Salkoff, 1994; Schreiber and Salkoff, 1997). Functional inferences and liganded structures of the gating ring (isolated Slo1 CTD structures (Yuan et al., 2012) and full-length aSlo1 structure (Tao et al., 2017)) have identified the residues Q892 (hQ889), D895 (hD892), D898 (hD895), D900 (hD897), as Ca^{2+}-coordinating residues (**Figures 4C**). Interestingly, residue N449 in the RCK1 domain forming part of the intersubunit assembly interface from an adjacent α-subunit was found to directly contact with the Ca^{2+} bound in the Ca^{2+} bowl, indicating that the Ca^{2+} bowl site may be influenced by Ca^{2+} occupancy status of RCK1 in a neighboring α-subunit.

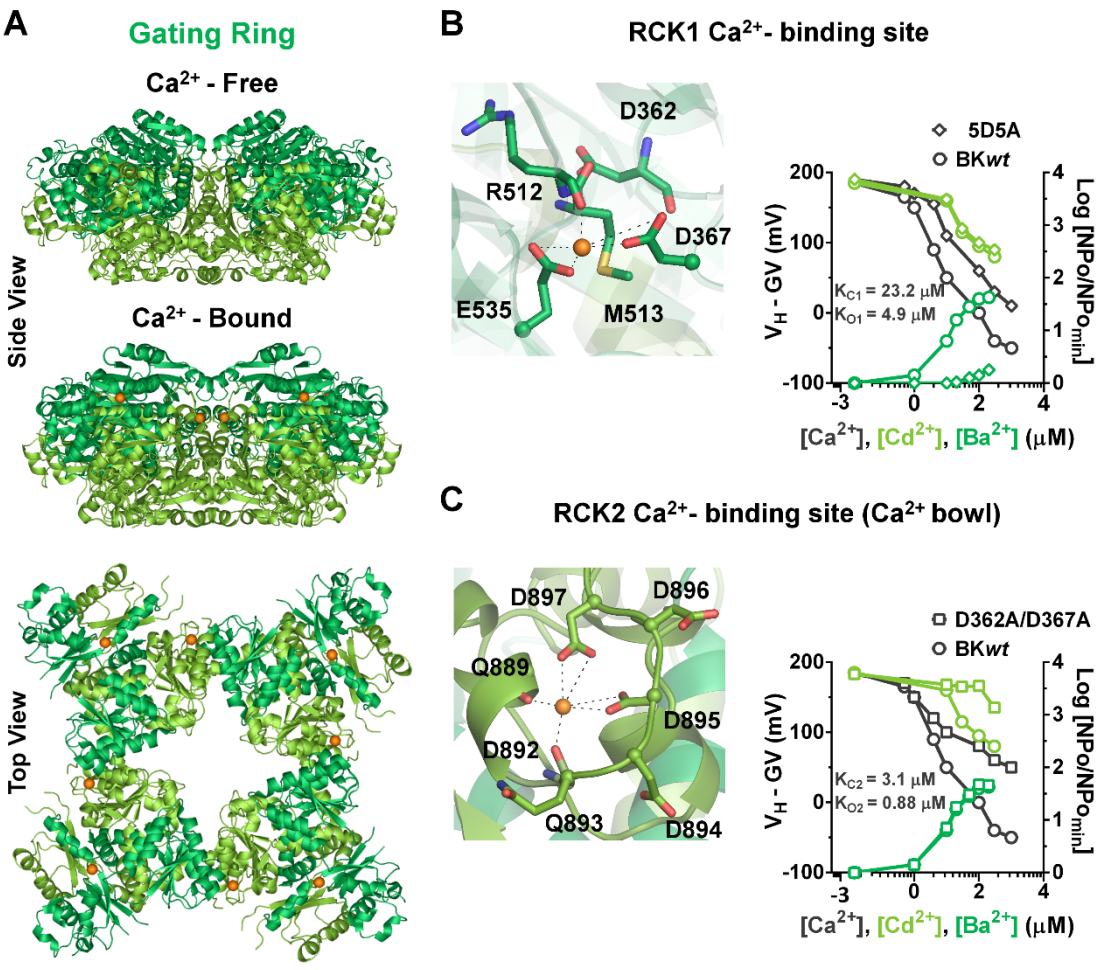

Figure 4. High-Affinity Ca^{2+}-binding sites in the gating ring.

(**A**) Cryo-EM structures of the aSlo1 gating ring in the unliganded (Side View; PDB ID: 5TJI) and Ca^{2+}-bound (Side and Top view; PDB ID: 5TJ6) conformation, in which Ca^{2+} (orange spheres) is bound at RCK1 site (green) and Ca^{2+} bowl (light green). (**B**-**C**) Structural and functional differences between the high-affinity Ca^{2+}-bindings sites located on RCK1 and RCK2 domains, respectively. (**B**) High-resolution view of the RCK1 binding site with coordination mediated by D367, E535, and R514 residues. D362 and M513 are proposed to stabilize the local structure of the Ca^{2+}-binding site. (**C**) High-resolution view of the RCK2 binding site. Cluster of aspartate residues forming the Ca^{2+} bowl and Ca^{2+} coordinating residues are labeled. Ca^{2+}-, Cd^{2+}- and Ba^{2+}-dependent activation mediated by the RCK1 Ca^{2+}-site (**B**) and Ca^{2+} bowl (**C**) are shown (Xia et al., 2002; Zeng et al., 2005; Zhou et al., 2012). Activation by Cd^{2+} (light green) and Ba^{2+} (green) occurs selectively through the RCK1 Ca^{2+}-site and Ca^{2+} bowl, respectively.

Electrophysiological studies of the mutants D362A/D367A (Xia et al., 2002) or M513I (Bao et al., 2002) and 5D5A (Schreiber and Salkoff, 1997) that selectively abolish the function of the RCK1 Ca^{2+}-site and Ca^{2+} bowl, respectively, show that each one is responsible for about half of the BK channel's Ca^{2+} sensitivity, while the double RCK sites mutants are only activated by Ca^{2+} at concentrations at concentrations greater than 1 mM (Bao et al., 2002; Xia et al., 2002). However, the RCK1 and RCK2 Ca^{2+}-binding sites have distinct functional properties conferred by their different molecular structures and relative positions within the gating ring (Wu et al., 2010; Yuan et al., 2010, 2012; Hite et al., 2017; Tao et al., 2017) Thus, the RCK sites differ in their Ca^{2+} binding affinities (Bao et al., 2002; Xia et al., 2002; Sweet and Cox, 2008), divalent cations selectivity (Oberhauser et al., 1988; Schreiber and Salkoff, 1997; Zeng et al., 2005; Zhou et al., 2012), voltage dependence (Sweet and Cox, 2008; Savalli et al., 2012; Miranda et al., 2018) and in their contribution to gating mechanism (Yang et al., 2010, 2015).

The apparent Ca^{2+} dissociation constants (K_D) estimated for each RCK sensor show that Ca^{2+} bowl has higher affinity for Ca^{2+} with values of 3.1 and 0.88 μM for closed and open channel (**Figure 4B**), respectively, whereas the RCK1 Ca^{2+}-site has an affinity of 23 μM when the channel is closed and 4.9 μM when the channel is open (**Figure 4C**) (Sweet and Cox, 2008). The structural differences between the RCK sites are also made evident by differential selectivity with other chemically distinct divalent cations (Oberhauser et al., 1988; Schreiber and Salkoff, 1997; Zeng et al., 2005; Zhou et al., 2012). For example, it has been established that Cd^{2+} selectively interacts with the RCK1 site, whereas Ba^{2+} acts exclusively through the Ca^{2+} bowl (**Figure 4B,C**) (Zeng et al., 2005). Additionally, only activation involving the RCK1 site was shown to be sensitive to voltage (Sweet and Cox, 2008; Miranda et al., 2013, 2016, 2018), and whereas the N-lobe of RCK1 is involved in the ability of RCK1 Ca^{2+} binding to act on the PD domain but does not participate in activation involving the Ca^{2+} bowl (Yang et al., 2010). Overall, considering the nonequivalence of these two Ca^{2+} sensors it is reasonable to assume that the pathway through

which Ca^{2+} binding in RCK1 leads to channel activation differs from that involving Ca^{2+} binding in the in the Ca^{2+} bowl.

Different from the two high-affinity Ca^{2+}-binding sites in the cytosolic RCK1 and RCK2 domain, another cation-binding site is formed between the RCK1 N-lobe domain and the cytosolic side TMD of adjacent α-subunits (**Figure 5A**). Both Ca^{2+} and Mg^{2+} ions can bind to this site with affinities in the millimolar range (Golowasch et al., 1986; Oberhauser et al., 1988; Shi and Cui, 2001; Zhang et al., 2001), but at physiological conditions the site is more likely occupied by Mg^{2+} being known as the Mg^{2+}-binding site.

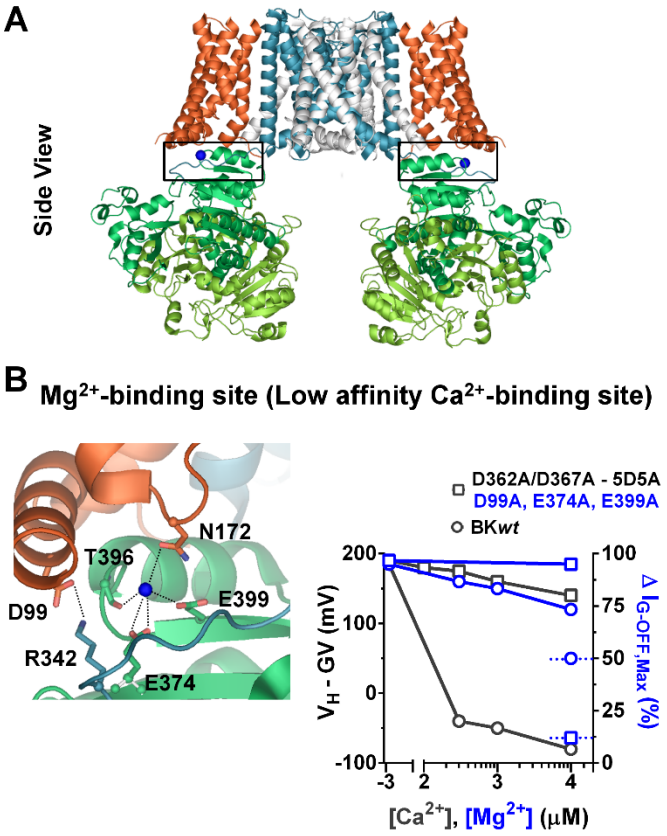

Figure 5. Low-Affinity Mg^{2+}-binding site.

(**A**) Cryo-EM structure of the aSlo1 in the Ca^{2+}/Mg^{2+}-bound state (PDB ID: 5TJ6). Mg^{2+} (blue spheres) is bound to the low-affinity site forming by the interface between the TMD of one α-subunit and the gating ring of the neighbor α-subunit. (**B**) High-resolution view of the Mg^{2+}-binding site. Residues E374, E399, and T396 (RCK1 domain) and N161 (VSD) appear to contribute to Mg^{2+} coordination. Residues D99 and R342 form a salt bridge that may help stabilize the bound Mg^{2+} structure. Ca^{2+}- (dark gray) and Mg^{2+}-dependent (blue) activation mediated by the Mg^{2+}-binding site (left axis) and the Mg^{2+} effect on $I_{G\text{-}OFF}$ peak (right axis) are shown (Xia et al., 2002; Yang et al., 2008a).

Mutagenesis studies in the N-terminus of the RCK1 domain identified that E374 and E399 are critical for Mg^{2+} sensing (Shi and Cui, 2001; Xia et al., 2002), which is in accordance with the structural evidence regarding the determinants of Mg^{2+} coordination, besides of the residue T396 (RCK1 domain) and the residue N172 located at the S2–S3 loop in the neighboring α-subunit (Tao et al., 2017) (**Figure 5B**). Additionally, the residue D99 located at the S0–S1 loop have been identified functionally as a key residue in the formation of the inter-subunit Mg^{2+}-binding site at the interface between the VSD and CTD (Yang et al., 2008a). However, the critical role of D99 on Mg^{2+} sensitivity appears to be related to stabilize the bound Mg^{2+} structure by interacting with some other nearby charged residues, including the R342 at the S6-RCK1 linker (Tao et al., 2017) (**Figure 5B**).

Allosteric gating mechanisms consistent with the modular structure of BK channels.

Gating mechanisms are best formulated in terms of what is known about the structure of an ion channel. Several kinetic models have been developed to understand the modular nature of the BK channel. Thus, the ability of VSD and CTD sense voltage and intracellular signaling molecules can enhance the PD opening by electromechanical and chemomechanical coupling in a nonobligatory fashion (functional independence of the three distinct structural modules) is well described in terms of allosteric mechanisms (Monod et al., 1965). The dual allosteric model proposed by Horrigan and Aldrich (2002) (**Figure 6**) stands out due to its optimum balance between simplicity and predictive capabilities providing a useful framework for analyzing BK channel gating mechanisms in terms of domain/domain interactions (Horrigan and Aldrich, 2002). Latorre et al. (Latorre et al., 2017) show a rational approach to the experimental study of BK channels using the HA kinetic model.

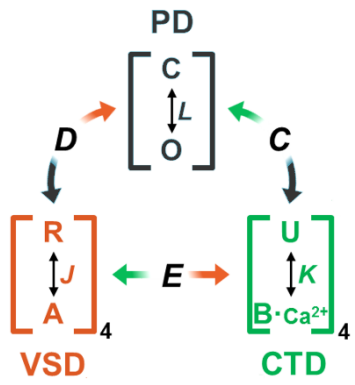

Figure 6. HA allosteric gating model of BK channels.

Scheme of HA allosteric model (Horrigan and Aldrich, 2002) indicates the possible conformations of the PD (C-O), VSD (R-A) and Ca^{2+} sensors (U-B·Ca^{2+}) in each of four α-subunits. Channel opening is defined by the equilibrium constant, L; VSD activation is defined by the equilibrium constant J, Ca^{2+} binding is defined by the binding constant K. The allosteric relationships between the modules are described by the allosteric factors D, C, and E.

I. VSD-PD allosteric coupling.

In the absence of voltage sensor activation and Ca^{2+} binding, the BK channel activation gate (PD) can transit between the closed (C) and open states (O) with an intrinsic open probability (Po) (Pallotta, 1985) of $\sim 10^{-7}$ (Horrigan and Aldrich, 1999; Cui and Aldrich, 2000). The C-O equilibrium is governed by the equilibrium constant L, which is regulated by four independent and identical voltage and Ca^{2+} sensors.

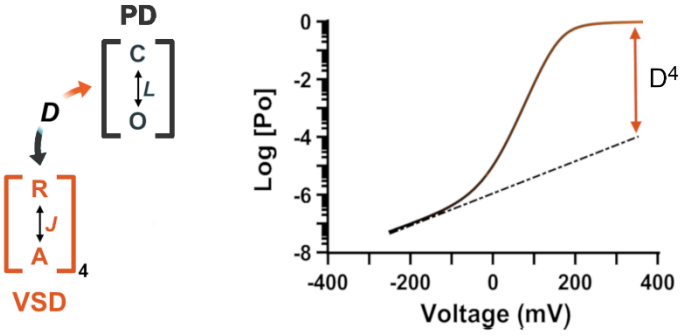

Figure 7. Voltage-gating of BK channels.

(*Left*): Allosteric gating model between the VSD and the PD in absence of Ca^{2+}. (*Right*): Activation of VSD increase the Po of the BK channel through the coupling factor D which describe the VSD-PD energetic interaction ($D = e^{-\Delta\Delta G^{V}_{C\leftrightarrow O}/RT}$).

In the absence of Ca^{2+} binding, depolarization membrane activates the VSD transiting from resting (R) to activated (A) state facilitating the channel opening (**Figure 7**). The function of each VSD is defined by the equilibrium constant $J(V)$, whereas that the VSD activation ability of affect the equilibrium of the PD is define by the allosteric factor D.

How the voltage-driven conformational changes of the VSD are coupled with the opening of the pore is yet unclear, although the S6 TM segment appears to play an important role. Interactions between E219 and E321/E324 (Zhang et al., 2014), located on the cytosolic side of S4 and S6, respectively, may contribute to VSD–PD coupling. Mutations of VSD residues (E180, E186, and R210) also were shown to produce effects consistent with a reduction in coupling energies between VSD and PD (Ma et al., 2006), which suggest that interactions between residues in different TM segments can impact on VSD-pore interaction. Additionally, based on functional data and molecular modeling it has been proposed that a “hydrophobic ring” may act as an integration node between the allosteric signals from both domains (Carrasquel-Ursulaez et al., 2014, 2018).

II. CTD-PD allosteric coupling.

Similarly, saturating Ca^{2+} binding increases BK channel open probability by four orders of magnitude from $\sim 10^{-7}$–10^{-3} when the voltage sensors are at the resting state (Horrigan and Aldrich, 2002; Yang et al., 2010), indicating a strong interaction between Ca^{2+} binding and channel opening (**Figure 8**). The transition of Ca^{2+} sensors between unbound (U) or Ca^{2+} bound (B-Ca^{2+}) conformations is defined by equilibrium constant K which depends on Ca^{2+} concentration ([Ca^{2+}]) and the Ca^{2+} dissociation constant (K_D). For simplicity, the two high-affinity Ca^{2+}-binding sites per α-subunit are treated as a single site in the HA model, giving four effective Ca^{2+}-binding sites. The VSD activation ability to affect the equilibrium of the PD is defined by the allosteric factor D. Thus, each Ca^{2+} sensor increase the Po by the allosteric factor C reflecting the energetic coupling between the Ca^{2+} binding and channel opening processes.

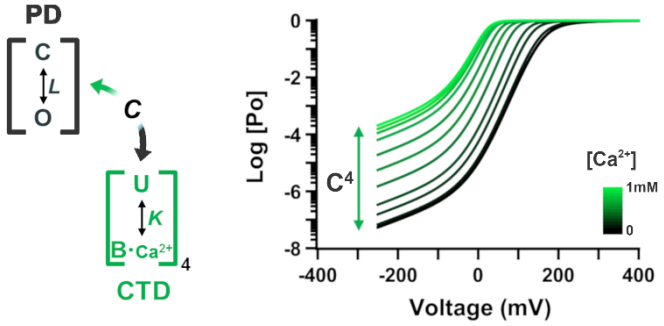

Figure 8. Ca^{2+}-gating of BK channels.

(*Left*): Allosteric gating model between the CTD and the PD at the resting state of the VSD. (*Right*): Ca^{2+} binding to sensors on CTD increase the Po of the BK channel through the coupling factor C which describe the CTD-PD energetic interaction ($C = e^{-\Delta\Delta G^{Ca}_{C\leftrightarrow O}/RT}$).

The molecular mechanism of chemomechanical coupling between the CTD and the PD in BK channels is the best understood at a molecular level. Ca^{2+}-induced rearrangements of the gating ring (Yusifov et al., 2008, 2010; Wu et al., 2010; Yuan et al., 2010, 2012; Javaherian et al., 2011; Miranda et al., 2013; Hite et al., 2017; Tao et al., 2017) is transmitted to the PD through the S6-RCK1 linker that connects these two domains. Shortening of the linker increases channel activity, while its elongation decreases Ca^{2+} sensitivity (Niu et al., 2004). This led to the proposal that the S6-RCK1 linker, the gating ring, or both acting in series operate like a passive spring such that the conformational change promoted by Ca^{2+} binding to the gating ring directly pulls the linker to open the gate. The recent structural information of aSlo1 suggests that the RCK1 N-lobe of the gating ring may contribute spring-like properties (Hite et al., 2017). Interestingly, the protein-protein interface formed by the non-covalent interaction between the RCK1 N-lobe, the VSD, and the S4-S5 linker may also play an important role to propagate any conformational changes in the CTD upon Ca^{2+} binding to the PD (Hite et al., 2017).

III. CTD-VSD allosteric coupling.

Ca^{2+} binding and VSD activation process are also directly influenced by the status of the voltage sensors and Ca^{2+} sensors, respectively, when the channel is closed (**Figure 9**). Such energetic

interaction is described by the allosteric factor E. For simplicity, the standard HA model assumes that Ca^{2+} and voltages sensors interact through a mechanism where the Ca^{2+} binding to one α-subunit affects only the VSD in the same subunit (Horrigan and Aldrich, 2002).

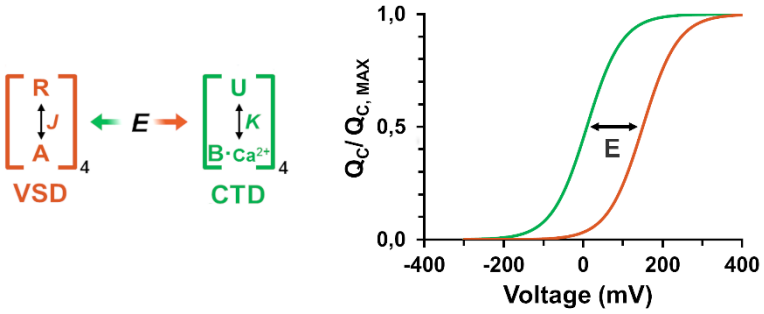

Figure 9. Ca^{2+}-voltage sensors coupling in BK channels.

(*Left*): CTD-VSD allosteric model in closed channels. (*Right*): Ca^{2+} binding to sensors on CTD increase the VSD activation through the coupling factor E describing the CTD-VSD energetic interaction ($E = e^{-\Delta\Delta G^{Ca}_{R\leftrightarrow A}/RT}$).

The extent of the CTD-VSD allosteric interaction as well its molecular nature is by far the least unclear within the framework of the dual allosteric gating mechanisms of BK channel. Interactions between VSD and CTD during BK gating have been revealed by results showing that Ca^{2+} binding alters the R-A equilibrium of voltage sensors (Horrigan and Aldrich, 2002; Savalli et al., 2012; Carrasquel-Ursulaez et al., 2014). Furthermore, fluorescence-based studies indicate that the structural rearrangements of the gating ring during channel gating show voltage dependence (Miranda et al., 2013). Again, the physical interface between the RCK1 N-lobe and VSD has been suggested to provide the structure capable of mediating the crosstalk between these sensory modules and their synergy in activating the pore domain (Yang et al., 2007; Sun et al., 2013; Tao et al., 2017; Zhang et al., 2017). However, different studies have put forth opposing conclusions

about the strength of functional interaction (in energetic terms) between voltage sensors and Ca^{2+} sensors (Horrigan and Aldrich, 2002) (Carrasquel-Ursulaez et al., 2014).

The full-length structures now provide a stronger basis for thinking about how VSD–CTD interactions may affect channel gating, suggesting that Ca^{2+}-induced rearrangements of the N-lobe RCK1 directly produce a displacement of the voltage sensors away from the pore axis, which in turn induces an equivalent displacement of the S5 helices near the plasma surface, favoring pore opening (Hite et al., 2017). The possibility that a major component of the VSD–CTD interaction through the RCK1-VSD, and then via linkers to the PD, contradict previous proposals that voltage and Ca^{2+} sensors are only weakly coupled leading to rethink the standard HA model for dual activation of BK channel.

So far, several questions regarding the structural and functional bases of the allosteric interplays that underlie the Ca^{2+} and voltage activation mechanisms of BK channel are still open such as: What is the extent of the allosteric interaction between Ca^{2+} binding and VSD activation and how relevant it is these specialized-sensory modules crosstalk on the BK channel gating? Mechanistically, how does the Ca^{2+}-VSD coupling occur? Given the nonequivalence of the two high-affinity Ca^{2+}- binding sites in the CTD, does each kind of Ca^{2+} site located on RCK1 and RCK2 domain distinct energetic contributions to the CTD-VSD interaction?

Hypothesis

Ca^{2+} binding and VSD activation process in BK channels are strongly coupled involving independent allosteric pathways via the two distinct RCK1 and RCK2 Ca^{2+} sensors interact with the voltage-sensing domains.

Main Aim

Evaluate the energetic coupling between Ca^{2+} binding and the voltage-sensing domain activation and determine the functional role of the two distinct high-affinity Ca^{2+}-binding sites on the CTD-VSD allosteric interaction.

SPECIFIC AIMS

- Characterize the Ca^{2+}-induced effect on voltage-sensing domain activation independently from the pore opening process.
- Elucidate the interaction mechanisms which the allosteric coupling between Ca^{2+} binding and VSD activation occurs.
- Evaluate the energetic contribution to the VSD equilibrium of the two high-affinity Ca^{2+}-binding sites contained in the RCK1 and RCK2 domains.

METHODOLOGY, RESULTS AND DISCUSSION

For the following sections refer to the attached manuscripts:

Lorenzo-Ceballos Y, Carrasquel-Ursulaez W, Castillo K, Alvarez O, Latorre R. (2019). *Calcium-driven regulation of voltage-sensing domains in BK channels*. bioRxiv. DOI:10.1101/520429.

Calcium-driven regulation of voltage-sensing domains in BK channels

Yenisleidy Lorenzo-Ceballos[1,2], Willy Carrasquel-Ursulaez[2], Karen Castillo[2], Osvaldo Alvarez[2,3] and Ramon Latorre[2 (*)]

[1]Doctorado en Ciencias Mención Neurociencia, Facultad de Ciencias, Universidad de Valparaíso, Valparaíso, Chile; [2]Centro Interdisciplinario de Neurociencia de Valparaíso, Facultad de Ciencias, Universidad de Valparaíso, Valparaíso, Chile; [3]Departamento de Biología, Facultad de Ciencias, Universidad de Chile, Santiago, Chile.

(*) Correspondence and Requests for materials should be addressed to Ramon Latorre (ramon.latorre@uv.cl)

Abstract

Allosteric interplays between the voltage-sensing domain (VSD), the Ca^{2+}-binding sites, and the pore domain govern the Ca^{2+}- and voltage-activated K^+ (BK) channel opening. However, the functional relevance of the Ca^{2+}- and voltage-sensing mechanisms crosstalk on BK channel gating is still debated. We examined the energetic interaction between Ca^{2+} binding and VSD activation measuring and analyzing the effects of internal Ca^{2+} on BK channels gating currents. Our results indicate that the Ca^{2+} sensors occupancy has a strong impact on the VSD activation through a coordinated interaction mechanism in which Ca^{2+} binding to a single α-subunit affects all VSDs equally. Moreover, the two distinct high-affinity Ca^{2+}-binding sites contained in the C-terminus domains, RCK1 and RCK2, appear to contribute equally to decrease the free energy necessary to activate the VSD. We conclude that voltage-dependent gating and pore opening in BK channels is modulated to a great extent by the interaction between Ca^{2+} sensors and VSDs.

Introduction

Diverse cellular events involve calcium ions as a primary mediator in the signal transduction pathways triggering, among other signaling processes, Ca^{2+}-activated conductances. Since the BK channels are regulated by cytosolic Ca^{2+} and depolarizing voltages (Marty, 1981; Pallotta et al., 1981; Latorre et al., 1982), they are integrators of physiological stimuli including intracellular Ca^{2+} elevation and membrane excitability. BK channels are modular proteins where each module accomplishes a specific channel function. Thus, different modules harbor voltage and Ca^{2+} sensors that communicate with the channel gate allosterically (Cox et al., 1997; Horrigan and Aldrich, 1999, 2002; Horrigan et al., 1999; Rothberg and Magleby, 1999, 2000; Cui and Aldrich, 2000). Functional BK channels are formed by homotetramers of α-subunits (Shen et al., 1994) each comprising a transmembrane voltage-sensing domain (VSD) and an intracellular Ca^{2+}-sensing C-terminal domain (CTD) that can independently modulate the ion conduction gate in the pore domain (PD) (Latorre et al., 2017). The CTDs consist of two non-identical regulators of the conductance of K^+ domains (RCK1 and RCK2) arranged into a ring-like tetrameric structure dubbed the gating ring (Wu et al., 2010; Yuan et al., 2010, 2012; Hite et al., 2017; Tao et al., 2017). Each RCK domain contains distinct ligand-binding sites capable of detecting Ca^{2+} in the micromolar range (Schreiber and Salkoff, 1997; Bao et al., 2002; Xia et al., 2002).

In the absence of Ca^{2+}, the activation of VSD decreases the free energy necessary to fully open the BK channels in an allosteric fashion (Horrigan and Aldrich, 1999; Horrigan et al., 1999). Under these experimental conditions, very positive membrane potentials are required to drive all voltage sensors to its activated conformation (Cui et al., 1997; Stefani et al., 1997; Horrigan et al., 1999; Contreras et al., 2012), ultimately leading to a significant activity of the BK channel. Hence, in cells like neurons, an appreciable open probability of BK channels at physiologically relevant voltages necessarily involves the activation of Ca^{2+} sensors on the gating ring. The allosteric interplays established between the functional and structural modules (VSD-PD, CTD-PD, and CTD-VSD)

are key in enabling BK channels to operate over a dynamic wide-range of internal Ca^{2+} and voltage conditions by fine-tuning the channel's gating machinery. Therefore, understanding the structure-functional bases that underlie the Ca^{2+} and voltage activation mechanisms interrelationship becomes essential.

The voltage dependence of Ca^{2+}-dependent gating ring rearrangements (Miranda et al., 2013, 2018) and RCK1 site occupancy (Sweet and Cox, 2008; Savalli et al., 2012; Miranda et al., 2018) as well as the perturbation of VSD movements by Ca^{2+} binding (Savalli et al., 2012) support the idea that the energetic interaction between both specialized sensors may be crucial to favor BK channel activation. The physical CTD-VSD interface has been suggested to provide the structure capable of mediating the crosstalk between these sensory modules and their synergy in activating the pore domain (Yang et al., 2007; Sun et al., 2013; Tao et al., 2017; Zhang et al., 2017). However, the strength of the interaction between voltage and Ca^{2+} sensors and their relevance to BK channel activation is still an unresolved matter (Horrigan and Aldrich, 2002; Carrasquel-Ursulaez et al., 2015). Also, the functional role that plays each of the high-affinity Ca^{2+}-binding sites on the CTD-VSD allosteric interaction is an open question. The RCK1 and RCK2 Ca^{2+}-binding sites have distinct functional properties conferred by their different molecular structures and relative positions within the gating ring (Wu et al., 2010; Yuan et al., 2010, 2012; Hite et al., 2017; Tao et al., 2017). Thus, the RCK sites differ in their Ca^{2+} binding affinities (Bao et al., 2002; Xia et al., 2002; Sweet and Cox, 2008), divalent cations selectivity (Oberhauser et al., 1988; Schreiber and Salkoff, 1997; Zeng et al., 2005; Zhou et al., 2012), voltage dependence (Sweet and Cox, 2008; Savalli et al., 2012; Miranda et al., 2018) and in their contribution to allosteric gating mechanism (Yang et al., 2010, 2015). In particular, only the RCK1 site appears to be involved in communicating the Ca^{2+}-dependent conformational changes towards the membrane-spanning VSD (Savalli et al., 2012; Miranda et al., 2018). Recently, the *Aplysia* BK structure shows that the N-lobe of RCK1 domain is in a non-covalent contact with the VSD and the S4-S5 linker

being this RCK1-VSD interaction surface rearranged when comparing the liganded and Ca^{2+}-free structures (Hite et al., 2017; Tao et al., 2017). Actually, it has been hypothesized that any Ca^{2+}-induced rearrangements of the gating ring should be ultimately transmitted to the pore domain via the VSD (Hite et al., 2017; Zhou et al., 2017). Thus, defining what extent Ca^{2+} binding influences to VSD is crucial in determining how important is the crosstalk between sensors in decreasing the free energy necessary to open the BK channel.

Here, we examined the Ca^{2+}-dependence of the VSD activation estimating the allosteric coupling between Ca^{2+} and voltage sensors. By analyzing gating currents under unliganded and Ca^{2+}-saturated conditions, we found a strong energetic influence of the Ca^{2+}-binding on the voltage sensors equilibrium in an independent manner of the channel opening. These findings point out that a major component in the synergistic Ca^{2+} and voltage activation of BK channels can reside on the sensory domains communication. We also found that the Ca^{2+}-dependent behavior of the voltage sensor activation is consistent with an CTD-VSD allosteric coupling that occurs through a concerted interaction scheme where each Ca^{2+}-bound to high-affinity sites affect equally all voltage sensors in the BK tetramer. Notably, we found that the two distinct RCK1 and RCK2 Ca^{2+} sensors exert equivalent contributions on VSD via independent allosteric pathways.

Results

Allosteric coupling between Ca^{2+}-binding and voltage sensor activation is strong. We characterized the effects of Ca^{2+}-binding on voltage sensor activation in BK channels by analyzing gating current measured on inside-out patches of *Xenopus laevis* oocyte membrane. Families of gating currents (I_G) were evoked at different intracellular Ca^{2+} concentrations ($[Ca^{2+}]_i$) ranging from 0.1 to 100 μM in K^+-free solution (***Figure 1A***). For all experiments, first we measured I_G in the nominal absence of Ca^{2+} ("zero Ca^{2+}" condition), and then we perfused the internal side with solutions containing Ca^{2+} at increasing concentrations. The amount of gating charge displaced ($\boldsymbol{Q_C}$) at each Ca^{2+} concentration was obtained by fitting the initial part of the ON-gating current decay to a single exponential (fast ON-gating; see *Methods*) and integrating it. In this manner, we determine only the gating charge displaced before the BK channel opening.

The increase in internal Ca^{2+} promotes a leftward shift of the Q_C versus voltage ($Q_C(V)$) curves (***Figure 1B,C***) which indicate that Ca^{2+}-binding facilitates the activation of the voltage sensor being more prominent as binding sites occupancy increases. Revealing a strong energetic interaction between both sensors, a significant Ca^{2+}-induced shift of voltage sensor activation occurs (ΔV_H = -142.6 ± 4.5 mV) under Ca^{2+}-saturated conditions for high-affinity binding sites (100 μM). Such large shift means that Ca^{2+}-binding to the RCK Ca^{2+}-binding sites alters the VSD equilibrium promoting a decrease in the free energy ($\Delta\Delta G_V^{Ca}$) that defines the voltage sensor resting-active (R-A) equilibrium by ~8 kJ/mol ($\Delta\Delta G_V^{Ca}$ = -7.98 ± 0.27 kJ/mol).

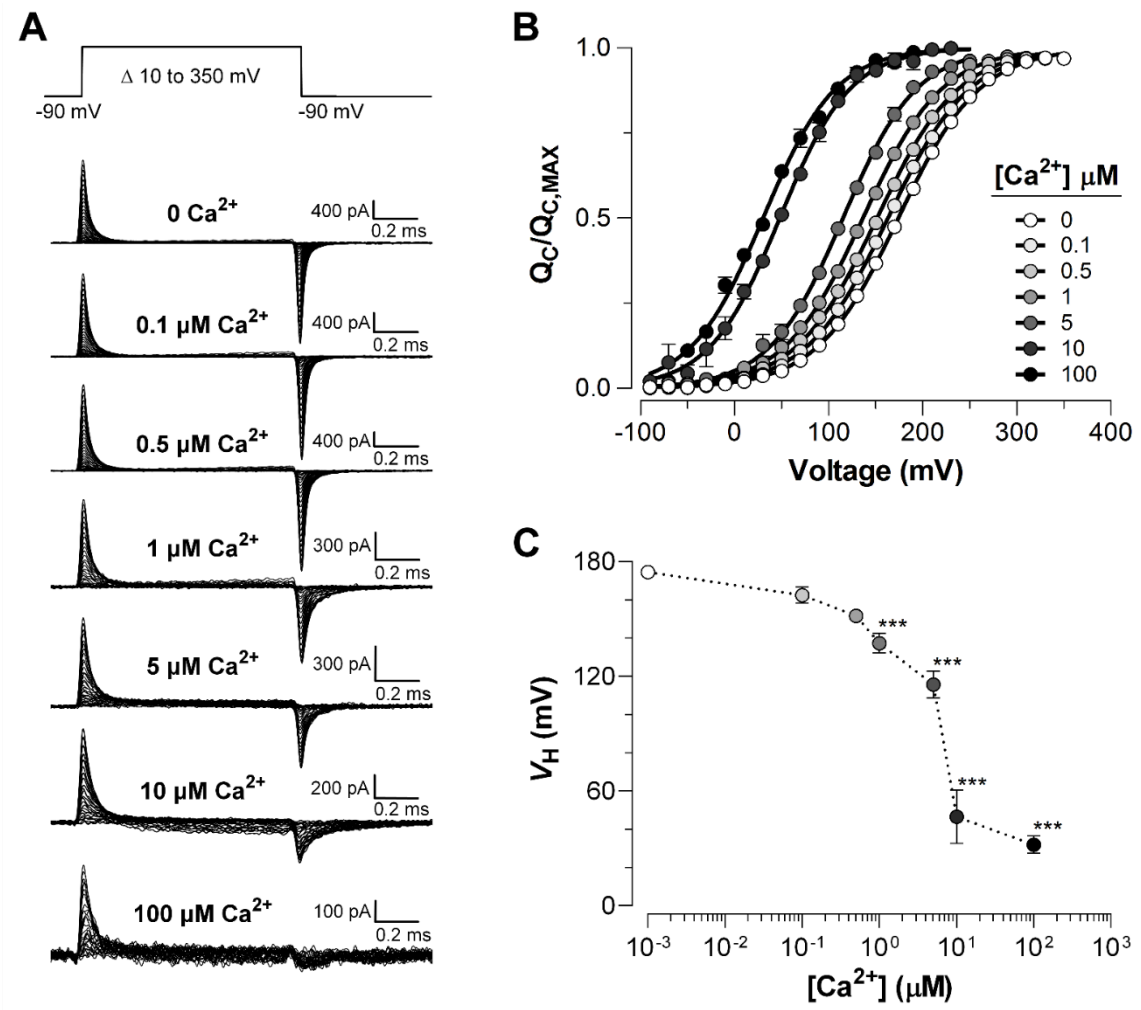

Figure 1. Effects of Ca^{2+}-binding on VSD activation in BK channels.

(**A**) Representative gating current (I_G) recordings at different internal Ca^{2+} concentrations (from 0 to 100 μM). I_G were evoked by the indicated voltage protocol of 1 ms duration. (**B**) Gating charge-voltage relationships ($Q_C(V)$) were obtained by integrating the fast component for each ON I_G trace. Normalized gating charge data $\left(Q_C(V)/Q_{C,\ MAX}\right)$ (mean ± SEM) were fitted using a single Boltzmann function (solid lines). (**C**) V_H obtained from the $Q_C(V)$ curves as a function of Ca^{2+} concentration (mean ± SEM). At zero" Ca^{2+} condition $V_{H\,(0\ Ca^{2+})}$ = 174.5 ± 2.4 mV (n = 25), whereas Ca^{2+} binding produce a leftward shift in V_H (ΔV_H): 0.1 μM Ca^{2+} (ΔV_H = -12.1 ± 3.5 mV, n = 5); 0.5 μM Ca^{2+} (ΔV_H = -22.9 ± 1.8 mV, n = 5); 1 μM Ca^{2+} (ΔV_H = -37.1 ± 3.5 mV, n = 5); 5 μM Ca^{2+} (ΔV_H = -58.8 ± 6.7 mV, n = 6); 10 μM Ca^{2+} (ΔV_H = -127.9 ± 13.9 mV, n = 6); 100 μM Ca^{2+} (ΔV_H = -142.6 ± 4.5 mV, n = 7). The one-way ANOVA followed by Dunnett's post-hoc test analysis was used to assess statistical significance of the Ca^{2+}-induced shifts in V_H (***p< 0.001).

A visual inspection of the current records indicates that the kinetics of the ON-gating current is not much affected by the concentration of Ca^{2+} present in the internal solution. However, it is apparent that the OFF-gating current is dramatically modified becoming smaller in amplitude and with slower kinetics as the internal Ca^{2+} concentration is increased (***Figure 1A*** and ***Figure 1—figure supplement 1A***). At least two components can be resolved in the OFF gating current decay (***Figure 1—figure supplement 1B,C***), and the relative contribution of the slower component increases as internal Ca^{2+} augmented reflecting an increase of the open probability of channel ***Figure 1—figure supplement 1D,E***). This kinetic behavior recapitulates the effect describe on gating charge displacement as a function of the depolarizing pulse duration (Horrigan and Aldrich, 2002; Contreras et al., 2012; Carrasquel-Ursulaez et al., 2015), and confirm that this phenomenon is associated with the time course of channel opening revealing the allosteric interaction between voltage sensors and the pore gate (Horrigan and Aldrich, 2002).

Ca^{2+} binding to single α-subunit affects the R-A voltage sensor equilibrium of all four subunits equally. Taking advantage of the dose-dependent effect of Ca^{2+} on voltage sensor activation we investigated the underlying mechanism of the Ca^{2+}-voltage sensors communication in the context of the well-established Horrigan-Aldrich (HA) allosteric gating model (Horrigan and Aldrich, 2002). Two different mechanisms were proposed by Horrigan and Aldrich for the interaction between the Ca^{2+}-binding sites and voltage sensors. The first mechanism supposes that Ca^{2+} binding to one α-subunit affects the VSD in the same subunit only (Scheme I) (***Figure 2A***), while the second mechanism assumes that the Ca^{2+} binding affects the four VSD equally (Scheme II) (***Figure 2B***). It should be noted that the standard HA model makes two simplifying assumptions by considering a single Ca^{2+}-binding site per α-subunit and the Scheme I as the Ca^{2+} binding-VSD interaction mechanism underlying BK channel gating (Horrigan and Aldrich, 2002).

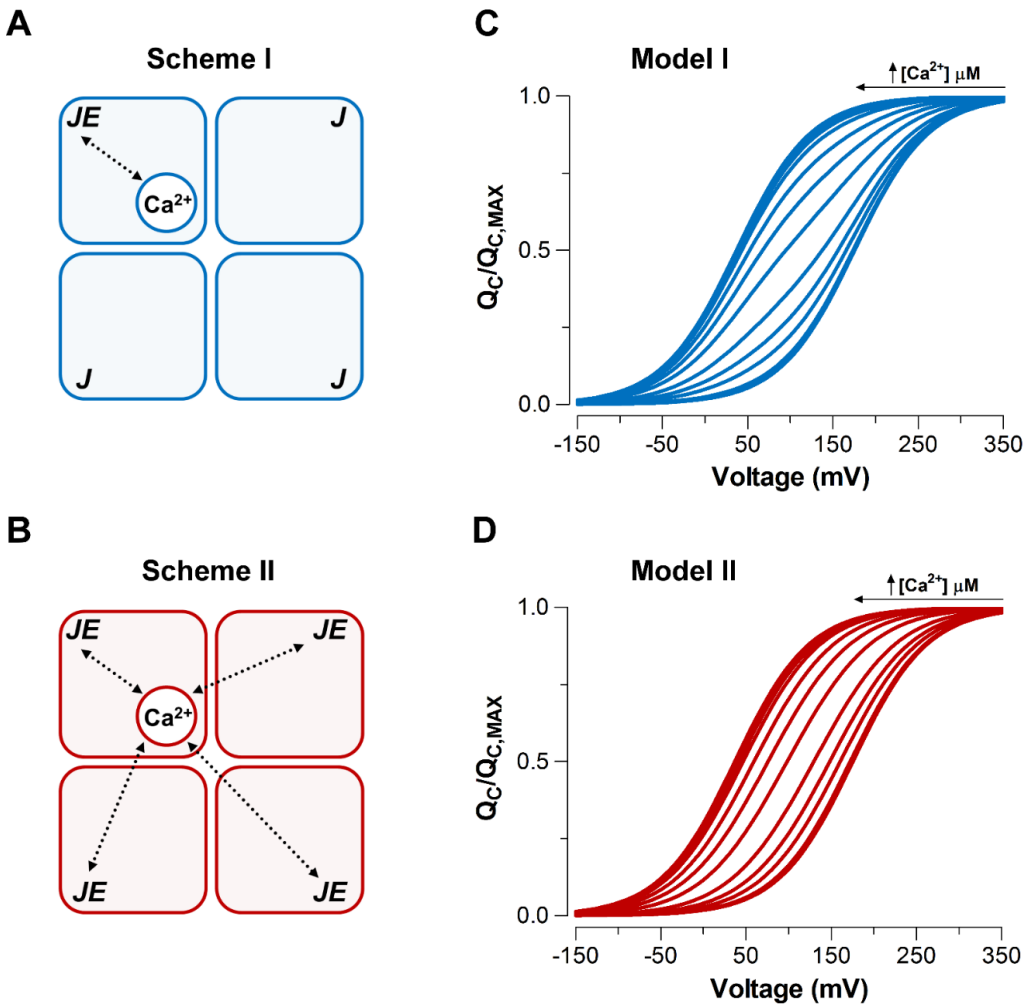

Figure 2. Model-dependent behavior of the $Q_C(V)$ curves based on the CTD-VSD interaction mechanisms according to the fractional occupancy of Ca^{2+}-binding sites.

(**A-B**) Cartoons representing two interaction schemes between voltage sensors and Ca^{2+}-binding sites (modify from Horrigan and Aldrich (2002)). The Scheme I (**A**) assume that Ca^{2+} binding only affects the voltage sensor of one α-subunit (E_{M1}). The Scheme II (**B**) predicts that binding of Ca^{2+} to one α-subunit affects VSD in all subunits equally, increasing the voltage sensor equilibrium constants (J) E_{M2}-fold in all four subunits (E_{M2}^4, when the four Ca^{2+} sites are occupied). In both schemes, a single Ca^{2+}-binding site is considered in each α-subunit. (**C-D**) Predictions of $Q_C(V)$ relationships at different internal calcium concentration (from 0 to 10 mM) by two distinctive interaction mechanisms between Ca^{2+}-binding sites and voltage sensors (Scheme I and Scheme II), respectively. $Q_C(V)$ curves were generated using Equation 4 (blue: Model I) or Equation 6 (red: Model II), and the following set of parameters: z_J= 0.58, J_0= 0.018, K_D= 11 µM and E_{M1}= E_{M2}^4= 25.

For a better comprehension, we simulated the normalized $Q_C(V)$ curves over a wide range of Ca^{2+} concentrations (from 0 to 10 mM) for each Ca^{2+}-VSD interaction scheme (***Figure 2C,D***). Here we assume that the measurement of the fast gating currents captures the charge displaced by R-A transitions and exclude the charge associated with the transition between the activated estates. This assumption is reasonable since the Ca^{2+}-binding rate constant estimated for BK is about 10^8 $M^{-1}s^{-1}$ (Hou et al., 2016) implying that at 10 μM internal Ca^{2+} (the highest non-saturating Ca^{2+} concentration tested) the time constant of the Ca^{2+} binding is 1 ms, while the VSD activates with a time constant of ~30 μs at the higher voltage tested (see the *Supplementary Information* for details of the simulations).

At extreme conditions of low (0.03 to 0.1 μM) and high (≥100 μM) internal Ca^{2+}, the VSD activation behaves in a mechanism-independent manner since all voltage sensors are in the same functional state (unliganded or saturated). However, the distinctive effects on $Q_C(V)$ curves at intermediate Ca^{2+} concentrations (1-10 μM) provide useful signatures to distinguish between these two mechanisms. Scheme I predicts two functional states of the VSD depending on occupancy status of the Ca^{2+} site (Ca^{2+} bound and unbound) such that the $Q_C(V)$ curve behavior is described by the fractional distribution of the unliganded and Ca^{2+}-saturated functional states like an all-or-none allosteric effect (***Figure 2C***; ***Figure 2—figure supplement 1B*** and Equation 4 in *Supplementary Information*). On the contrary, the Ca^{2+}-binding effect on the VSD activation according to the Scheme II is characterized by a five-component Boltzmann function (***Figure 2—figure supplement 1C*** and Equation 6 in *Supplementary Information*). Each component represents a single functional state determined by the number of Ca^{2+} bound to the channel (from 0 to 4). In such case, the $Q_C(V)$ curves resulting from a distribution of functional states behaves as an equivalent single Boltzmann leftward shifted by an incremental allosteric effect (from E to E^4) as the number of Ca^{2+} bound to the channel increases (***Figure 2D***).

To elucidate the mechanism by which Ca^{2+} and voltage sensors interact, we performed fits of the $Q_C(V)$ data using the two different models represented in the Scheme I and Scheme II (***Figure 3A,B***). The allosteric factor E that accounts for the coupling between the Ca^{2+}-binding sites and the voltage sensors was constrained to values calculated from the experimental data of the $Q_C(V)$ shift at the Ca^{2+} saturating conditions (100 μM) in relation to the same curve in the absence of Ca^{2+}. The z_J, J_0 and K_D parameters obtained during the fitting procedure of each model are very similar (***Figure 3C***). The fitted values of the affinity constant (K_D = 3 - 5 μM) agree with previous reports (Cox et al., 1997; Horrigan and Aldrich, 2002) although slightly smaller than those estimated on the closed conformation of the channel (K_D = 11 μM). However, we found that the fit with the Scheme II to the $Q_C(V)$ curves (***Figure 3B***) is better than the fit to the data using Scheme I (***Figure 3A***) as indicated by the Akaike model selection criteria (AIC) (Akaike, 1974). Moreover, Model II generates a V_H-$\log[Ca^{2+}]$ curve (solid line) that accounts for the dose-response V_H-$\log[Ca^{2+}]$ experimental data reasonable well (***Figure 3D***). Also, the behavior of $Q_C(V)$ curves at intermediate Ca^{2+} concentrations (1-10 μM) is qualitatively consistent with the phenotype exhibit by the Ca^{2+}-VSD scheme II (***Figure 2D*** **and** ***Figure 3B***). Thus, the experimental dose-dependent effect of Ca^{2+} on voltage sensor activation reveals that Ca^{2+}-binding to a single α-subunit of BK channels increases E-fold the equilibrium constant J that defines the equilibrium between resting and active conformations of the voltage sensors in all four subunits.

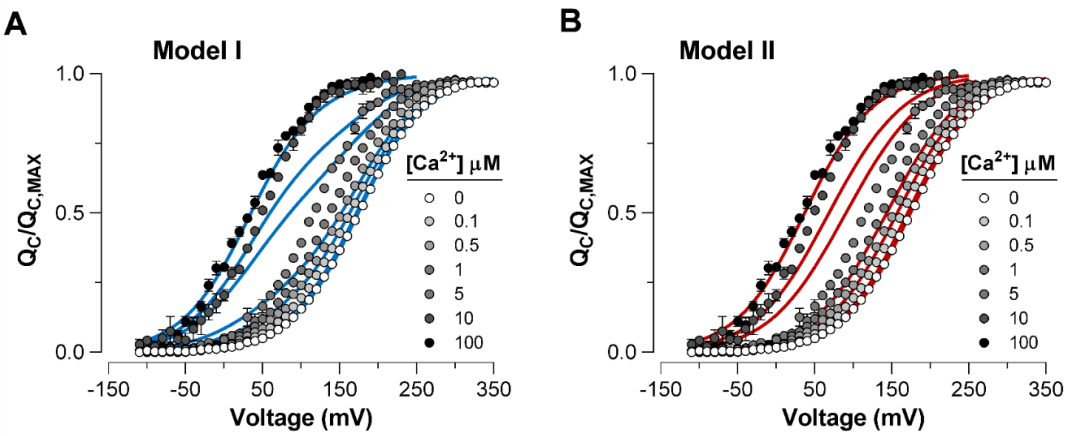

C

Model Parameters	Model I	Model II
z_J	0.58	0.58
J_0	0.018	0.018
E_M	26.4*	2.27*
K_D (µM)	3.9	4.3
AIC	-784.1	-946.5

* Fixed parameters in the model fitting. AIC values correspond to Akaike Information Criterion to select the best fit model.

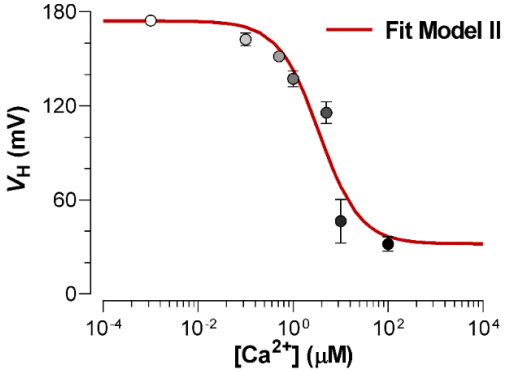

Figure 3. Dose-dependent effect of Ca^{2+} on voltage sensor activation is predicted by a Ca^{2+}-VSD interaction mechanism defining that Ca^{2+}-binding equally affects the VSD in all four α-subunits.

(**A-B**) The experimental $Q_C(V)$ data were fitted with the two possible allosteric interaction mechanisms between voltage and calcium sensors described by the Scheme I and Scheme II. The blue and red lines represent the global fits by Model I and Model II, respectively. The allosteric factor E (E_{M1} and E_{M2}) was constrained to the value obtained from the individual fitting of the $Q_C(V)/Q_{C,\ MAX}$ curves at 0 and 100 µM Ca^{2+} (experimental E (E_{exp}) equal to 26.4). The z_J, J_0 and K_D parameters were allowed to vary freely. (**C**) Parameters for the best fits of the $Q_C(V)$ data. Note that the allosteric factor E for Model I (E_{M1}) and Model II (E_{M2}) have different interpretations, being $E_{M2} = E_{exp}$ whereas $E_{M2} = \sqrt[4]{E_{exp}}$ given that the four voltage sensor will be altered in 2.3-fold (E_{M2} = 2.27) with each additional Ca^{2+} bound. Based on the Akaike Information Criterion (AIC), the best model fit to the $Q_C(V, [Ca^{2+}])$ data is achieved using the Ca^{2+}-VSD interaction scheme described by Model II. (**D**) The Ca^{2+}-dependence of V_H-$Q_C(V)$ curves are superimposed with the predicted V_H by Model II (red line).

High-affinity Ca^{2+}-binding sites in RCK1 and RCK2 domains contribute equally to the allosteric coupling between Ca^{2+} and voltage sensors. Under physiological conditions, the RCK1 and RCK2 high-affinity Ca^{2+}-binding sites are responsible by all calcium sensitivity of the activation of BK channel (Schreiber and Salkoff, 1997; Bao et al., 2002, 2004; Xia et al., 2002). However, distinct physiological roles of the RCK1 Ca^{2+}-sensor and Ca^{2+} bowl may be based in their functionally and structurally distinctive properties (Zeng et al., 2005; Sweet and Cox, 2008; Yang et al., 2010; Savalli et al., 2012; Tao et al., 2017). Below, we asked what the energetic contribution to VSD equilibrium is of the two high-affinity Ca^{2+}-binding sites contained in the RCK1 and RCK2 domains.

To elucidate the effect of each Ca^{2+}-sensor on the VSD activation we used mutations that selectively and separately abolish the function of the two differents RCK Ca^{2+}-sites. Disruption of the RCK1 Ca^{2+}-sensor by the double mutant D362A/D367A (Xia et al., 2002) reduces significantly (48%, $\Delta V_{H\ (D362A/D367A)}$ = -74.9 ± 4.7 mV) the leftward shifted of the $Q_C(V)$ curves at 100 μM Ca^{2+} compared with the wild-type (WT) BK channel (***Figure 4A,C***).We also examined the effect of the mutant M513I (Bao et al., 2002) which have been shown to eliminate the Ca^{2+} sensitivity derived from the RCK1 site (Bao et al., 2002, 2004; Zhang et al., 2010). In this mutant, the 100 μM Ca^{2+}-induced shift in V_H of VSD activation curve is also considerably smaller relative to WT (about 54%, $\Delta V_{H\ (M513I)}$ = -65.4 ± 2.6 mV) (***Figure 5***). Therefore, both mutations affect the Ca^{2+}-induced enhancement of activation of voltage sensor very similarly through the RCK1 site (***Figure 5C***), although their mechanisms action could be quite different. The M513 residue appears to participate in the stabilization of the proper conformation RCK1 Ca^{2+}-site whereas D367 is a key residue in the coordination of Ca^{2+} ion (Wu et al., 2010; Zhang et al., 2010; Tao et al., 2017). On the other hand, neutralization of the residues forming part of the Ca^{2+} bowl (Schreiber and Salkoff, 1997) (5D5A mutant, see *Methods*) on the RCK2 domain decreases the leftward shift of the $Q_C(V)$ curve when Ca^{2+} is increased to 100 μM by approximately 54% ($\Delta V_{H(5D5A)}$= -65.7 ± 4.7 mV).

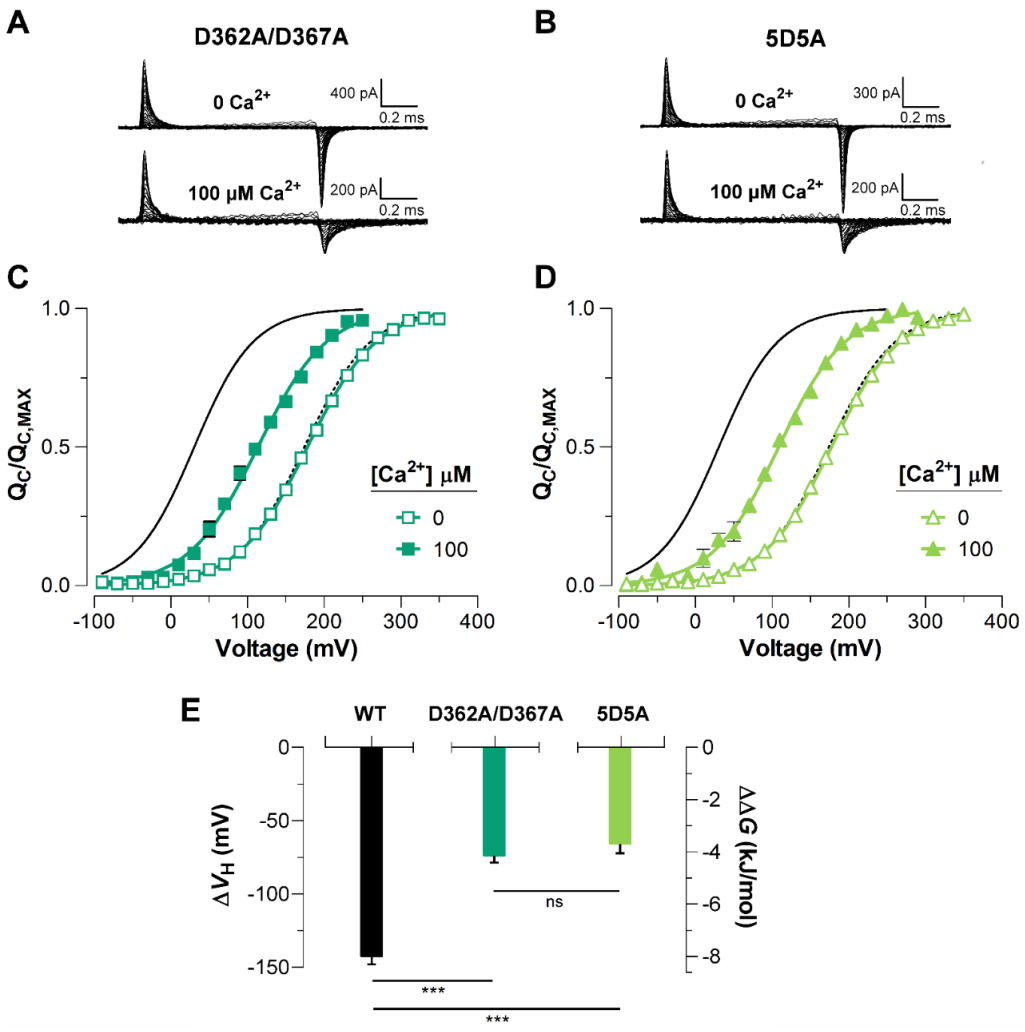

Figure 4. The high-affinity Ca^{2+}-binding sites contribute equally to allosteric coupling between calcium and voltage sensors in BK channels.

(**A-B**) Representative gating current (I_G) recordings at 0 and 100 µM of $[Ca^{2+}]_i$ for the RCK1 site mutant (D362A/D367A) and the RCK2 site mutant (5D5A), respectively. (**C-D**) Gating charge-voltage curves ($Q_C(V)$) were obtained at 0 Ca^{2+} (open symbols) and 100 µM Ca^{2+} (filled symbols) for D362A/D367A and 5D5A mutants, respectively. Boltzmann fitting to the experimental data (mean ± SEM) is indicated by solid lines ($V_{H(D362A/D367A)}$ = 178.0 ± 2.7 mV, n = 12 and $V_{H(5D5A)}$ = 176.4 ± 4.6 mV, n = 17 at "zero" Ca^{2+}; $V_{H(D362A/D367A)}$ = 104.2 ± 7.3 mV, n = 7 and $V_{H(5D5A)}$ = 110.8 ± 6.7 mV, n = 6 at 100 µM Ca^{2+}). For comparison, all $Q_C(V)$ plots include the Boltzmann fit of the $Q_C(V)$ curves for WT at 0 Ca^{2+} (dashed black line) and 100 µM Ca^{2+} (solid black line). (**e**) Quantification of the V_H shift (ΔV_H) in the $Q_C(V)$ curves and the free energy change ($\Delta\Delta G_V^{Ca}$) induced by 100 µM Ca^{2+}. The non-parametric *t*-test was used to evaluate statistical significances between WT BK channel and the RCK sites mutants (***p<0.001).

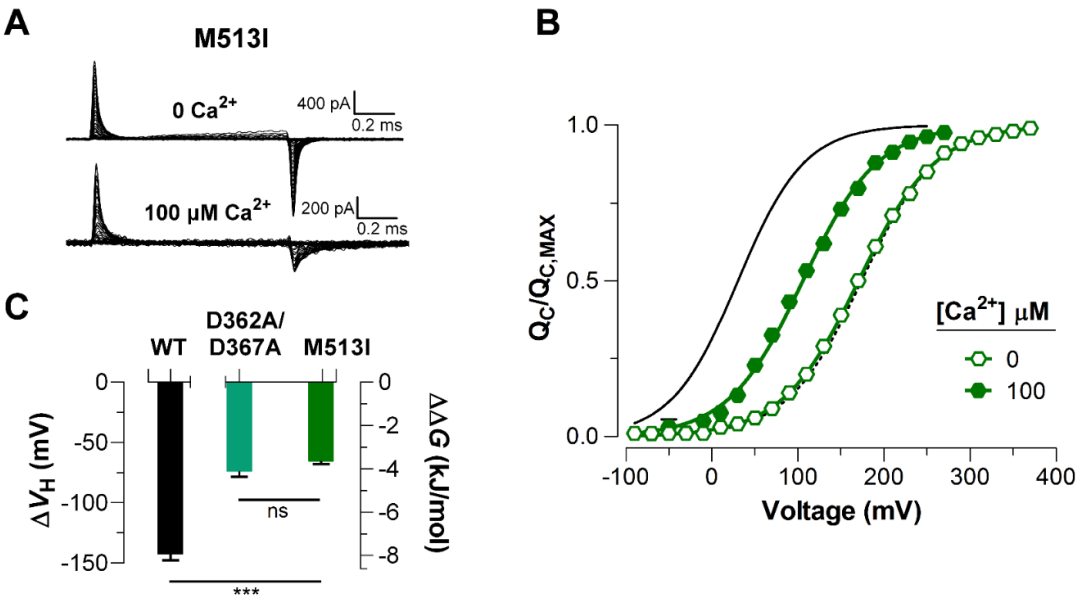

Figure 5. Mutations abolishing Ca^{2+}-sensing by the RCK1 binding-site reduce the Ca^{2+}-induced effect on voltage sensors activation similarly.

(**A**) Representative gating current (I_G) recordings at 0 and 100 µM of $[Ca^{2+}]_i$ for the RCK1 site mutant M513I. (**B**) Gating charge-voltage curves $Q_C(V)$ were obtained at 0 Ca^{2+} and 100 µM Ca^{2+} (open and filled symbols) for the M513I mutant. Boltzmann fitting to the experimental data (mean ± SEM) is indicated by solid lines ($V_{H(M513I)}$ = 170.4 ± 4.4 mV, n = 17 at "zero" Ca^{2+} and $V_{H(M513I)}$ = 105.0 ± 6.3 mV, n = 4 at 100 µM Ca^{2+}). For comparison, the $Q_C(V)$ plot includes the Boltzmann fit of the $Q_C(V)$ curves for WT at 0 Ca^{2+} and 100 µM Ca^{2+} (dashed and solid black line). (**C**) Quantification of the V_H (ΔV_H) shift in the $Q_C(V)$ curves and the free energy change induced by 100 µM Ca^{2+} ($\Delta\Delta G_V^{Ca}$). The non-parametric t-test was used to compare statistical significances between WT BK channel and the RCK1-site mutants (***p<0.001).

Surprisingly, the effect of Ca^{2+} binding on ΔV_{H} from each high-affinity Ca^{2+} site is roughly half relative to WT channels with both intact sites (***Figure 4E***). Therefore, both high-affinity Ca^{2+}-binding sites contribute equally to decrease the free energy necessary to activate the VSD. Thus, the change of free energy of the resting-active equilibrium of the voltage sensor in response to Ca^{2+}-binding at RCK2 site is ~ -4 kJ/mol ($\Delta\Delta G_V^{Ca}$(D362A/D367A) = -4.2 ± 0.3 kJ/mol and $\Delta\Delta G_V^{Ca}$(M513I) = -3.6 ± 0.5 kJ/mol) (***Figure 4C*** and ***Figure 5C***). In the same way, the occupation of the RCK1 Ca^{2+}-binding site decreases the free energy necessary to activate the VSD in -3.8 ± 0.4 kJ/mol ($\Delta\Delta G_V^{Ca}$(5D5A)). Remarkably, these findings reveal an additive effect of Ca^{2+}-binding to the RCK1 and Ca^{2+} bowl sites on the VSD activation which suggest independent allosteric pathways through which they exert their modulation on the VSD.

Taking these results into account, we expanded the Ca^{2+}-VSD interaction model described by Scheme II considering the energetic contribution of the two kinds of Ca^{2+} sensors on the VSD per α-subunit ($E_{WT} = E_{S1} * E_{S2}$) (***Figure 2—figure supplement 1E***). As described in the above model fittings, the allosteric factors E of each one RCK1 and RCK2 sites (E_{S1} and E_{S2}) were constrained to values equivalent to the Ca^{2+}-induced energetic perturbations of the voltage sensor equilibrium for the 5D5A and D362A/D367A mutants, respectively. However, the inclussion of the two Ca^{2+} sensors in the Ca^{2+}-VSD interaction model does not produce better fits to $Q_{\mathrm{C}}(V, [\mathrm{Ca}^{2+}])$ according to the AIC criteria (***Table 1*** and ***Figure 3B***), the estimated K_D parameters for each Ca^{2+}-binding sites (K_{D1} = 15.6 μM and K_{D2} = 1.9 μM) by the experimental data fitting agrees very well with the apparent Ca^{2+} affinities previously reported in the literature (Bao et al., 2002; Xia et al., 2002; Sweet and Cox, 2008). Interestingly, modest positive cooperativity (G = 2.6) between the two Ca^{2+}-binding sites located in the same α-subunit is required to achieve a good estimation of the K_D parameters (***Table 1***), where the Ca^{2+} bowl site has an affinity for Ca^{2+} about 8-fold greater than does the RCK1 Ca^{2+}-sensor.

Discussion

Recent insights into a major interplay between voltage- and Ca^{2+}-sensing modules in the BK channel are supported by functional and structural studies (Yuan et al., 2010; Savalli et al., 2012; Miranda et al., 2013, 2016, 2018; Carrasquel-Ursulaez et al., 2015; Hite et al., 2017; Tao et al., 2017; Zhang et al., 2017), offering a new perspective in our understanding of its multimodal gating mechanism. However, the CTD-VSD allosteric coupling as well its molecular nature has yet to be firmly established since their direct assessment is subject to great experimental challenges. Based on the functional independence of the distinct structural domains (PD, CTD, and VSD), the energetic relationship between the sensory modules can be directly defined comparing the voltage sensor equilibrium change at extreme Ca^{2+} stimulus conditions limiting the status of the Ca^{2+}-binding sites to two well-defined configurations: unliganded and saturated (Horrigan and Aldrich, 2002).

Using this approach, this work straightforwardly establishes that Ca^{2+}-binding to high-affinity sites make a significant and direct energetic contribution to the equilibrium of the resting-activated transition (R-A) of the VSD facilitating their activation (ΔV_{H} = -142.6 ± 4.5 mV and $\Delta\Delta G_V^{Ca}$ = -7.98 ± 0.27 kJ/mol). This result resolves a previous debate regarding to the magnitude of the Ca^{2+}-driven shift of the $Q_{\mathrm{C}}(V)$ curve, because it has been reported a similar leftward shift (ΔV_{H} = -140 mV and $\Delta\Delta G_V^{Ca}$ = -7.9 kJ/mol; at $[Ca^{2+}]_i$ = 100 μM) (Carrasquel-Ursulaez et al., 2015) and a smaller leftward shift (ΔV_{H} = -33 mV and $\Delta\Delta G_V^{Ca}$ = -1.9 kJ/mol; at $[Ca^{2+}]_i$ = 70 μM) (Horrigan and Aldrich, 2002) at saturating Ca^{2+} concentration. The reason for the contradictory findings is not clear to us; since we used a similar experimental approach. Even if we assumed that the calcium effect on

VSD is underestimated at 70 μM Ca^{2+} (Horrigan and Aldrich, 2002) compared to 100 μM as saturating condition of the binding sites, we observed a significative greater effect in Ca^{2+} concentrations (1, 5 and 10 μM, ***Figure 1C***) where less than 50% of the Ca^{2+} sensors are occupied (K_D = 11 μM (Cox et al., 1997; Horrigan and Aldrich, 2002)).

Fluorescence studies that optically track the motions of the voltage sensor or gating ring provide two lines of evidence that support these findings. First, conformational rearrangements of the voltage sensors detected using voltage-clamp fluorometry can be provoked by Ca^{2+}-binding to the high-affinity sites. The sudden rise of intracellular [Ca^{2+}] by UV flash induced-photolysis of caged Ca^{2+} prompts a leftward shift in both conductance-voltage ($G(V)$) and fluorescence-voltage ($F(V)$) relationships. These results suggest that functional activation of the gating ring is propagated to VSD leading to structural perturbations of voltages sensors, thereby favoring its active conformation (Savalli et al., 2012). Second, the structural rearrangement of gating ring in response to Ca^{2+} has a voltage dependence (Miranda et al., 2013, 2018) attributable to the voltage sensor operation. The origin of these voltage-dependent motions has been recently established via modifications on the voltage-sensing function of the BK channel using the patch-clamp fluorometry technique (Miranda et al., 2018). Both the charged residue mutations on the S4 transmembrane segment (R210, R213, and E219) and the co-expression of β1-subunit with BKα channel modify the conformational changes of the gating ring triggered by depolarization in correspondence to the observed $G(V)$ shift for these channel constructs. In contrast, perturbations of pore opening equilibrium like the F315A mutation or the assembly of BKα channel with γ1-subunit does not modify on the voltage-dependent reorganization of the gating ring (Miranda et al., 2018).

Mechanistically and in a channel opening-independent fashion, how does the CTD-VSD coupling occur? Taking into account the homotetrameric configuration of the BK channel, Horrigan and Aldrich (Horrigan and Aldrich, 2002) defined the general gating scheme of BK channel considering the simplest CTD-VSD interaction model in which voltage sensors and Ca^{2+}-binding sites solely interact within the same subunit. However, the VSD movement at non-saturating Ca^{2+} conditions which entail distinct functional states of the Ca^{2+} sites (unliganded and liganded), unveiled that the standard HA model can not explain the mechanistic interaction governing the allosteric coupling between the Ca^{2+} and voltage sensors. Given that Ca^{2+}-binding will influence only a fraction of voltage sensors, Scheme I would evidence $Q_{\mathrm{C}}(V)$ curves characteristic of an all-or-none model showing two well-distinguishable components Boltzmann that correspond to Ca^{2+}-affected and unaffected VSD fractions (***Figure 3A***). Conversely, an energetic effect of each Ca^{2+}-site on all the voltage sensors of the tetramer would lead to an equivalent functional status of each VSD, so that the $Q_{\mathrm{C}}(V)$ curves behaving in an incremental shifted fashion as increasing the fractional occupancy of the Ca^{2+} sites. The VSD and Ca^{2+} sites interacting in such a fashion (Scheme II) reproduce reasonably well the behavior of the Ca^{2+}-dependent gating charge movement observed in our experiments (***Figure 3B***). This concerted CTD-VSD communication may underlie a mechanism analogous to the mechanical strategy of interaction between the homooctameric ring of RCK domains and the pore module described for bacterial K^+ channels (Jiang et al., 2002; Ye et al., 2006; Lingle, 2007; Pau et al., 2011; Smith et al., 2012, 2013). Both in MthK and BK channels, the Ca^{2+}-site occupancy triggers a conformational change conveying to a symmetric overall rearrangement of the cytosolic tetrameric structure that finally is

propagated to the transmembrane regions (TMD) via C-linker and in the BK channel also via the protein-protein interfaces between the gating ring and the TMD (Jiang et al., 2002, 2003; Ye et al., 2006; Yuan et al., 2010, 2012; Pau et al., 2011; Smith et al., 2012; Tao et al., 2017). Consequently, we can speculate that each Ca^{2+}-binding event produces a gradual conformational expansion of the gating ring affecting the four voltage sensors in each step through the progressive perturbations within the protein-protein interfaces.

As mentioned above, the communication pathway through which the Ca^{2+}-driven conformational changes are propagated to the voltage sensors appears to critically reside on the CTD-VSD interface that involves non-covalent interactions between RCK1 N-lobe and S0-S4 transmembrane segments (Yang et al., 2007, 2008, 2010; Sun et al., 2013; Hite et al., 2017; Tao et al., 2017). Scanning mutagenesis of RCK1-N terminal subdomain indicated that residues on the βA-αC region are involved into the allosteric connection of the Ca^{2+}-dependent activation mediated by RCK1 site occupancy but not to the Ca^{2+} bowl (Yang et al., 2010). In line with this study, the selective activation of the RCK1 domain was identified to be responsible for the Ca^{2+}-induced VSD rearrangement (Savalli et al., 2012) and the voltage dependence of the Ca^{2+}-driven motions of gating ring (Miranda et al., 2016, 2018), suggesting that CTD-VSD allosteric coupling is primarily determined by the RCK1 site. However, our results are inconsistent with this picture. The constructs D362A/D367A and 5D5A (D894A-D898A) selectively impaired the Ca^{2+}-sensitivity of the RCK1- and RCK2-sensors, respectively, by neutralization of residues that are involved in contributing to Ca^{2+}-coordination (Zhang et al., 2010; Tao et al., 2017). Comparing the fast gating charge movement at 0 Ca^{2+} and saturating Ca^{2+} conditions reflects that the energetic effect of Ca^{2+}-binding on voltage sensor equilibrium is practically identical (~ -

4 kJ/mol) for either the D362A/D367A mutations or 5D5A mutations (***Figure 4***). Thus, our findings establish that the RCK2-driven contribution to CTD-VSD energetic coupling is quite similar to the RCK1-driven contribution. The functional role of the RCK2-sensor on Ca^{2+}-sensitivity of VSD activation was further corroborated using the M513I mutation (***Figure 5***). This point mutation hinders the Ca^{2+}-dependent activation associated with the RCK1-sensor presumably by disrupting the structural integrity of the binding site and the transduction via through the βA-αC region (Zhang et al., 2010). Thus, another residue involved in the BK Ca^{2+}-dependent activation mediated by the RCK1 Ca^{2+}-binding site but not forming part of the site itself decreases the $Q_{\mathrm{C}}(V)$ leftward shift almost in the same amount as it does the D362A/D367A mutant.

Interestingly, beyond the energetic contribution of each RCK site to the voltage sensor equilibrium is the same, its addition mimics the VSD Ca^{2+}-sensitivity of the fully occupied sites. These findings remind us of early reports showing that each RCK site mutant shifts the Ca^{2+}-dependent $G(V)$ by approximately half relative to WT channels (Bao et al., 2002; Xia et al., 2002). Our results suggest an autonomy of the two RCK-sensors indicating independent allosteric pathways through which they exert their modulation on the VSD but does not discard some cooperativity effect between them. Indeed, various lines of evidence indicate albeit modest a cooperativity between the two high-affinity Ca^{2+}-binding sites although their nature is still unclear (Qian et al., 2006; Sweet and Cox, 2008; Savalli et al., 2012). Intra and intersubunit structural connectivity support the putative cooperative interactions between the Ca^{2+} sensors at the gating ring (Yuan et al., 2012; Hite et al., 2017). Actually, a recently functional study of the intrasubunit connections between the RCK1 site and Ca^{2+} bowl (R514-Y904/E902 interactions) has shown that such

connections are potential candidates of the structural determinants underlying to a cooperative mechanism between the RCK1- and RCK2-sensor involving either to preserve the integrity of RCK1 Ca^{2+}-binding site or the allosteric propagation pathway towards transmembrane domains (Kshatri et al., 2018). On the basis of the cryo-EM structure of *Aplysia californica* BK channel, Hite *et al*. (Hite et al., 2017) proposed that there should be a positive cooperativity of the Ca^{2+}-binding at RCK1 site and Ca^{2+} bowl since the Ca^{2+}-induced conformational change of the RCK1-N lobes from closed to open configuration depends on functional state (unliganded and liganded) of both RCK sites. Our analysis based on the CTD-VSD interaction model predicted a small and positive cooperative relation (G = 2.6) among the two high-affinity Ca^{2+} sites within the same α-subunit, which has been suggested by an earlier study (Qian et al., 2006). It is noteworthy that K_D parameters achieved for each Ca^{2+}-binding sites (K_{D1} = 15.6 μM and K_{D2} = 1.9 μM) by the experimental data fitting agrees very well with the apparent Ca^{2+} affinities previously reported in the literature (Bao et al., 2002; Xia et al., 2002; Sweet and Cox, 2008). Together, all this new information recapitulate a more relevant functional role of the cooperative interactions between RCK sensors within the same subunit on Ca^{2+}-dependent activation of the channel (Qian et al., 2006).

In conclusion, our results depict a remarkable, and direct energetic direct interplay between the specialized sensory modules (VSD and CTD). Our findings together with the emerging structural-functional information establish a new paradigm about how the stimuli integration (depolarization and intracellular Ca^{2+}) modulates the BK channel activation and its relevance within a physiological context. Notable and unexpected is the equivalent role of the distinct ligand-binding sites at the cytosolic domain to the allosteric

regulation on voltage sensing. Additional studies to discern the molecular bases underlying in the Ca^{2+} and voltage propagation pathways and the cooperative interactions of the RCK1 and RCK2 regulatory domains may provide new clues about the dual gating mechanism of BK channel.

Methods

Channel Expression.

Xenopus laevis oocytes were used as a heterologous system to express BK channels. The cDNA coding for the human BK α-subunit (U11058) was provided by L. Toro (University of California, Los Angeles, CA). The cDNA coding for independent mutants of each two high-affinity Ca^{2+} site from BK channel, the double mutant D362A/D367A (Xia et al., 2002) and the mutant M513I (Bao et al., 2002) in the RCK1 Ca^{2+}-binding site and the mutant 5D5A (Schreiber and Salkoff, 1997) (D894A/D895A/D896A/D897A/D898A) in the RCK2 Ca^{2+}-binding site or calcium bowl, were kindly provided by M. Holmgren (National Institutes of Health, Bethesda, MD). The cRNA was prepared by using mMESSAGE mMACHINE (Ambion) for *in vitro* transcription. *Xenopus laevis* oocytes were injected with 50 ng of cRNA and incubated in an ND96 solution (in mM: 96 NaCl, 2 KCl, 1.8 $CaCl_2$, 1 $MgCl_2$, 5 HEPES, pH 7.4) at 18°C for 4–8 days before electrophysiological recordings.

Electrophysiological recordings.

All recordings were made by using the patch-clamp technique in the inside-out configuration. Data were acquired with an Axopatch 200B (Molecular Devices) amplifier and the Clampex 10 (Molecular Devices) acquisition software. Gating current (I_G) records were elicited by 1-ms voltage steps from −90 to 350 mV in increments of 10 mV. Both the voltage command and current output were filtered at 20 kHz with 8-pole Bessel low-pass filter (Frequency Devices). Current signals were sampled with a 16-bit A/D converter (Digidata 1550B; Molecular Devices), using a sampling rate of 500 kHz. Linear membrane capacitance and leak subtraction were performed based on a P/4 protocol (Armstrong and Bezanilla, 1974).

Borosilicate capillary glasses (1B150F-4, World Precision Instruments) were pulled in a horizontal pipette puller (Sutter Instruments). After fire-polished, pipette resistance was 0.5-1 MΩ. The external (pipette) solution contained (in mM): 110 tetraethylammonium (TEA)-$MeSO_3$, 10 HEPES, 2 $MgCl_2$; pH was adjusted to 7.0. The internal solution (bath) contained (in mM): N-methyl-D-

glucamine (NMDG)-$MeSO_3$, 10 HEPES, and 5 EGTA for "zero Ca^{2+}" solution (~0.8 nM, based on the presence of ~10 μM contaminant [Ca^{2+}] (Cui et al., 1997). For test solutions at different Ca^{2+} concentrations (0.1-100 μM), $CaCl_2$ was added to reach the desired free [Ca^{2+}], and 5 mM EGTA (0.1-0.5 μM) or HEDTA (1-10 μM) was used as calcium buffer. No Ca^{2+} chelator was used in 100 μM free Ca^{2+} solutions. Free calcium concentration was estimated using the WinMaxChelator Software and checked with a Ca^{2+}-electrode (Hanna Instruments). All experiments were performed at room temperature (20-22 °C). To measure I_G at different Ca^{2+} concentrations in the same oocyte, the patch was excised and washed with an appropriate internal solution at least 10 times the chamber volume.

Data Analysis.

All data analysis was performed using Clampfit 10 (Molecular Devices), Matlab (MathWorks) and Excel 2007 (Microsoft). The first 50-100 μs of the ON-gating currents were fitted to a single exponential function and the area under the curve was integrated to obtain the charge displaced between closed states (Q_{C}) (Horrigan and Aldrich, 1999, 2002; Contreras et al., 2012; Carrasquel-Ursulaez et al., 2015). $Q_{\mathrm{C}}(V)$ data for each [Ca^{2+}]$_i$ were fitted using a Boltzmann function: $Q_{\mathrm{C}}(V) = \frac{Q_{\mathrm{C,\ MAX}}}{1+e^{\left(\frac{-z_Q F(V-V_{\mathrm{H}})}{RT}\right)}}$, where $Q_{\mathrm{C,\ MAX}}$ is the maximum charge, z_Q is the voltage dependency of activation, V_{H} is the half-activation voltage, T is the absolute temperature (typically 295 K), F is the Faraday's constant, and R is the universal gas constant. $Q_{\mathrm{C,\ MAX}}$, V_{H}, and z_Q were determined using least square minimization. $Q_{\mathrm{C}}(V)$ curves were aligned by shifting them along the voltage axis by the mean $\Delta V = (\langle V_{\mathrm{H}} \rangle - V_{\mathrm{H}})$ to generate a mean curve that did not alter the voltage dependence (Horrigan and Aldrich, 1999). All error estimates are SEM.

The Ca^{2+}-induced effect on VSD activation was quantified as the V_{H} shift relative to "zero" Ca^{2+} condition: $\Delta V_{\mathrm{H}} = V_{\mathrm{H}\left([\mathrm{Ca}^{2+}]_i\right)} - V_{\mathrm{H}\left(0\,[\mathrm{Ca}^{2+}]_i\right)}$. For wild-type (WT) BK channel and the RCK Ca^{2+}-sensor mutants (D362A/D367A, M513I and 5D5A), the energetic contribution of Ca^{2+}-binding on resting-active (R-A) equilibrium of the voltage sensor was calculated as changes in Gibbs free energy of

VSD activation induced by 100 μM Ca^{2+}: $\Delta\Delta G_V^{Ca} = F\left(z_{Q\left(100\ \mu M\ [Ca^{2+}]_i\right)} V_{H\left(100\ \mu M\ [Ca^{2+}]_i\right)} - z_{Q\left(0\ [Ca^{2+}]_i\right)} V_{H\left(0\ [Ca^{2+}]_i\right)}\right)$.

Model fitting.

We fit the $Q_C(V, [Ca^{2+}])$ experimental data using two distinct interaction mechanism between Ca^{2+}-binding sites and voltage sensor (see Scheme I and Scheme II in the ***Figure 2A,B***) within the framework of Horrigan-Aldrich (HA) general allosteric model (Horrigan and Aldrich, 2002). Assumptions and considerations for the equations that describe each one of the Ca^{2+}-VSD interaction schemes are given in the *Supplementary Information*. In terms of the HA allosteric mechanisms, the voltage sensor R-A equilibrium is defined by the equilibrium constant J according to the relation $J = e^{\frac{z_J F(V - V_H)}{RT}} = J_0 e^{\frac{z_J FV}{RT}}$, where J_0 is the zero voltage equilibrium constant and z_J the gating charges displacement per voltage sensor. In this fashion, the fraction of the total charge displaced essentially between closed states, $\left(Q_C(V)/Q_{C,\ MAX}\right)$ in the absence of calcium can be written as: $Q_C(V)/Q_{C,\ MAX}\ (Ca^{2+} \ll K_D) = \frac{1}{1+J^{-1}}$, where K_D is the dissociation constant of the high-affinity calcium-binding site with all voltage sensors at rest and the channel closed. In the presence of saturating Ca^{2+} (100 μM), the equilibrium of the R-A transition J becomes amplified by the allosteric factor E, which defines the coupling between Ca^{2+}-binding sites and voltage sensors, being $Q_C(V)/Q_{C,\ MAX}\ (Ca^{2+} \gg K_D) = \frac{1}{1+(JE)^{-1}}$ and $JE = J_0 e^{\frac{RT\ln(E) + z_J FV}{RT}}$. The $Q_C(V)/Q_{C,\ MAX}$ measured in the presence of high $[Ca^{2+}]$ and "zero Ca^{2+}" condition at the same voltage (so that J be canceled out) but in the limit where voltage where $J^{-1} \gg 1$ is:

$$\frac{Q_C(V)/Q_{C,\ MAX}\ (Ca^{2+} \gg K_D)}{Q_C(V)/Q_{C,\ MAX}\ (Ca^{2+} \ll K_D)}_{(\lim J^{-1} \gg 1)} = \frac{JE}{J} = E$$

Thus, the Gibbs free energy perturbation of the voltage sensor R-A equilibrium when the high-affinity binding sites are approximately 100% occupied by Ca^{2+} (100 μM) is a straightforward measure of the allosteric factor E: $E = e^{-\Delta\Delta G_V^{Ca}/RT}$.

Based on these conditions, the allosteric parameter E values were calculated and introduced in each of the two Ca^{2+}-VSD interaction models as a fixed parameter. Once E was obtained, the families of $Q_C(V, [Ca^{2+}])$ curves were simultaneously fitted to the model equations (Equation 3 and Equation 6) (see *Supplementary information*) by minimizing least-squares estimating the z_J, J_0 and K_D parameters for each model. To select the better Ca^{2+}-VSD interaction scheme that describes the experimental data, the model fits were compared according to their Akaike Information Criterion (AIC) (Akaike, 1974) values, calculated as $\mathrm{AIC} = 2p - 2\ln(L)$, where p is the number of free parameters and $\ln(L)$ is the maximum log-likelihood of the model. The best model fitting is that achieving the lowest AIC values. Minimum AIC values were used as model selection criteria.

The best model fit of the Ca^{2+}-VSD interaction scheme was extended including two high-affinity Ca^{2+}-binding sites per α-subunit (***Figure 2—figure supplement 2D,E***). The contribution of each Ca^{2+}-binding site to the free energy of the voltage sensor equilibrium may be split in two, such as $E = E_{S1} * E_{S2} = e^{-\left(\Delta\Delta G_V^{Ca}(S1) + \Delta\Delta G_V^{Ca}(S2)\right)/RT}$, where E_{S1} and E_{S2} are the allosteric factor E for the RCK1 and RCK2 sites. Thus, for the global fit of the $Q_C(V, [Ca^{2+}])$ curves, we constrained the allosteric parameter E_{S1} and E_{S2} obtained experimentally for the RCK2 Ca^{2+}-sensor mutant (5D5A) and RCK1 Ca^{2+}-sensor mutant (D362A/D367A), respectively, as described above. The rest of the parameters z_J, J_0, K_{D1}, K_{D2}, and G, where K_{D1} and K_{D2} are the dissociation constants of the RCK1 and RCK2 sites and G is a cooperativity factor between the two sites within the same α-subunit of the BK channel, were allowed to vary freely.

References

Akaike H. 1974. A new look at the statistical model identification. *IEEE Trans Automat Contr* **19**:716–723. DOI:10.1109/TAC.1974.1100705

Armstrong CM, Bezanilla F. 1974. Charge movement associated with the opening and closing of the activation gates of the Na channels. *J Gen Physiol* **63**:533–552. DOI:10.1085/jgp.63.5.533

Bao L, Rapin AM, Holmstrand EC, Cox DH. 2002. Elimination of the BKCa Channel's High-Affinity Ca2+ Sensitivity. *J Gen Physiol* **120**:173–189. DOI:10.1085/jgp.20028627

Bao L, Kaldany C, Holmstrand EC, Cox DH. 2004. Mapping the BK Ca Channel's "Ca2+ Bowl." *J Gen Physiol* **123**:475–489. DOI:10.1085/jgp.200409052

Carrasquel-Ursulaez W, Contreras GF, Sepúlveda R V, Aguayo D, González-Nilo F, González C, Latorre R. 2015. Hydrophobic interaction between contiguous residues in the S6 transmembrane segment acts as a stimuli integration node in the BK channel. *J Gen Physiol* **145**:61–74. DOI:10.1085/jgp.201411194

Contreras GF, Neely A, Alvarez O, Gonzalez C, Latorre R. 2012. Modulation of BK channel voltage gating by different auxiliary β subunits. *Proc Natl Acad Sci USA* **109**:18991–6. DOI:10.1073/pnas.1216953109

Cox DH, Cui J, Aldrich RW. 1997. Allosteric gating of a large conductance Ca-activated K+ channel. *J Gen Physiol* **110**:257–281. DOI:10.1085/jgp.110.3.257

Cui J, Cox DH, Aldrich RW. 1997. Intrinsic voltage dependence and Ca2+ regulation of mslo large conductance Ca-activated K+ channels. *J Gen Physiol* **109**:647–673. DOI:10.1085/jgp.109.5.647

Cui J, Aldrich RW. 2000. Allosteric Linkage between Voltage and Ca2+-Dependent Activation of BK-Type mslo1 K+ Channels. *Biochemistry* **39**:15612–15619. DOI:10.1021/bi001509+

Hite RK, Tao X, MacKinnon R. 2017. Structural basis for gating the high-conductance Ca2+-

activated K+ channel. *Nature* **541**:52–57. DOI:10.1038/nature20775

Horrigan FT, Cui J, Aldrich RW. 1999. Allosteric voltage gating of potassium channels I. Mslo ionic currents in the absence of Ca2+. *J Gen Physiol* **114**:277–304.

Horrigan FT, Aldrich RW. 1999. Allosteric voltage gating of potassium channels II. Mslo channel gating charge movement in the absence of Ca2+. *J Gen Physiol* **114**:305–336. DOI:10.1085/jgp.114.2.305

Horrigan FT, Aldrich RW. 2002. Coupling between voltage sensor activation, Ca2+ binding and channel opening in large conductance (BK) potassium channels. *J Gen Physiol* **120**:267–305. DOI:10.1085/jgp.20028605

Hou P, Xiao F, Liu H, Yuchi M, Zhang G, Wu Y, Wang W, Zeng W, Ding M, Cui J, Wu Z, Wang L-Y, Ding J. 2016. Extrapolating microdomain Ca2+ dynamics using BK channels as a Ca2+ sensor. *Sci Rep* **6**:17343. DOI:10.1038/srep17343

Jiang Y, Lee A, Chen J, Cadene M, Chait BT, Mackinnon R. 2002. Crystal structure and mechanism of a calcium-gated potassium channel 515–522.

Jiang Y, Ruta V, Chen J, Lee A, Mackinnon R. 2003. The principle of gating charge movement in a voltage-dependent K channel. *Nature* **423**:42–48.

Kshatri AS, Gonzalez-Hernandez AJ, Giraldez T. 2018. Functional validation of Ca2+-binding residues from the crystal structure of the BK ion channel. *BBA - Biomembr* **1860**:943–952. DOI:10.1016/j.bbamem.2017.09.023

Latorre R, Castillo K, Carrasquel-Ursulaez W, Sepulveda R V, Gonzalez-Nilo F, Gonzalez C, Alvarez O. 2017. Molecular Determinants of BK Channel Functional Diversity and Functioning. *Physiol Rev* **97**:39–87. DOI:10.1152/physrev.00001.2016

Latorre R, Vergara C, Hidalgo C. 1982. Reconstitution in planar lipid bilayers of a Ca2+-dependent K+ channel from transverse tubule membranes isolated from rabbit skeletal muscle. *Proc Natl*

Acad Sci USA **79**:805–809. DOI:10.1073/pnas.79.3.805

Lingle CJ. 2007. Gating Rings Formed by RCK Domains: Keys to Gate Opening. *J Gen Physiol* **129**:101–107. DOI:10.1085/jgp.200709739

Marty A. 1981. Ca-dependent K channels with large unitary conductance in chromaffin cell membranes. *Nature* **291**:497–500.

Miranda P, Contreras JE, Plested AJR, Sigworth FJ, Holmgren M, Giraldez T. 2013. State-dependent FRET reports calcium- and voltage-dependent gating-ring motions in BK channels. *Proc Natl Acad Sci USA* **110**:5217–5222. DOI:10.1073/pnas.1219611110

Miranda P, Holmgren M, Giraldez T. 2018. Voltage-dependent dynamics of the BK channel cytosolic gating ring are coupled to the membrane-embedded voltage sensor. *Elife* **7**:e40664. DOI:10.7554/eLife.40664

Miranda P, Giraldez T, Holmgren M. 2016. Interactions of divalent cations with calcium binding sites of BK channels reveal independent motions within the gating ring. *Proc Natl Acad Sci USA* **113**:14055–14060. DOI:10.1073/pnas.1611415113

Oberhauser A, Alvarez O, Latorre R. 1988. Activation by divalent cations of a Ca2+-activated K+ channel from skeletal muscle membrane. *J Gen Physiol* **92**:67–86. DOI:10.1085/jgp.92.1.67

Pallotta BS, Magleby KL, Barrett JN. 1981. Single channel recordings of Ca2+-activated K+ currents in rat muscle cell culture. *Nature* **293**:471–474.

Pau VPT, Smith FJ, Taylor AB, Parfenova L V, Samakai E, Callaghan MM, Abarca-Heidemann K, Hart PJ, Rothberg BS. 2011. Structure and function of multiple Ca2+-binding sites in a K+ channel regulator of K+ conductance (RCK) domain. *Proc Natl Acad Sci USA* **108**:17684–17689. DOI:10.1073/pnas.1107229108

Qian X, Niu X, Magleby KL. 2006. Intra- and Intersubunit Cooperativity in Activation of BK Channels by Ca2+. *J Gen Physiol* **128**:389–404. DOI:10.1085/jgp.200609486

Rothberg BS, Magleby KL. 1999. Gating kinetics of single large-conductance Ca2+-activated K+ channels in high Ca2+ suggest a two-tiered allosteric gating mechanism. *J Gen Physiol* **114**:93–124. DOI:10.1085/jgp.114.1.93

Rothberg BS, Magleby KL. 2000. Voltage and Ca2+ activation of single large-conductance Ca2+-activated K+ channels described by a two-tiered allosteric gating mechanism. *J Gen Physiol* **116**:75–99. DOI:10.1085/jgp.116.1.75

Savalli N, Pantazis A, Yusifov T, Sigg D, Olcese R. 2012. The contribution of RCK domains to human BK channel allosteric activation. *J Biol Chem* **287**:21741–21750. DOI:10.1074/jbc.M112.346171

Schreiber M, Salkoff L. 1997. A novel calcium-sensing domain in the BK channel. *Biophys J* **73**:1355–1363. DOI:10.1016/S0006-3495(97)78168-2

Shen KZ, Lagrutta A, Davies NW, Standen NB, Adelman JP, North RA. 1994. Tetraethylammonium block of Slowpoke calcium-activated potassium channels expressed in Xenopus oocytes: evidence for tetrameric channel formation. *Pflugers Arch* **426**:440–445.

Smith FJ, Pau VPT, Cingolani G, Rothberg BS. 2012. Crystal structure of a Ba2+-bound gating ring reveals elementary steps in RCK domain activation. *Structure* **20**:2038–2047. DOI:10.1016/j.str.2012.09.014

Smith FJ, Pau VPT, Cingolani G, Rothberg BS. 2013. Structural basis of allosteric interactions among Ca2+-binding sites in a K+channel RCK domain. *Nat Commun* **4**:1–10. DOI:10.1038/ncomms3621

Stefani E, Ottolia M, Noceti F, Olcese R, Wallner M, Latorre R. 1997. Voltage-controlled gating in a large conductance Ca2+ sensitive K+ channel (hslo). *Proc Natl Acad Sci USA* **94**:5427–5431.

Sun X, Shi J, Delaloye K, Yang X, Yang H, Zhang G, Cui J. 2013. The Interface between

Membrane-Spanning and Cytosolic Domains in Ca2+-Dependent K+ Channels Is Involved in Subunit Modulation of Gating. *J Neurosci* **33**:11253–11261. DOI:10.1523/JNEUROSCI.0620-13.2013

Sweet T-B, Cox DH. 2008. Measurements of the BKCa channel's high-affinity Ca2+ binding constants: effects of membrane voltage. *J Gen Physiol* **132**:491–505. DOI:10.1085/jgp.200810094

Tao X, Hite RK, MacKinnon R. 2017. Cryo-EM structure of the open high-conductance Ca2+-activated K+ channel. *Nature* **541**:46–51. DOI:10.1038/nature20608

Wu Y, Yang Y, Ye S, Jiang Y. 2010. Structure of the gating ring from the human large-conductance Ca2+-gated K+ channel. *Nature* **466**:393–397. DOI:10.1038/nature09252

Xia X-M, Zeng X, Lingle CJ. 2002. Multiple regulatory sites in large-conductance calcium-activated potassium channels. *Nature* **418**:880–884. DOI:10.1038/nature00956

Yang H, Hu L, Shi J, Delaloye K, Horrigan FT, Cui J. 2007. Mg2+ mediates interaction between the voltage sensor and cytosolic domain to activate BK channels. *Proc Natl Acad Sci USA* **104**:18270–5. DOI:10.1073/pnas.0705873104

Yang H, Shi J, Zhang G, Yang J, Delaloye K, Cui J. 2008. Activation of Slo1 BK channels by Mg2+ coordinated between the voltage sensor and RCK1 domains. *Nat Struct Mol Biol* **15**:1152–1159. DOI:10.1038/nsmb.1507

Yang H, Zhang G, Cui J. 2015. BK channels: multiple sensors, one activation gate. *Front Physiol* **6**:1–16. DOI:10.3389/fphys.2015.00029

Yang J, Krishnamoorthy G, Saxena A, Zhang G, Shi J, Yang H, Delaloye K, Sept D, Cui J. 2010. An Epilepsy/Dyskinesia-Associated Mutation Enhances BK Channel Activation by Potentiating Ca2+ Sensing. *Neuron* **66**:871–883. DOI:10.1016/j.neuron.2010.05.009

Ye S, Li Y, Chen L, Jiang Y. 2006. Crystal Structures of a Ligand-free MthK Gating Ring: Insights

into the Ligand Gating Mechanism of K+ Channels. *Cell* **126**:1161–1173. DOI:10.1016/j.cell.2006.08.029

Yuan P, Leonetti MD, Pico AR, Hsiung Y, MacKinnon R. 2010. Structure of the Human BK Channel Ca2+-Activation Apparatus at 3.0 Å Resolution. *Science (80-)* **329**:182–186. DOI:10.1126/science.1190414.Structure

Yuan P, Leonetti MD, Hsiung Y, MacKinnon R. 2012. Open structure of the Ca2+ gating ring in the high-conductance Ca2+-activated K+ channel. *Nature* **481**:94–97. DOI:10.1038/nature10670

Zeng X-H, Xia X-M, Lingle CJ. 2005. Divalent Cation Sensitivity of BK Channel Activation Supports the Existence of Three Distinct Binding Sites. *J Gen Physiol* **125**:273–286. DOI:10.1085/jgp.200409239

Zhang G, Huang S-Y, Yang J, Shi J, Yang X, Moller A, Zou X, Cui J. 2010. Ion sensing in the RCK1 domain of BK channels. *Proc Natl Acad Sci USA* **107**:18700–18705. DOI:10.1073/pnas.1010124107

Zhang G, Geng Y, Jin Y, Shi J, McFarland K, Magleby KL, Salkoff L, Cui J. 2017. Deletion of cytosolic gating ring decreases gate and voltage sensor coupling in BK channels. *J Gen Physiol* **149**:373–387.

Zhou Y, Zeng X-H, Lingle CJ. 2012. Barium ions selectively activate BK channels via the Ca2+-bowl site. *Proc Natl Acad Sci USA* **109**:11413–11418. DOI:10.1073/pnas.1204444109

Zhou Y, Yang H, Cui J, Lingle CJ. 2017. Threading the biophysics of mammalian Slo1 channels onto structures of an invertebrate Slo1 channel. *J Gen Physiol* **149**:985–1007. DOI:10.1085/jgp.201711845

Acknowledgments

We thank Mrs. Luisa Soto (University of Valparaiso) for excellent technical assistance. This research was supported by FONDECYT Grant No. 1150273 and AFOSR No. FA9550-16-1- 0384 to R.L.; CONICYT-PFCHA Doctoral fellowships to Y.L.C.; FONDECYT Grant No. 1180999 to K.C. The Centro Interdisciplinario de Neurociencia de Valparaiso is a Millennium Institute supported by the Millennium Scientific Initiative of the Chilean Ministry of Economy, Development, and Tourism (P029-022-F).

Competing interests

The authors declare no competing financial interests.

Supplementary Information

Assumptions and model predictions. We assume that the four voltage sensors act independently transiting between two states, resting (R) and active (A), governed by the voltage-dependent equilibrium constant $\boldsymbol{J}$. The R–A equilibrium is displaced toward the active state by membrane depolarization generating a fast gating charge movement ($\boldsymbol{Q_C}$) before channels opening. Additionally, the Ca^{2+}-binding to high-affinity sites shifts the voltage sensor equilibrium toward their active configuration through an allosteric coupling described by the factor $\boldsymbol{E}$ (***Figure 2—figure supplement 1A***). By assuming the simplified standard model for the BK channels (Horrigan and Aldrich, 2002), where each α-subunit has a single Ca^{2+}-binding site, we established the possible states and their connections through which each voltage sensor transit in presence of Ca^{2+} (***Figure 2—figure supplement 1B;C***) following the CTD-VSD interaction mechanisms described by the Scheme I and Scheme II (***Figure 2A,B***).

For Scheme I, in which Ca^{2+}-binding sites and voltage sensors can only interact within the same α-subunit, the activation of each VSD can occur through the R_0-A_0 or R_1-A_1 transitions according to the functional state of the Ca^{2+} site (unbound or Ca^{2+} bound). The equilibrium of such transitions is governed by J or JE_{M1}, respectively (***Figure 2—figure supplement 2B***). In the case of Scheme II, in which binding of Ca^{2+} to a single α-subunit affects the four voltage sensors equally, the R-A equilibrium of each VSD would be affected by the number of Ca^{2+} bound in the channel (0-4) depicted in the model (Model II) as five possible R-A transitions. According to this model, the J constant increase E_{M2}-fold for each occupied Ca^{2+} site (***Figure 2—figure supplement 1C***). For both schemes, the horizontal transitions R-R and A-A represent the Ca^{2+}-binding equilibrium (K or KE) when the VSD is in the resting or active conformation, respectively. The K equilibrium constant is defined as the bound/unbound probability ratio for each Ca^{2+}-binding site and depends on Ca^{2+} concentration ($[Ca^{2+}]$) and the Ca^{2+} dissociation constant (K_D): $K = [Ca^{2+}]/K_D$.

Here, we assume that the voltage sensor movement at ON-gating currents is in equilibrium relative to the binding of Ca^{2+}. The assumption is reasonable since the Ca^{2+}-binding rate constant estimated for BK channel is about $10^8\ M^{-1}s^{-1}$ (Hou et al., 2016) implying that at 10 μM internal Ca^{2+} the association time constant is 1 ms. Thus, Ca^{2+} binding at this Ca^{2+} concentration proceeds at a pace about 33-fold slower than the voltage sensor movement (~30 μs). Based on this consideration, the R-A transitions in the models would be predominant transitions whose proportion will be determined by the [Ca^{2+}] and K_D. Therefore, predictions of the $Q_{\mathrm{C}}(V)$ curves at different Ca^{2+} concentrations for Model I and Model II were based on a given fractional occupancy of Ca^{2+} sites established by the probability of Ca^{2+} bound (b) and unbound $(1-b)$ for each Ca^{2+}-sensor, and the energetic contribution to VSD equilibrium.

Simulations of the $Q_{\mathrm{C}}(V)$ curves using the Scheme I (Model I) were obtained using the equation

$$\frac{Q_{\mathrm{C}}(V)}{Q_{\mathrm{C,\ MAX}}} = (1-b)\left(\frac{1}{1+J^{-1}}\right) + b\left(\frac{1}{1+(JE_{M1})^{-1}}\right) \qquad (1);$$

where

$$b = \frac{1}{1+K^{-1}} = \frac{1}{1+\frac{K_D}{[Ca^{2+}]}} = \frac{[Ca^{2+}]}{[Ca^{2+}]+K_D} \qquad (2);$$

and

$$J = J_0 e^{\frac{z_J FV}{RT}} \qquad (3)$$

Substituting b and J into Equation (1), the Ca^{2+}-dependent voltage sensor activation for Model I is given by the equation

$$\frac{Q_{\mathrm{C}}(V)}{Q_{\mathrm{C,\ MAX}}} = \left(\frac{K_D}{[Ca^{2+}] + K_D}\right)\left(\frac{1}{1 + \frac{e^{\frac{-z_J FV}{RT}}}{J_0}}\right) + \left(\frac{[Ca^{2+}]}{[Ca^{2+}] + K_D}\right)\left(\frac{1}{1 + \frac{e^{\frac{-z_J FV}{RT}}}{J_0 E_{M1}}}\right) \quad (4)$$

Thus, the $Q_{\mathrm{C}}(V)$ curves are determined by the proportion of two functional VSD populations with a distinctive effect (unliganded effect or Ca^{2+}-saturated effect) Consequently, the $Q_{\mathrm{C}}(V)$ curves are represented by a weighted sum of two Boltzmann functions.

Meanwhile, for the concerted CTD-VSD interaction Scheme II (Model II), the $Q_{\mathrm{C}}(V, [\mathrm{Ca}^{2+}])$ curves would be determined using the general equation:

$$\frac{Q_{\mathrm{C}}(V)}{Q_{\mathrm{C,\ MAX}}} = \sum_{x=0}^{n} \binom{n}{x} (1-b)^{n-x} b^x \left(\frac{1}{1 + (JE_{M2}^x)^{-1}}\right) \quad (5)$$

The expression in the first bracket represents the fraction of VSD belonging to a channel with x (0 to 4) Ca^{2+} bound, according to a binomial probability distribution. Thus, the $Q_{\mathrm{C}}(V)$ curves result in a weighted sum of five distinct Boltzmann functions corresponding to the five possible R-A transitions (***Figure 2—figure supplement 1C***). By stating $n = 4$ because the tetrameric symmetry of the channels, and substituting b and J into the previous equation (Equation 5) we have

$$\frac{Q_{\mathrm{C}}(V)}{Q_{\mathrm{C,\ MAX}}} = \sum_{x=0}^{4} \binom{4}{x} \left(\frac{K_D}{[Ca^{2+}] + K_D}\right)^{4-x} \left(\frac{[Ca^{2+}]}{[Ca^{2+}] + K_D}\right)^{x} \left(\frac{1}{1 + \frac{e^{\frac{-z_J FV}{RT}}}{J_0 E_{M2}^x}}\right) \quad (6)$$

It should be noted that at limiting Ca^{2+} conditions, both schemes become equivalent where the VSD activation is characterized by a single Boltzmann function. At zero Ca^{2+}, the $Q_{\mathrm{C}}(V)$ curves are described by

$$\frac{Q_{\mathrm{C}}(V)}{Q_{\mathrm{C,\ MAX}}} = \left(\frac{1}{1 + \frac{e^{\frac{-z_J FV}{RT}}}{J_0}} \right),$$

whereas Ca^{2+} saturating concentration J is multiply by the allosteric factor E, where $E = E_{M1} = E_{M2}^4$ depending on the model (Model I or Model II):

$$\frac{Q_{\mathrm{C}}(V)}{Q_{\mathrm{C,\ MAX}}} = \left(\frac{1}{1 + \frac{e^{\frac{-z_J FV}{RT}}}{J_0 E}} \right)$$

Given that each α-subunit has two Ca^{2+}-binding sites, we expanded the CTD-VSD interaction Scheme II (***Figure 2—figure supplement 1C***) considering the existence of two Ca^{2+}-binding sites (***Figure 2—figure supplement 1D,E***). The Model II includes the energetic contribution of RCK1 and RCK2 Ca^{2+}-sites to the VSD activation. The factor $E = E_{S1} * E_{S2}$ where E_{S1} and E_{S1} are the allosteric coupling between the VSD and the RCK1 Ca^{2+}-site and RCK2 Ca^{2+}-site, respectively. The K_1 and K_2 constants define the bound/unbound transition for each RCK1 and RCK2 sites being $K_1 = [Ca^{2+}]/\ K_{D1}$ and $K_2 = [Ca^{2+}]/\ K_{D2}$. Assuming that the Ca^{2+} sensors of distinct α-subunit do not interact, we only consider intrasubunit cooperativity between the RCK1 and RCK2 sites defined by the factor G. Thus, the occupancy of one RCK site will affect Ca^{2+}-binding equilibrium to the other RCK site in the α-subunit (GK_1 and GK_2) (***Figure 2—figure supplement 1E***). The equilibrium J of the VSD increase E_{S1}-fold and E_{S2}-fold for the each Ca^{2+} bound to RCK1 and RCK2 sites, respectively, reaching to $JE_{S1}^4 E_{S2}^4$ when the eight Ca^{2+} sites are occupied.

Supplementary Figures

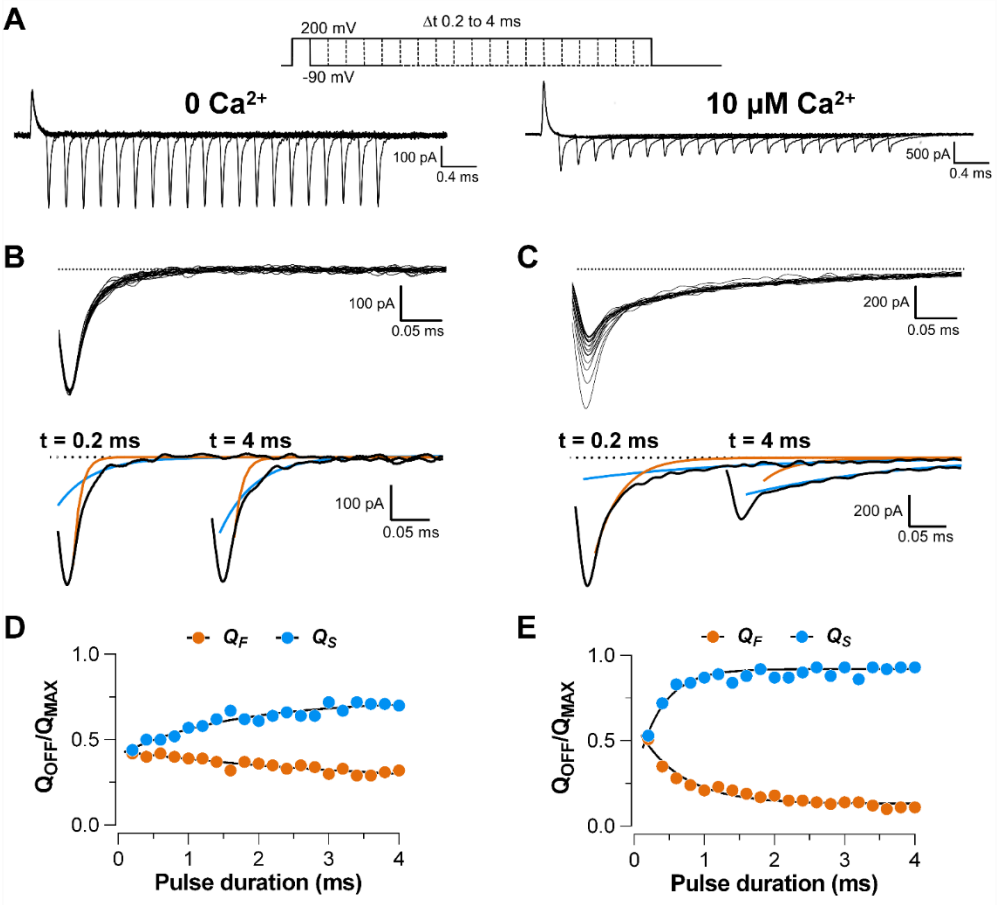

Figure 1—figure supplement 1. Ca^{2+} increase the slow component of the OFF gating currents.

(**A**) Gating current (I_G) recordings evoked by 200 mV pulses with different durations (from 0.2 to 4 ms) at 0 and 10 µM [Ca^{2+}] conditions, respectively. (**B-C**) The top panels show the superimposed traces of the I_G-OFF recorded at -90 mV evidencing a decrease in amplitude and a slower decay of the OFF current as the duration of the pulse increases at 10 µM Ca^{2+}. The dashed line represents the baseline for each experiment. I_G-OFF were fitted with an exponential function of two-components (fast and slow components). I_G-OFF traces at 0.2 ms and 4 ms pulse duration are displayed for each Ca^{2+} condition. Orange and blue lines correspond to fast and slow components of the two-exponential fits, respectively: (**B**) "zero" Ca^{2+} (τ_F = 10 µs and τ_S= 44 µs) and (**C**) 10 µM Ca^{2+} (τ_F = 25 µs and τ_S = 212 µs). (**D-E**) The relative amplitude of the OFF-charge components, the fast (Q_F) and slow (Q_S) charge components were plotted against the pulse duration and fitted with an exponential function representing the time course of the opening of the channel: (**D**) "zero" Ca^{2+} ($\tau_{0Ca^{2+}}$ = 1.8 ms) and (**E**) 10 µM Ca^{2+} ($\tau_{10\,\mu M}$ = 536 µs).

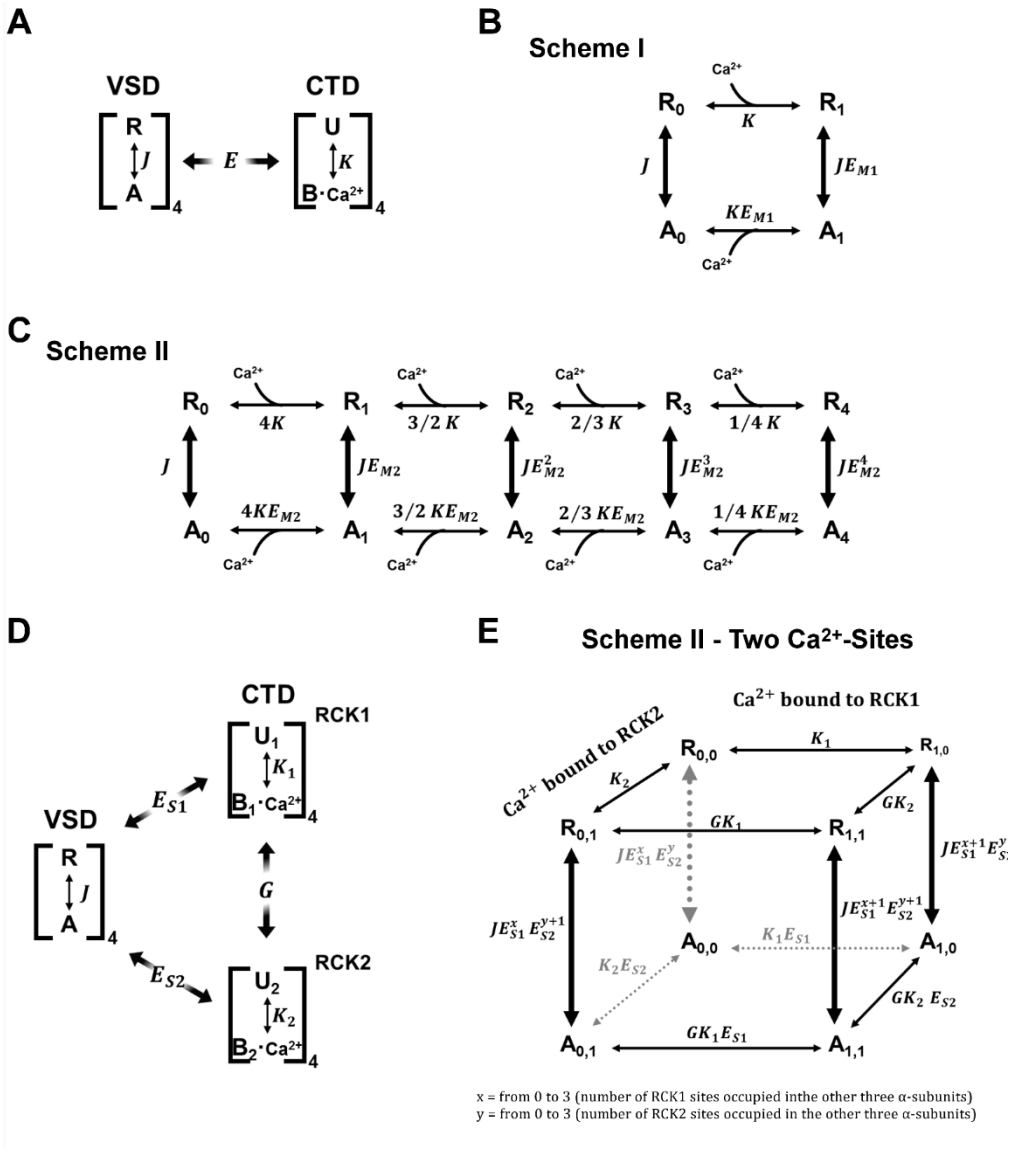

Figure 2—figure supplement 1. Kinetic models of the VSD activation according to the CTD-VSD interaction schemes.

(**A**) Sub-scheme describing calcium and voltage allosteric interaction for closed channels. The VSD transit between two resting (R) and active (A) configuration governed by the equilibrium constant J, whereas each Ca^{2+} site undergoes unbound (U) - Ca^{2+} bound (**B**) transitions governed by the equilibrium constant K. The allosteric factor E accounts for the coupling between the calcium and voltage sensors (CTD-VSD) (**B-C**) VSD kinetic models in presence of Ca^{2+} according to CTD-VSD interaction schemes I and II (*Figure 2A,B*), respectively, where the vertical transitions (R-A) represent the VSD movement and the horizontal transitions (R-R and A-A) are Ca^{2+}-binding

reactions when the VSD is in the resting or active conformation. For the Scheme I (**B**), each VSD can undergo R_0-A_0 or R_1-A_1 transitions depending on the unbound or bound state of the Ca^{2+} site in the α-subunit, respectively. Thus, the R_1-A_1 equilibrium is defined by J increased E_{M1}-fold (JE_{M1}). For the Scheme II (**C**), the R_0-A_0 to R_4-A_4 transitions represent the VSD equilibrium with 0, 1, 2, 3, and 4 occupied Ca^{2+} sites in the channel. Thus, for each Ca^{2+} bound the equilibrium constant J increase E_{M2}-fold reaching to JE_{M2}^4 when the four Ca^{2+} sites are occupied. The thickness of the arrows indicates the probability of transitions. (**D**) General sub-scheme of the CTD-VSD interaction including two Ca^{2+} sites for each CTD (RCK1 and RCK2 sites). For each RCK1 and RCK2 site the unbound-Ca^{2+} bound transitions are governed by the equilibrium constants K_1 and K_2. The factor G describe the cooperativity between the sites within the same α-subunit; and the E_{S1} and E_{S2} factors define the allosteric coupling between the RCK1 and RCK2 sites and the VSD, respectively. (**E**) Schematic representation of VSD kinetic model according to the extended version of the Scheme II (**C**) accounting for both RCK1 and RCK2 Ca^{2+}-sites on each α-subunit. For sake of simplicity, are only depicted the VSD transitions depending on the unbound or bound state of the RCK sites within the same α-subunit: RCK1 site ($R_{1,0}$-$A_{1,0}$), RCK2 site ($R_{0,1}$-$A_{0,1}$) and both sites ($R_{1,1}$-$A_{1,1}$).

ADDITIONAL RESULTS AND DISCUSSION

Total voltage-sensing charges per channel in BK channels.

Characterization of voltage sensing process in BK channel has been widely approached including the voltage-sensing residues (Díaz et al., 1998; Ma et al., 2006; Zhang et al., 2014), the allosteric interaction with the pore and modulation (Horrigan and Aldrich, 1999; Horrigan et al., 1999; Ma et al., 2006; Budelli et al., 2013; Zhang et al., 2017) by auxiliary subunits (Bao and Cox, 2005; Contreras et al., 2012; Castillo et al., 2015). An important parameter of the voltage sensitivity is the number of charges translocated during the gating process (Z). However, the total gating charges per channel displaced during the activation process of the BK channel remains unclear (Stefani et al., 1997; Horrigan et al., 1999).

Thus, the number of gating charges per channel in BK channel was determined by the $\mathrm{Q/N}$ method ($Z_{Q/N} = Q_{MAX}/Ne_0$). The number of channels (N) in the membrane patch was estimated using non-stationary noise analysis (Sigworth, 1980) of ionic currents whereas the maximum value of the charge (Q_{MAX}) was calculated from the gating current recorded in the same membrane patch (**Figure 10**). From the ionic current recordings was calculated the mean current ($\langle I \rangle$) and variance (σ^2) in each isochrone, and the σ^2- $\langle I \rangle$ relationship was fitted using the theoretical variance function: $\sigma^2 = i\langle I \rangle - \langle I \rangle^2/N$ (**Figure 10B**). This type of analysis is used to relate macroscopically observable parameters, such as the total ionic current with microscopic parameters like the number of functional channels in the patch of membrane N, as well as, the single-channel current (i) and the maximum open probability, $P_O = I_{MAX}/iN$ where I_{MAX} is the maximum mean current measured (Alvarez et al., 2002; Lingle, 2006).

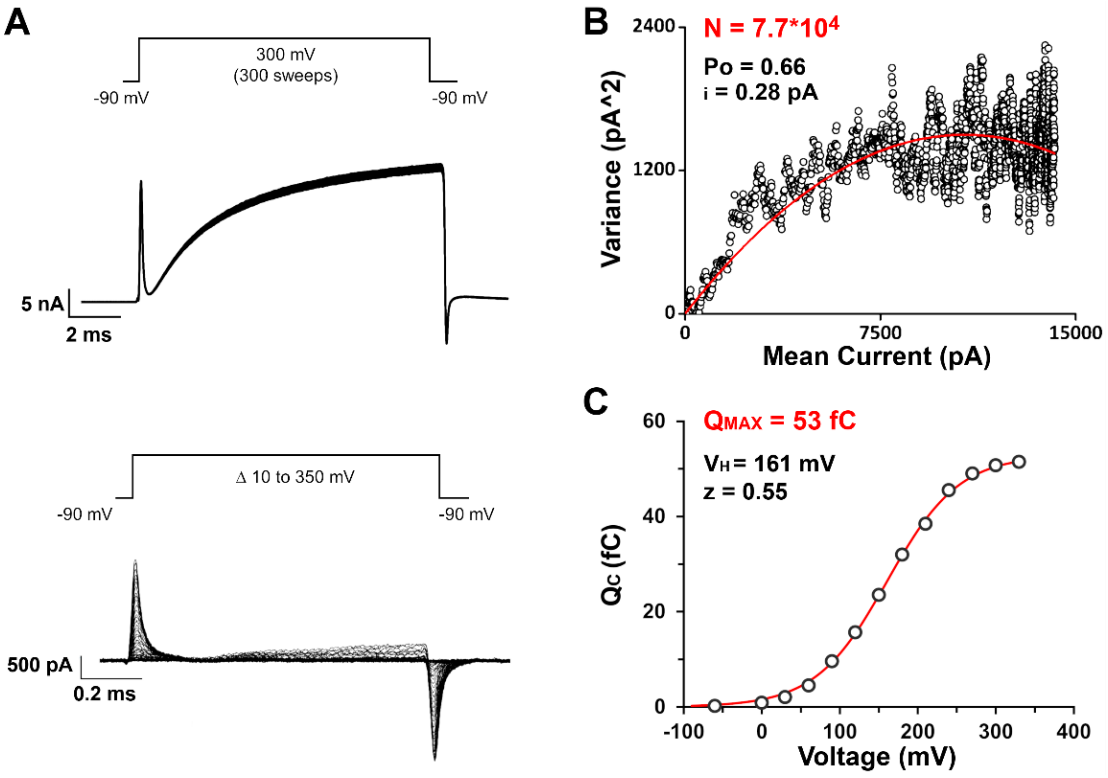

Figure 10. Determination of total gating charge displaced per channel from Q/N method in BK channels.

(**A**) Representative experiment using Q/N method for BK channel. Ionic currents (Top) were evoked by repeated voltage pulses (300 sweeps) to 300 mV, and then in the same membrane patch, after perfusing with K^+ free internal solution, gating currents (Bottom) were elicited by 1-ms voltage steps from -90 to 350 mV. (**B**) Experimental variance (σ^2) - mean current ($\langle I \rangle$) plot was fitted using the theoretical variance function $\sigma^2 = i\langle I \rangle - \langle I \rangle^2/N$ (red line) in order to obtain the number of channels, N. (**C**) Maximum value of the charge, Q_{MAX}, was obtained by fitted to a single exponential function ON-gating currents and integrating the area under the curve described by the monoexponential fitting. $Q_C(V)$ data were fitted using a Boltzmann function (red line).

According to the fact that the voltage-sensing charges in the BK channel are fewer than those observed the other Kv channels, during activation of the voltage-sensing domain in the BK channel the total number of charges displaced per channel is approximately 4.3 electronic charges (e_0) (**Table 1)** which fully agrees with early reports (4-5 e_0) (Stefani et al., 1997). The smaller number of gating charges indicates that more membrane depolarization is needed to move the VSD of BK channels into the fully activated state. This weaker voltage sensitivity is critical to the physiological role of BK channels because it enables BK channels to operate in a wide range of membrane potentials to fine-tune channel activation and in turn the membrane voltage (Yang et al., 2015). On the other hand, these findings indicate that the gating charges in BK channel is moving in multiple steps and not between two states (R-A; single step) as is assumed by the HA model (Horrigan and Aldrich, 1999; Horrigan et al., 1999). Thus, the estimations of Ze_0 from the slope of a single-Boltzmann fit to the $Q(V)$ curve (z_J = 0.6 per VSD, **Figure 10D**) underestimates the total number of charges per channel ($Z = 4z_J$ = 2.4 e_0) (Bezanilla and Villalba-Galea, 2013), and in turn, the distinct contributions of the gating-sensing charges to the overall voltage dependence of the BK channel (Ma et al., 2006).

Table 1. Summary of the experimental $Z_{Q/N}$ (e_0) values obtained by Q/N method.

	Q/N Method		
Experiments	N	Q_{MAX} **(fC)**	$Z_{Q/N}$ (e_0)
1	7.7*10^4	53	**4.3**
2	7.8*10^4	58	**4.1**
3	6.8*10^3	4.8	**4.4**
			4.3 ± 0.2

Modulatory β-subunits effects on VSD.

At least some diversity in BK channel properties can arise from the cell-specific molecular composition of the BK channel complex, including co-assembly with various accessory subunits such as the β- and γ-subunits (Knaus et al., 1994; Wallner et al., 1996; Brenner et al., 2000; Uebele et al., 2000; Xia et al., 2000; Yan and Aldrich, 2010). In particular, the tissue-specific expression of β-subunits dramatically modify the BK gating properties. β-subunits (β1–β4) are encoded by four different genes (KCNMB1–4). All of them share a similar predicted topology, containing two TM segments, TM1 and TM2, joined together by an external loop, and short intracellular N- and C-terminal regions. β1, β2, and β3 exhibit high degrees of homology, whereas β4 is genetically more distant from the other β subunits. Several gating properties are potential targets for regulation by auxiliary β-subunits including not only Ca^{2+} sensitivity and voltage-dependent gating of BK channels (McManus et al., 1995; Cox and Aldrich, 2000; Bao and Cox, 2005; Orio and Latorre, 2005; Sweet and Cox, 2009) but also inactivation behavior (Wallner et al., 1999; Uebele et al., 2000; Xia et al., 2000) and pharmacology (Dworetzky et al., 1996; Meera et al., 2000).

Effect of β-subunits on allosteric CTD-VSD coupling.

Specifically, BK voltage-sensing properties are affected differentially by the β-subunits. β1, β2, and β4 modify the R-A equilibrium constant stabilizing the voltage sensor in its active conformation. Whereas β1 and β2 (albeit to a lesser extent) induce a leftward shift of the VSD activation without changes in the apparent gating charge (Bao and Cox, 2005; Yang et al., 2008b; Contreras et al., 2012), β4-subunit modify mainly the R-A equilibrium by decreasing in the number of apparent gating charges per voltage sensor. β3-subunit has no effect on VSD equilibrium (Contreras et al., 2012).

Functional and structural characteristics of β-subunit modulation have led to the idea of the association of β-subunits alters the VSD–CTD interface and the interactions among CTD, PD and

VSD that are key in the Ca^{2+}- and voltage-dependent activation of BK channels, providing a novel perspective on how subunits modify BK channel activation (Lee et al., 2010; Horrigan, 2012; Sun et al., 2013). For example, perturbations of the VSD–CTD interface by mutations of residues N172 and E399 alter the ability of the β1- subunit to modify Ca^{2+} sensitivity without affecting the VSD modulation, which suggests that β1 primarily interacts with the VSD to alter voltage-dependent gating (Yang et al., 2008b; Contreras et al., 2012), and in turn, such an interaction changes the VSD–CTD interface to alter Ca^{2+}-dependent gating (Sun et al., 2013). Thus, the VSD–CTD interface changes may provide an allosteric mechanism to propagate the effects of different β1 subunits to all aspects of BK channel gating.

Could β-subunits modulate energetically to the allosteric VSD–CTD interaction being part of their modulatory mechanism? To examine the effect of β-subunits on the interaction between Ca^{2+}-binding sites and VSD, gating current recordings at different internal [Ca^{2+}] were obtained for BK channel (BK(α)) co-expressed with β1-subunit (**Figure 11A**) and β3b-subunit (**Figure 12A**). Electrophysiological recordings and data analysis were performed following the same protocol described in Lorenzo-Ceballos et al. (*Submitted Manuscript*: (Lorenzo-Ceballos et al., 2019)).

Preliminary results show that similar to the VSD behavior in BK(α) channel, the increase in internal Ca^{2+} promotes a leftward shift voltage $Q_C(V)$ curves obtained in presence of β1 (**Figure 11B,C**) and β3b (**Figure 12B,C**) facilitating the activation of the voltage sensor. Given the difficulties of detecting gating currents at saturating [Ca^{2+}], the I_G recordings under these Ca^{2+} conditions are not available for the BK(α/β1) and BK(α/β3b) constructs. However, despite it is not possible to determine the energetic interaction between the specialized-sensory modules for BK(α/β1) and BK(α/β3b) channels, the Ca^{2+}-induced effect on VSD activation seems not to be affected by the presence of β1 nor β3b (**Figure 13**).

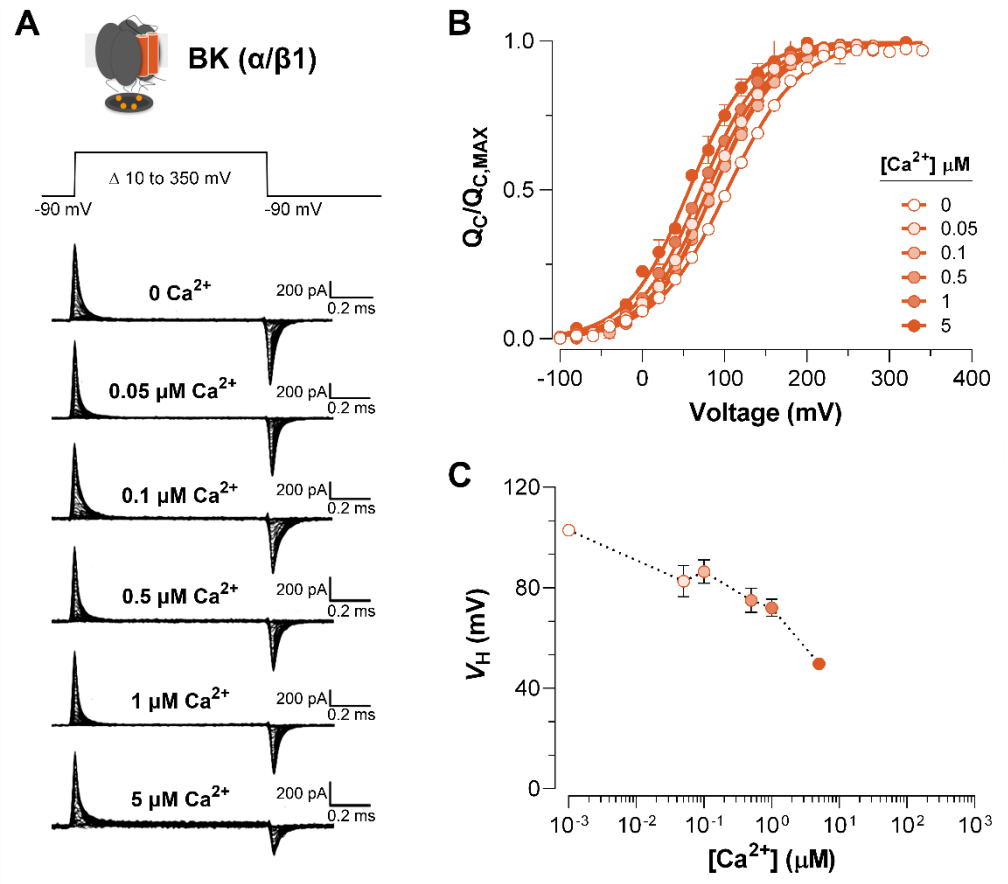

Figure 11. Ca^{2+}-induced effects of on VSD activation in BK channels co-expressed with β1-subunit.

(**A**) Representative gating current (I_G) recordings at different internal Ca^{2+} concentrations (from 0 to 5 µM). I_G were evoked by the indicated voltage protocol of 1 ms duration. (**B**) Gating charge-voltage relationships ($Q_C(V)$) were obtained by integrating the fast component for each ON I_G trace. Normalized gating charge data $\left(Q_C(V)/Q_{C,\ MAX}\right)$ (mean ± SEM) were fitted using a single Boltzmann function (solid lines). (**C**) V_H obtained from the $Q_C(V)$ curves as a function of Ca^{2+} concentration (mean ± SEM): zero" Ca^{2+} condition ($V_{H\,(0\ Ca^{2+})}$ = 102.9 ± 1.6 mV, n = 13); 0.05 µM Ca^{2+} (V_H = 82.7 ± 6.2 mV, n = 5); 0.1 µM Ca^{2+} (V_H = 86.4 ± 4.6 mV, n = 3); 0.5 µM Ca^{2+} (V_H 75.0 ± 4.8 mV, n = 4); 1 µM Ca^{2+} (V_H = 72.0 ± 3.4 mV, n = 8); 5µM Ca^{2+} (V_H = 49.8 mV, n = 2).

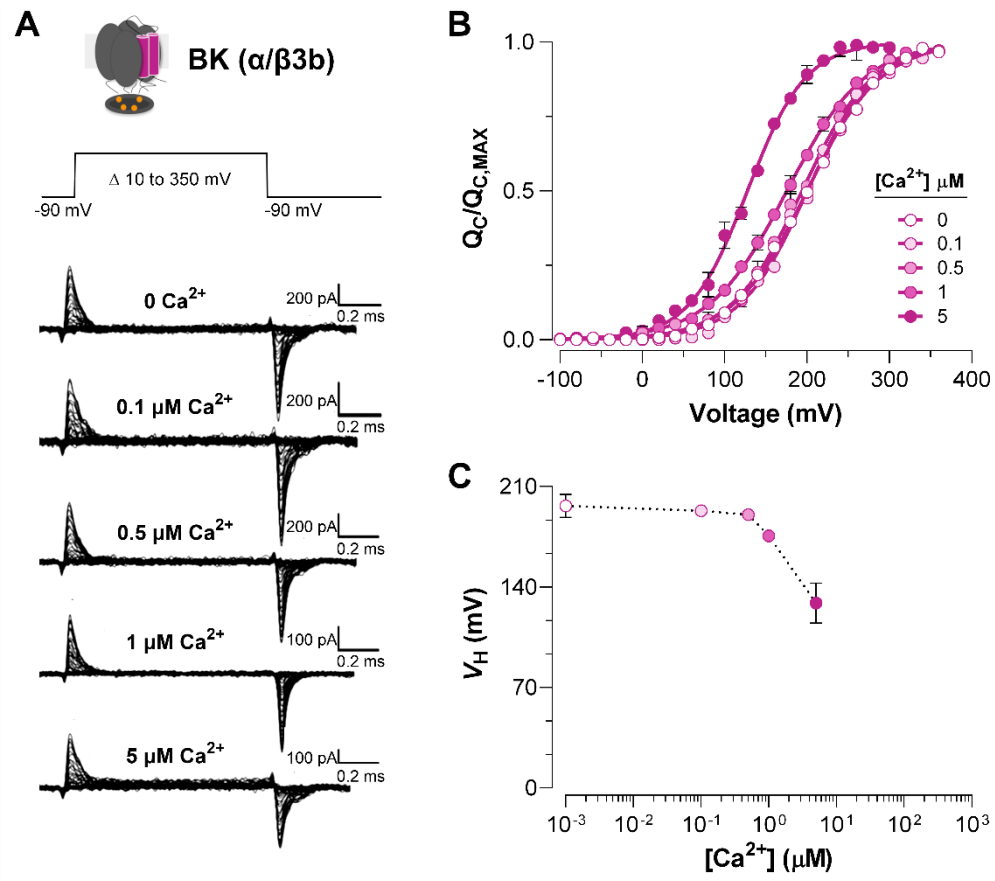

Figure 12. Ca^{2+}-induced effects of on VSD activation in BK channels co-expressed with β3b-subunit.

(**A**) Representative gating current (I_G) recordings at different internal Ca^{2+} concentrations (from 0 to 5 µM). I_G were evoked by the indicated voltage protocol of 1 ms duration. (**B**) Gating charge-voltage relationships ($Q_C(V)$) were obtained by integrating the fast component for each ON I_G trace. Normalized gating charge data $\left(Q_C(V)/Q_{C,\ MAX}\right)$ (mean ± SEM) were fitted using a single Boltzmann function (solid lines). (**C**) V_H obtained from the $Q_C(V)$ curves as a function of Ca^{2+} concentration (mean ± SEM): zero" Ca^{2+} condition ($V_{H\,(0\ Ca^{2+})}$ = 196.5 ± 7.2 mV, n = 5); 0.1 µM Ca^{2+} (V_H = 193.1 mV, n = 1); 0.5 µM Ca^{2+} (V_H = 190.4 mV, n = 2); 1 µM Ca^{2+} (V_H = 175.6 mV, n = 2); 5µM Ca^{2+} (V_H = 128.8 ± 13.9 mV, n = 3).

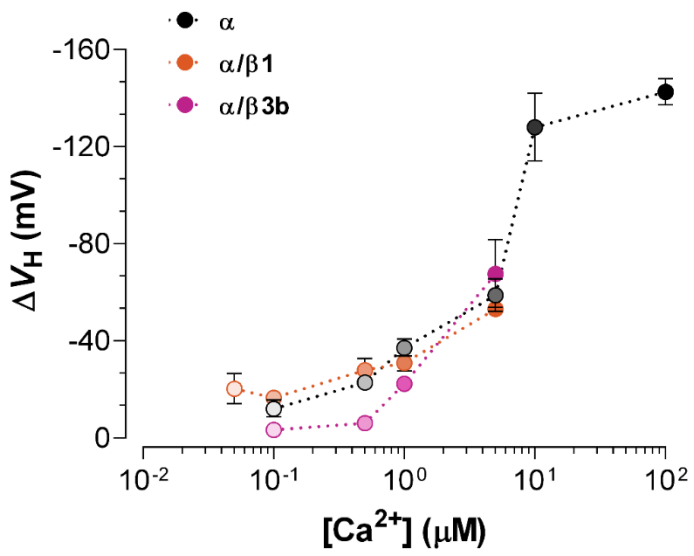

Figure 13. Comparison of Ca^{2+}- induced effects on VSD of BK(α) channel and in presence of β1- and β3b-subunits.

Quantification of ΔV_{H} obtained from of the $Q_{\mathrm{C}}(V)$ curves (mean ± SEM) as a function of Ca^{2+} concentration for BK(α) (black), BK(α/β1) (orange) and BK(α/β3b) (pink) channels.

Given the β3b-subunit do not produce appreciable modifications in the BK channel Ca^{2+} sensitivity (Xia et al., 2000) nor does it affect the VSD activation (Contreras et al., 2012) it would be expected that the β3b do not play a modulatory role on the coupling between Ca^{2+} sensor and the voltage sensors. On the other hand, the β1-induced effect on VSD has been proposed to account for the most modulatory properties including the apparent enhancement of the Ca^{2+} sensitivity (Yang et al., 2008b; Contreras et al., 2012). The idea is that by stabilizing of the active configuration of the voltage sensor, the work that Ca^{2+} binding must do to open the channel is decreased, and the net effect is an apparent enhancement of the Ca^{2+} sensitivity (Contreras et al., 2012). However, some reports indicate that a true Ca^{2+} affinity change it is necessary to fully account for the effects of β1-subunit on Ca^{2+} sensitivity (Cox and Aldrich, 2000; Bao and Cox, 2005; Sweet and Cox, 2009). The strong energetic coupling between Ca^{2+} and voltage sensors (Lorenzo-Ceballos et al., 2019)

can be taken into account to another potential mechanism in the β1-induced Ca^{2+} sensitivity such that the stabilization of the voltage sensor in its active conformation favors the Ca^{2+} binding. Although these preliminary results do not allow us to rule out β-induced effects on the CTD-VSD coupling and should be approached any mechanistic interpretation with caution, the ostensible non-modify of Ca^{2+}-voltage sensor interaction by β1 agrees with the voltage sensor as the primary target regulated by the β1-subunit for all the functional consequences of β1 association (Yang et al., 2008b; Contreras et al., 2012).

β1-subunit decrease the voltage sensitivity of VSD.

In addition to the dramatic leftward shift (about 60 to 70 mV) of the VSD activation induced by β1 (Bao and Cox, 2005; Contreras et al., 2012), has been suggested that β1 alter the function of the voltage sensors affecting their voltage sensitivity (Orio and Latorre, 2005). However, this finding is provided by the maximum voltage dependence of the $\ln Po(V)$ relationship (maximum slope) (Sigg and Bezanilla, 1997). Although the maximum slope is related to the voltage sensor-associated activation of the channels, it is important to note that the steepness of the $\ln Po(V)$ curve is altered by other variables besides the number of voltage-sensing charges, including the strength of coupling between the VSD and the PD (allosteric factor D).

To assess if the β-induced effect on VSD promotes also a reduction of the voltage dependence of the voltage sensor movement, the total number of gating charges displaced per channel in presence of β1- and β3b-subunits was determined by the Q/N method using the same experimental strategies described above. Representative experiments for BK(α/β1) and BK(α/β3b) constructs are presented in **Figure 14** and **Figure 15**, respectively. Preliminary results (**Figure 16**), shows that in presence of the β3-subunit the number of gating charges displaced per channel did not change relative to BK(α) channels showing a value of 4.1 electronic charges which indicate that in presence of β3 VSD behaves as the α-subunit alone (Contreras et al., 2012).

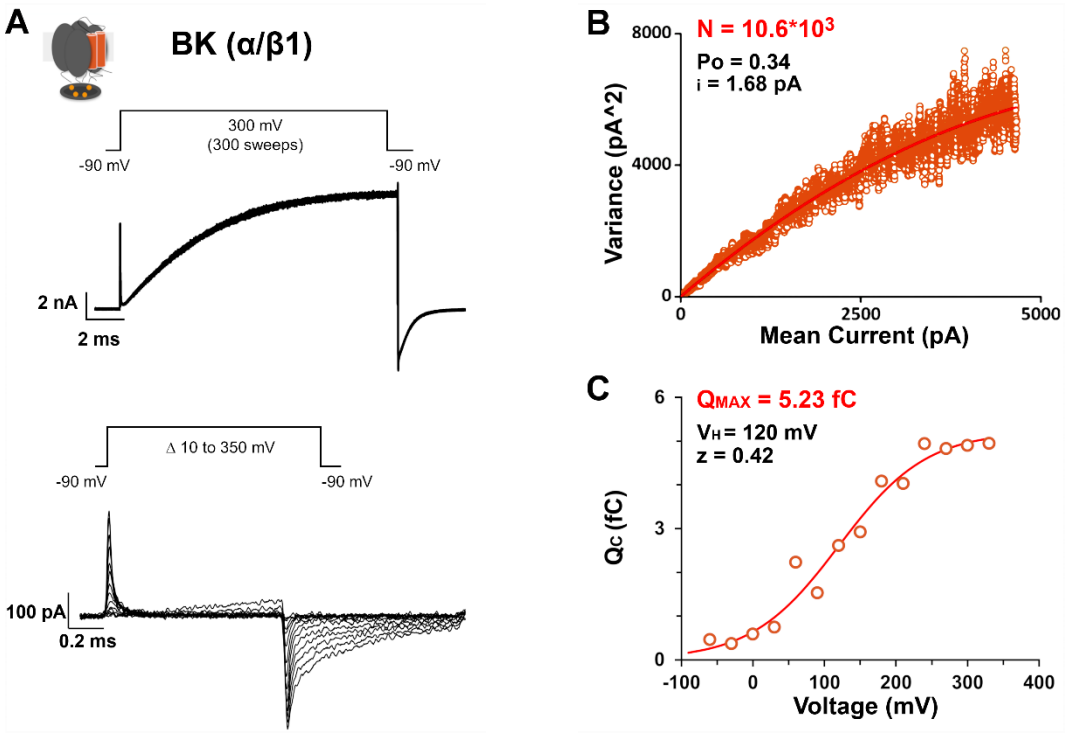

Figure 14. Determination of total gating charge displaced per channel from Q/N method in BK channels co-expressed with β1-subunit.

(**A**) Representative experiment using Q/N method for BK(α/β1) channel. Ionic currents (top) were evoked by repeated voltage pulses (300 sweeps) to 300 mV, and then in the same membrane patch, after perfusing with K^+ free internal solution, gating currents (bottom) were elicited by 1-ms voltage steps from -90 to 350 mV. (**B**) Experimental variance (σ^2) - mean current ($\langle I \rangle$) plot was fitted using the theoretical variance function $\sigma^2 = i\langle I \rangle - \langle I \rangle^2/N$ (red line) in order to obtain the number of channels, N. (**C**) Maximum value of the charge, Q_{MAX}, was obtained by fitted to a single exponential function ON-gating currents and integrating the area under the curve described by the monoexponential fitting. $Q_C(V)$ data were fitted using a Boltzmann function (red line).

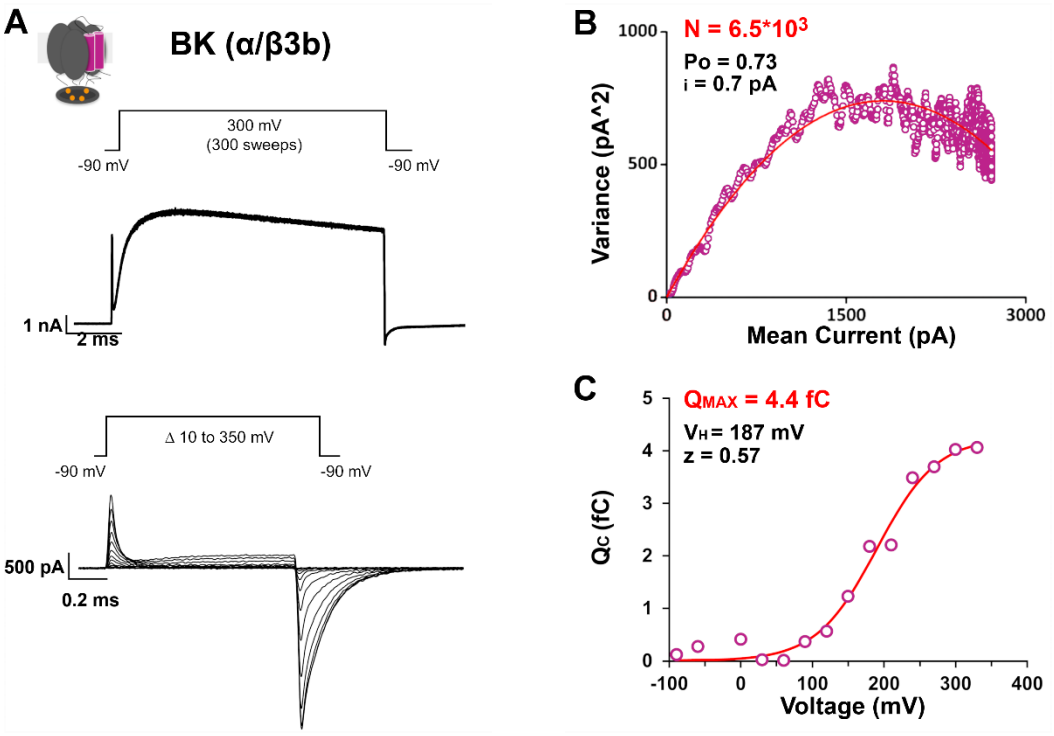

Figure 15. Determination of total gating charge displaced per channel from Q/N method in BK channels co-expressed with β3b-subunit.

(**A**) Representative experiment using Q/N method for BK(α/β3b) channel. Ionic currents (top) were evoked by repeated voltage pulses (300 sweeps) to 300 mV, and then in the same membrane patch, after perfusing with K^+ free internal solution, gating currents (bottom) were elicited by 1-ms voltage steps from -90 to 350 mV. (**B**) Experimental variance (σ^2) - mean current ($\langle I \rangle$) plot was fitted using the theoretical variance function $\sigma^2 = i\langle I \rangle - \langle I \rangle^2/N$ (red line) in order to obtain the number of channels, N. (**C**) Maximum value of the charge, Q_{MAX}, was obtained by fitted to a single exponential function ON-gating currents and integrating the area under the curve described by the monoexponential fitting. $Q_C(V)$ data were fitted using a Boltzmann function (red line).

In agreement with the previous report (Orio and Latorre, 2005), β1-subunit appears to affect also the voltage dependence of VSD. In presence of β1-subunit, the number of gating charges displaced during VSD activation per channel was less relative to BK α-subunit alone decreasing from 4.3 electronic charges in BK(α) channels to 3.2 electronic charges in BK(α/β1) channels (**Figure 16)**. Reduction of the total charges in the presence of β1 suggest that the interaction the voltage sensor in α-subunit with β1-subunit promotes a decreasing of the extension of VSD displacement during channel activation and/or modifying the pattern of the membrane electric field. Thus, the modulatory function of β1 to VSD in BK channels could involve a change in the effective valence of the voltage sensor activation process

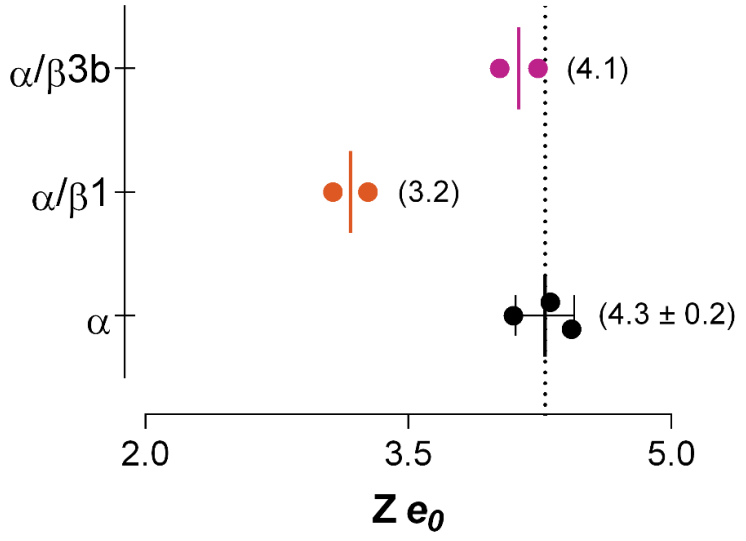

Figure 16. β-subunits effect on total gating charges displaced during VSD activation of BK(α) channel.

Scatter plot of $Z_{Q/N}$ values (mean ± SEM) for BK(α) (black), BK(α/β1) (orange) and BK(α/β3b) (pink) channels. Each filled circle represents an Q/N experiment as are shown in the Figure 10, Figure 14, and Figure 15. The vertical lines between the experiments (circles) represent the $Z_{Q/N}$ mean value.

Concluding Remarks

The work presented in this thesis focuses mainly in the characterization of the Ca^{2+}-driven effects on VSD activation, trying to understand the allosteric interplay between Ca^{2+} and voltage sensors in the framework of the dual activation of the BK channel. The new structural information provides insights into the physical basis underlying several features of the BK channels functionality including a new perspective on how voltage sensing may affect the ability of the CTD to gate the BK channel. Nevertheless, the molecular and mechanistic nature of the different transduction pathways through which the specialized sensors converge to fine-tune of the channel gating is yet not well understood. In this thesis is shown that the synergistic Ca^{2+} and voltage activation of BK channels is largely mediated by a remarkable sensory domains communication. The evaluation of interaction schemes between voltage and Ca^{2+} sensor proposed that a concerted interaction mechanism appears to underlie in these allosteric CTD-VSD coupling. In addition, was identified an equivalent modulatory role of the two high-affinity Ca^{2+}-binding sites to the allosteric Ca^{2+}-regulation of the voltage-sensing process. Regarding the molecular bases underlying in the allosteric propagation pathways and the cooperative interactions of the RCK1 and RCK2 regulatory domains, additional functional studies are needed to provide new clues on the dual gating mechanism of BK channel. Preliminary findings suggested that the modulatory effects of the auxiliary β1-subunit on the gating properties of BK channels occur by modifying the VSD function including its voltage sensitivity but without affecting its allosteric relation with the Ca^{2+} sensors.

REFERENCES

Adelman JP, Shen KZ, Kavanaugh MP, Warren RA, Wu YN, Lagrutta A, Bond CT, Alan North R. 1992. Calcium-activated potassium channels expressed from cloned complementary DNAs. *Neuron* **9**:209–216. DOI:10.1016/0896-6273(92)90160-F

Aggarwal SK, MacKinnon R. 1996. Contribution of the S4 segment to gating charge in the Shaker K+ channel. *Neuron* **16**:1169–77. DOI:10.1016/S0896-6273(00)80143-9

Alvarez O, Gonzalez C, Latorre R. 2002. COUNTING CHANNELS : A TUTORIAL GUIDE ON ION CHANNEL. *Advan Physiol Edu* **26**:327–341. DOI:10.1152/advan.00006.2002

Atkinson NS, Robertson GA, Ganetzky B. 1991. A Component of Calcium-Activated Potassium Channels Encoded by the Drosophila slo Locus. *Science (80-)* **253**:551–555. DOI:10.1126/science.1857984

Bao L, Rapin AM, Holmstrand EC, Cox DH. 2002. Elimination of the BKCa Channel's High-Affinity Ca2+ Sensitivity. *J Gen Physiol* **120**:173–189. DOI:10.1085/jgp.20028627

Bao L, Cox DH. 2005. Gating and ionic currents reveal how the BKCa channel's Ca2+ sensitivity is enhanced by its beta1 subunit. *J Gen Physiol* **126**:393–412. DOI:10.1085/jgp.200509346

Berridge MJ, Lipp P, Bootman MD. 2000. The versatility and universality of calcium signalling. *Nat Rev Mol Cell Biol* **1**:11–21. DOI:10.1038/35036035

Bezanilla F. 2000. The voltage sensor in voltage-dependent ion channels. *Physiol Rev* **80**:555–92. DOI:10.1152/physrev.2000.80.2.555

Bezanilla F. 2018. Gating currents. *J Gen Physiol* **150**:911–932. DOI:10.1085/jgp.201812090

Bezanilla F, Villalba-Galea CA. 2013. The gating charge should not be estimated by fitting a two-state model to a Q-V curve. *J Gen Physiol* **142**:575–8. DOI:10.1085/jgp.201311056

Blatz AL, Magleby KL. 1984. Ion conductance and selectivity of single calcium-activated potassium channels in cultured rat muscle. *J Gen Physiol* **84**:1–23. DOI:10.1085/jgp.84.1.1

Brelidze TI, Niu X, Magleby KL. 2003. A ring of eight conserved negatively charged amino acids doubles the conductance of BK channels and prevents inward rectification. *Proc Natl Acad Sci USA* **100**:9017–9022. DOI:10.1073/pnas.1532257100

Brelidze TI, Magleby KL. 2005. Probing the Geometry of the Inner Vestibule of BK Channels with Sugars. *J Gen Physiol* **126**:105–121. DOI:10.1085/jgp.200509286

Brenner R, Jegla TJ, Wickenden A, Liu Y, Aldrich RW. 2000. Cloning and functional characterization of novel large conductance calcium-activated potassium channel beta subunits, hKCNMB3 and hKCNMB4. *J Biol Chem* **275**:6453–6461.

Budelli G, Geng Y, Butler A, Magleby KL, Salkoff L. 2013. Properties of Slo1 K + channels with and without the gating ring. *PNAS* **110**:16657–16662. DOI:10.1073/pnas.1313433110

Butler A, Tsunoda S, McCobb DP, Wei A, Salkoff L. 1993. mSlo, a complex mouse gene encoding "maxi" calcium-activated potassium channels. *Science (80-)* **261**:221–224. DOI:10.1126/science.7687074

Carrasquel-Ursulaez W, Contreras GF, Sepúlveda R V, Aguayo D, González-Nilo F, González C, Latorre R. 2014. Hydrophobic interaction between contiguous residues in the S6 transmembrane segment acts as a stimuli integration node in the BK channel. *J Gen Physiol* **145**:61–74. DOI:10.1085/jgp.201411194

Carrasquel-Ursulaez W, Lorenzo Y, Echeverria F, Latorre R. 2018. Large Conductance Potassium Channels in the Nervous System In: Bhattacharjee A, editor. The Oxford Handbook of Neuronal Ion Channels. Oxford University Press. pp. 1–75. DOI:10.1093/oxfordhb/9780190669164.013.11

Carvacho I, Gonzalez W, Torres YP, Brauchi S, Alvarez O, Gonzalez-Nilo FD, Latorre R. 2008. Intrinsic Electrostatic Potential in the BK Channel Pore: Role in Determining Single Channel Conductance and Block. *J Gen Physiol* **131**:147–161. DOI:10.1085/jgp.200709862

Castillo K, Contreras GF, Pupo A, Torres YP, Neely A, Gonzalez C, Latorre R. 2015. Molecular mechanism underlying β1 regulation in voltage- and calcium-activated potassium (BK) channels. *PNAS* **112**:4809–14. DOI:10.1073/pnas.1504378112

Clapham DE. 2007. Calcium Signaling. *Cell* **131**:1047–1058. DOI:10.1016/j.cell.2007.11.028

Contet C, Goulding SP, Kuljis DA, Barth AL. 2016. BK Channels in the Central Nervous System, 1st ed, International Review of Neurobiology. Elsevier Inc. DOI:10.1016/bs.irn.2016.04.001

Contreras GF, Neely A, Alvarez O, Gonzalez C, Latorre R. 2012. Modulation of BK channel voltage gating by different auxiliary β subunits. *Proc Natl Acad Sci USA* **109**:18991–6. DOI:10.1073/pnas.1216953109

Cox DH, Aldrich RW. 2000. Role of the beta1 subunit in large-conductance Ca2+-activated K+ channel gating energetics. Mechanisms of enhanced Ca2+ sensitivity. *J Gen Physiol* **116**:411–32.

Cui J, Aldrich RW. 2000. Allosteric Linkage between Voltage and Ca2+-Dependent Activation of BK-Type mslo1 K+ Channels. *Biochemistry* **39**:15612–15619. DOI:10.1021/bi001509+

Díaz-Franulic I, Sepúlveda R V., Navarro-Quezada N, González-Nilo F, Naranjo D. 2015. Pore dimensions and the role of occupancy in unitary conductance of Shaker K channels. *J Gen Physiol* **146**:133–146. DOI:10.1085/jgp.201411353

Díaz L, Meera P, Amigo J, Stefani E, Alvarez O, Toro L, Latorre R. 1998. Role of the S4 segment in a voltage-dependent calcium-sensitive potassium (hSlo) channel. *J Biol Chem* **273**:32430–32436. DOI:10.1074/jbc.273.49.32430

Dopico AM, Bukiya AN, Jaggar JH. 2018. Calcium- and voltage-gated BK channels in vascular smooth muscle. *Pflugers Arch Eur J Physiol* **470**:1271–1289. DOI:10.1007/s00424-018-2151-y

Dworetzky SI, Trojnacki JT, Gribkoff VK. 1994. Cloning and expression of a human large-conductance calcium-activated potassium channel. *Mol Brain Res* **27**:189–193. DOI:10.1016/0169-328X(94)90203-8

Dworetzky SI, Boissard CG, Lum-Ragan JT, Mckay MC, Post-Munson DJ, Trojnacki JT, Chang CP, Gribkoff VK. 1996. Phenotypic alteration of a human BK (hSlo) channel by hSlobeta subunit coexpression: changes in blocker sensitivity, activation/relaxation and inactivation kinetics, and protein kinase A modulation. *J Neurosci* **16**:4543–4550.

Eisenman G, Latorre R, Miller C. 1986. Multi-ion conduction and selectivity in the high-conductance Ca++-activated K+ channel from skeletal muscle. *Biophys J* **50**:1025–1034. DOI:10.1016/S0006-3495(86)83546-9

Elkins T, Ganetzky B, Wu CF. 1986. A Drosophila mutation that eliminates a calcium-dependent potassium current. *Proc Natl Acad Sci USA* **83**:8415–8419. DOI:10.1073/pnas.83.21.8415

Gandhi CS, Isacoff EY. 2002. Perspective Molecular Models of Voltage Sensing. *J Gen Physiol* **120**:455–463. DOI:10.1085/jgp.20028678

Gárdos G. 1958. The function of calcium in the potassium permeability of human erythrocytes. *BBA - Biochim Biophys Acta* **30**:653–654. DOI:10.1016/0006-3002(58)90124-0

Geng Y, Niu X, Magleby KL. 2011. Low resistance, large dimension entrance to the inner cavity of BK channels determined by changing side-chain volume. *J Gen Physiol* **137**:533–548. DOI:10.1085/jgp.201110616

Ghosh A, Greenberg ME. 1995. Calcium Signaling in Neurons: Molecular Mechanisms and Cellular Consequences. *Science (80-)* **268**:239–247. DOI:10.1126/science.7716515

Giraldez T, Rothberg BS. 2017. Understanding the conformational motions of RCK gating rings. *J Gen Physiol* 1–11. DOI:10.1085/jgp.201611726

Golowasch J, Kirkwood A, Miller C. 1986. Allosteric effects of Mg2+ on the gating of Ca2+-activated K+ channels from mammalian skeletal muscle. *JExpBiol* **124**:5–13.

Griguoli M, Sgritta M, Cherubini E. 2016. Presynaptic BK channels control transmitter release: physiological relevance and potential therapeutic implications. *J Physiol* **594**:3489–3500. DOI:10.1113/JP271841

Haug T, Olcese R, Toro L, Stefani E. 2004. Regulation of K+ Flow by a Ring of Negative Charges in the Outer Pore of BKCa Channels. Part II: Neutralization of Aspartate 292 Reduces Long Channel Openings and Gating Current Slow Component. *J Gen Physiol* **124**:185–197.

Heginbotham L, Lu Z, Abramson T, MacKinnon R. 1994. Mutations in the K+ channel signature sequence. *Biophys J* **66**:1061–7. DOI:10.1016/S0006-3495(94)80887-2

Hille B. 2001. Gating: Voltage Sensing and InactivationIon Channels of Excitable Membranes. Sunderland, Massachusetts: Sinauer Associates, Inc. pp. 603–634.

Hite RK, Tao X, MacKinnon R. 2017. Structural basis for gating the high-conductance Ca2+-activated K+ channel. *Nature* **000**:52–57. DOI:10.1038/nature20775

Horrigan FT. 2012. Perspectives on: conformational coupling in ion channels: conformational coupling in BK potassium channels. *J Gen Physiol* **140**:625–34. DOI:10.1085/jgp.201210849

Horrigan FT, Aldrich RW. 1999. Allosteric voltage gating of potassium channels II. Mslo channel gating charge movement in the absence of Ca2+. *J Gen Physiol* **114**:305–336.

DOI:10.1085/jgp.114.2.305

Horrigan FT, Cui J, Aldrich RW. 1999. Allosteric voltage gating of potassium channels I. Mslo ionic currents in the absence of Ca2+. *J Gen Physiol* **114**:277–304. DOI:10.1085/jgp.114.2.277

Horrigan FT, Aldrich RW. 2002. Coupling between voltage sensor activation, Ca2+ binding and channel opening in large conductance (BK) potassium channels. *J Gen Physiol* **120**:267–305. DOI:10.1085/jgp.20028605

Hu L, Shi J, Ma Z, Krishnamoorthy G, Sieling F, Zhang G, Horrigan FT, Cui J. 2003. Participation of the S4 voltage sensor in the Mg2+-dependent activation of large conductance (BK) K+ channels. *Proc Natl Acad Sci U S A* **100**:10488–93. DOI:10.1073/pnas.1834300100

Islas LD, Sigworth FJ. 1999. Voltage Sensitivity and Gating Charge in Shaker and Shab Family Potassium Channels. *J Gen Physiol* **114**:723–741. DOI:10.1085/jgp.114.5.723

Jaffe DB, Wang B, Brenner R. 2011. Shaping of action potentials by type I and type II large-conductance Ca2+-activated K+ channels. *Neuroscience* **192**:205–218. DOI:10.1016/j.neuroscience.2011.06.028

Javaherian AD, Yusifov T, Pantazis A, Franklin S, Gandhi CS, Olcese R. 2011. Metal-driven operation of the human large-conductance voltage- and Ca 2+-dependent potassium channel (BK) gating ring apparatus. *J Biol Chem* **286**:20701–20709. DOI:10.1074/jbc.M111.235234

Jensen MØ, Jogini V, Borhani DW, Leffler AE, Dror RO, Shaw DE, The. 2012. Mechanism of Voltage Gating in Potassium Channels. *Science (80-)* **336**:229–234. DOI:10.1126/science.1216533

Jiang Y, Pico A, Cadene M, Chait BT, MacKinnon R. 2001. Structure of the RCK domain from the E. coli K+channel and demonstration of its presence in the human BK channel. *Neuron* **29**:593–601. DOI:10.1016/S0896-6273(01)00236-7

Kaczmarek LK, Aldrich RW, Chandy KG, Grissmer S, Wei AD, Wulff H. 2017. International Union of Basic and Clinical Pharmacology . C . Nomenclature and Properties of Calcium-Activated and Sodium-Activated Potassium Channels 1–11. DOI:10.1124/pr.116.012864

Kimm T, Khaliq ZM, Bean BP. 2015. Differential Regulation of Action Potential Shape and Burst-Frequency Firing by BK and Kv2 Channels in Substantia Nigra Dopaminergic Neurons. *J Neurosci* **35**:16404–16417. DOI:10.1523/JNEUROSCI.5291-14.2015

Knaus HG, Folander K, Garcia-Calvo M, Garcia ML, Kaczorowski GJ, Smith M, Swanson R. 1994. Primary sequence and immunological characterization of beta-subunit of high conductance Ca(2+)-activated K+ channel from smooth muscle. *J Biol Chem* **269**:17274–17278.

Krnjevij K, Lisjewicz A. 1972. Injections of calcium ions into spinal motoneurones. *J Physiol* **225**:363–390. DOI:10.1113/jphysiol.1972.sp009945

Latorre R, Castillo K, Carrasquel-Ursulaez W, Sepulveda R V., Gonzalez-Nilo F, Gonzalez C, Alvarez O. 2017. Molecular Determinants of BK Channel Functional Diversity and Functioning. *Physiol Rev* **97**:39–87. DOI:10.1152/physrev.00001.2016

Latorre R, Vergara C, Hidalgo C. 1982. Reconstitution in planar lipid bilayers of a Ca2+-dependent

K+ channel from transverse tubule membranes isolated from rabbit skeletal muscle. *Proc Natl Acad Sci USA* **79**:805–809. DOI:10.1073/pnas.79.3.805

Latorre R, Miller C. 1983. Conduction and selectivity in potassium channels. *J Membr Biol* **71**:11–30. DOI:10.1007/BF01870671

Latorre R, Coronado R, Vergara C. 1984. K+ channels gated by voltage and ions. *Annu Rev Physiol* **46**:485–95. DOI:10.1146/annurev.ph.46.030184.002413

Lee US, Shi J, Cui J. 2010. Modulation of BK channel gating by the ß2 subunit involves both membrane-spanning and cytoplasmic domains of Slo1. *J Neurosci* **30**:16170–9. DOI:10.1523/JNEUROSCI.2323-10.2010

Li B, Jie W, Huang L, Wei P, Li S, Luo Z, Friedman AK, Meredith AL, Han MH, Zhu XH, Gao TM. 2014. Nuclear BK channels regulate gene expression via the control of nuclear calcium signaling. *Nat Neurosci* **17**:1055–1063. DOI:10.1038/nn.3744

Lingle CJ. 2006. Empirical considerations regarding the use of ensemble-variance analysis of macroscopic currents. *J Neurosci Methods* **158**:121–32. DOI:10.1016/j.jneumeth.2006.05.027

Lingle CJ. 2007. Gating Rings Formed by RCK Domains: Keys to Gate Opening. *J Gen Physiol* **129**:101–107. DOI:10.1085/jgp.200709739

Long SB, Campbell EB, MacKinnon R. 2005. Crystal Structure of a Mammalian Voltage-Dependent Shaker Family K+ Channel. *Science (80-)* **309**:897–903. DOI:10.1524/ncrs.2006.0153

Long SB, Tao X, Campbell EB, MacKinnon R. 2007. Atomic structure of a voltage-dependent K+ channel in a lipid membrane-like environment. *Nature* **450**:376–382. DOI:10.1038/nature06265

Lorenzo-Ceballos Y, Carrasquel-Ursulaez W, Castillo K, Alvarez O, Latorre R. 2019. Calcium-driven regulation of voltage-sensing domains in BK channels, bioRxiv. DOI:10.1101/520429

Ma Z, Lou XJ, Horrigan FT. 2006. Role of Charged Residues in the S1–S4 Voltage Sensor of BK Channels. *J Gen Physiol* **127**:309–328. DOI:10.1085/jgp.

Marty A. 1981. Ca-dependent K channels with large unitary conductance in chromaffin cell membranes. *Nature* **291**:497–500. DOI:10.1038/291497a0

Marty A. 1983. Ca2+-dependent K+ channels with large unitary conductance. *Trends Neurosci* **6**:262–265. DOI:10.1016/0166-2236(83)90115-7

McCobb DP, Fowler NL, Featherstone T, Lingle CJ, Saito M, Krause JE, Salkoff L. 1995. A human calcium-activated potassium channel gene expressed in vascular smooth muscle. *Am J Physiol Circ Physiol* **269**:H767–H777. DOI:10.1006/gyno.1997.4695

McManus OB, Helms LM, Pallanck L, Ganetzky B, Swanson R, Leonard RJ. 1995. Functional role of the beta subunit of high conductance calcium-activated potassium channels. *Neuron* **14**:645–650. DOI:10.1016/0896-6273(95)90321-6

Meech RW. 1978. Calcium-dependent potassium activation in nervous tissues. *Ann Rev Biophys*

Bioeng **7**:1–18. DOI:10.1146/annurev.bb.07.060178.000245

Meera P, Wallner M, Song M, Toro L. 1997. Large conductance voltage- and calcium-dependent K+ channel, a distinct member of voltage-dependent ion channels with seven N-terminal transmembrane segments (S0-S6), an extracellular N terminus, and an intracellular (S9-S10) C terminus. *Proc Natl Acad Sci USA* **94**:14066–14071. DOI:10.1073/pnas.94.25.14066

Meera P, Wallner M, Toro L. 2000. A neuronal β subunit (KCNMB4) makes the large conductance, voltage- and Ca2+-activated K+ channel resistant to charybdotoxin and iberiotoxin. *Proc Natl Acad Sci USA* **97**:1–6. DOI:10.1073/pnas.100118597

Meredith AL, Wiler SW, Miller BH, Takahashi JS, Fodor AA, Ruby NF, Aldrich RW. 2006. BK calcium-activated potassium channels regulate circadian behavioral rhythms and pacemaker output. *Nat Neurosci* **9**:1041–1049. DOI:10.1038/nn1740

Miranda P, Contreras JE, Plested AJR, Sigworth FJ, Holmgren M, Giraldez T. 2013. State-dependent FRET reports calcium- and voltage-dependent gating-ring motions in BK channels. *Proc Natl Acad Sci USA* **110**:5217–5222. DOI:10.1073/pnas.1219611110

Miranda P, Holmgren M, Giraldez T. 2018. Voltage-dependent dynamics of the BK channel cytosolic gating ring are coupled to the membrane-embedded voltage sensor. *Elife* **7**:e40664. DOI:10.7554/eLife.40664

Miranda P, Giraldez T, Holmgren M. 2016. Interactions of divalent cations with calcium binding sites of BK channels reveal independent motions within the gating ring. *Proc Natl Acad Sci* **113**:14055–14060. DOI:10.1073/pnas.1611415113

Monod J, Wyman J, Changeux JP. 1965. On the nature of allosteric transitions: A plausible model. *J Mol Biol* **12**:88–118. DOI:10.1016/S0022-2836(65)80285-6

Naranjo D, Moldenhauer H, Pincuntureo M, Díaz-Franulic I. 2016. Pore size matters for potassium channel conductance. *J Gen Physiol* **148**:277–291. DOI:10.1085/jgp.201611625

Nimigean CM, Chappie JS, Miller C. 2003. Electrostatic tuning of ion conductance in potassium channels. *Biochemistry* **42**:9263–9268. DOI:10.1021/bi0348720

Niu X, Qian X, Magleby KL. 2004. Linker-gating ring complex as passive spring and Ca(2+)-dependent machine for a voltage- and Ca(2+)-activated potassium channel. *Neuron* **42**:745–756. DOI:10.1016/j.neuron.2004.05.001

Noceti F, Baldelli P, Wei X, Qin N, Toro L, Birnbaumer L, Stefani E. 1996. Effective gating charges per channel in voltage-dependent K+ and Ca2+ channels. *J Gen Physiol* **108**:143–55. DOI:10.1085/jgp.108.3.143

Oberhauser A, Alvarez O, Latorre R. 1988. Activation by divalent cations of a Ca2+-activated K+ channel from skeletal muscle membrane. *J Gen Physiol* **92**:67–86. DOI:10.1085/jgp.92.1.67

Orio P, Latorre R. 2005. Differential effects of beta 1 and beta 2 subunits on BK channel activity. *J Gen Physiol* **125**:395–411. DOI:10.1085/jgp.200409236

Pallotta BS. 1985. N-Bromoacetamide Removes a Calcium- dependent Component of Channel Opening from Calcium-activated Potassium Channels in Rat Skeletal Muscle. *J Gen Physiol* **86**:601–611. DOI:10.1085/jgp.86.5.601

Pallotta BS, Magleby KL, Barrett JN. 1981. Single channel recordings of Ca2+-activated K+ currents in rat muscle cell culture. *Nature* **293**:471–474. DOI:10.1038/293471a0

Pantazis A, Gudzenko V, Savalli N, Sigg D, Olcese R. 2010. Operation of the voltage sensor of a human voltage- and Ca2+-activated K+ channel. *Proc Natl Acad Sci* **107**:4459–4464. DOI:10.1073/pnas.0911959107

Pantazis A, Olcese R. 2012. Relative transmembrane segment rearrangements during BK channel activation resolved by structurally assigned fluorophore–quencher pairing. *J Gen Physiol* **140**:207–218. DOI:10.1085/jgp.201210807

Pau VPT, Smith FJ, Taylor AB, Parfenova L V, Samakai E, Callaghan MM, Abarca-Heidemann K, Hart PJ, Rothberg BS. 2011. Structure and function of multiple Ca2+-binding sites in a K+ channel regulator of K+ conductance (RCK) domain. *Proc Natl Acad Sci USA* **108**:17684–17689. DOI:10.1073/pnas.1107229108

Peng Yuan, Leonetti MD, Pico AR, Hsiung Y, MacKinnon R. 2010. Structure of the Human BK Channel Ca2+-Activation Apparatus at 3.0 Å Resolution. *Science (80-)* **329**:182–186. DOI:10.1126/science.1190414

Pyott SJ, Duncan RK. 2016. BK Channels in the Vertebrate Inner Ear, 1st ed, International Review of Neurobiology. Elsevier Inc. DOI:10.1016/bs.irn.2016.03.016

Quirk JC, Reinhart PH. 2001. Identification of a novel tetramerization domain in large conductance KCa channels. *Neuron* **32**:13–23. DOI:10.1016/S0896-6273(01)00444-5

Saito M, Wu CF. 1991. Expression of ion channels and mutational effects in giant Drosophila neurons differentiated from cell division-arrested embryonic neuroblasts. *J Neurosci* **11**:2135–2150. DOI:10.1523/JNEUROSCI.11-07-02135.1991

Savalli N, Pantazis A, Yusifov T, Sigg D, Olcese R. 2012. The contribution of RCK domains to human BK channel allosteric activation. *J Biol Chem* **287**:21741–21750. DOI:10.1074/jbc.M112.346171

Schoppa NE, Sigworth FJ. 1998. Activation of Shaker potassium channels. I. Characterization of Voltage-dependent Transitions N. *J Gen Physiol* **111**:271–294. DOI:10.1085/jgp.111.2.295

Schreiber M, Salkoff L. 1997. A novel calcium-sensing domain in the BK channel. *Biophys J* **73**:1355–1363. DOI:10.1016/S0006-3495(97)78168-2

Schwarz W, Passow H. 1983. Ca2+-Activated K+ Channels in Erythrocytes and Excitable Cells. *PhysioL* **45**:359–74. DOI:10.1146/annurev.ph.45.030183.002043

Seoh S, Sigg D, Papazian DM, Bezanilla F. 1996. Voltage-sensing residues in the S2 and S4 segments of the Shaker K+ channel. *Neuron* **16**:1159–1167. DOI:10.1016/S0896-6273(00)80142-7

Shen KZ, Lagrutta A, Davies NW, Standen NB, Adelman JP, North RA. 1994. Tetraethylammonium block of Slowpoke calcium-activated potassium channels expressed in Xenopus oocytes: evidence for tetrameric channel formation. *Pflugers Arch* **426**:440–445. DOI:10.1007/BF00388308

Shi J, Cui J. 2001. Intracellular Mg2+ Enhances the Function of BK-type Ca2+ -activated K+

Channels. *J Gen Physiol* **118**:589–605. DOI:10.1085/jgp.118.5.589

Sigg D, Bezanilla F. 1997. Total charge movement per channel. The relation between gating charge displacement and the voltage sensitivity of activation. *J Gen Physiol* **109**:27–39. DOI:10.1085/jgp.109.1.27

Sigworth FJ. 1980. The variance of sodium current fluctuations at the node of Ranvier. *J Physiol* **307**:97–129. DOI:10.1113/jphysiol.1980.sp013426

Singh S, Wu CF. 1989. Complete separation of four potassium currents in drosophila. *Neuron* **2**:1325–1329. DOI:10.1016/0896-6273(89)90070-6

Stefani E, Ottolia M, Noceti F, Olcese R, Wallner M, Latorre R. 1997. Voltage-controlled gating in a large conductance Ca2+ sensitive K+ channel (hslo). *Proc Natl Acad Sci USA* **94**:5427–5431.

Sun X, Shi J, Delaloye K, Yang X, Yang H, Zhang G, Cui J. 2013. The Interface between Membrane-Spanning and Cytosolic Domains in Ca2+-Dependent K+ Channels Is Involved in Subunit Modulation of Gating. *J Neurosci* **33**:11253–11261. DOI:10.1523/JNEUROSCI.0620-13.2013

Sweet T-B, Cox DH. 2009. Measuring the influence of the BKCa {beta}1 subunit on Ca2+ binding to the BKCa channel. *J Gen Physiol* **133**:139–150. DOI:10.1085/jgp.200810129

Sweet T-BT-B, Cox DH. 2008. Measurements of the BKCa channel's high-affinity Ca2+ binding constants: effects of membrane voltage. *J Gen Physiol* **132**:491–505. DOI:10.1085/jgp.200810094

Tao X, Hite RK, MacKinnon R. 2017. Cryo-EM structure of the open high-conductance Ca2+-activated K+ channel. *Nature* **000**:1–14. DOI:10.1038/nature20608

Uebele VN, Lagrutta A, Wade T, Figueroa DJ, Liu Y, McKenna E, Austin CP, Bennett PB, Swanson R. 2000. Cloning and functional expression of two families of β-subunits of the large conductance calcium-activated K+ channel. *J Biol Chem* **275**:23211–23218. DOI:10.1074/jbc.M910187199

Vandael DH, Marcantoni A, Mahapatra S, Caro A, Ruth P, Zuccotti A, Knipper M, Carbone E. 2010. Cav1.3 and BK channels for timing and regulating cell firing. *Mol Neurobiol* **42**:185–198. DOI:10.1007/s12035-010-8151-3

Wallner M, Meera P, Toro L. 1996. Determinant for beta-subunit regulation in high-conductance voltage-activated and Ca(2+)-sensitive K+ channels: an additional transmembrane region at the N terminus. *Proc Natl Acad Sci USA* **93**:14922–14927. DOI:10.1073/pnas.93.25.14922

Wallner M, Meera P, Toro L. 1999. Molecular basis of fast inactivation in voltage and Ca2+-activated K+ channels: A transmembrane -subunit homolog. *Proc Natl Acad Sci USA* **96**:4137–4142. DOI:10.1073/pnas.96.7.4137

Wei A, Salkoff L. 1994. Calcium Sensitivity of BK-Type Kca Channels Determined by a Separable Domain. *Neuron* **13**:671–681. DOI:10.1016/0896-6273(94)90034-5

Wu Y, Xiong Y, Wang S, Yi H, Li H, Pan N, Horrigan FT, Wu Y, Ding J. 2009. Intersubunit coupling in the pore of BK channels. *J Biol Chem* **284**:23353–23363. DOI:10.1074/jbc.M109.027789

Wu Y, Yang Y, Ye S, Jiang Y. 2010. Structure of the gating ring from the human large-conductance Ca2+-gated K+ channel. *Nature* **466**:393–397. DOI:10.1038/nature09252

Xia X-M, Zeng X, Lingle CJ. 2002. Multiple regulatory sites in large-conductance calcium-activated potassium channels. *Nature* **418**:880–884. DOI:10.1038/nature00956

Xia XM, Ding JP, Zeng XH, Duan KL, Lingle CJ. 2000. Rectification and rapid activation at low Ca2+ of Ca2+-activated, voltage-dependent BK currents: consequences of rapid inactivation by a novel beta subunit. *J Neurosci* **20**:4890–4903. DOI:doi.org/10.1523/JNEUROSCI.20-13-04890.2000

Yan J, Aldrich RW. 2010. LRRC26 auxiliary protein allows BK channel activation at resting voltage without calcium. *Nature* **466**:513–6. DOI:10.1038/nature09162

Yang H, Hu L, Shi J, Delaloye K, Horrigan FT, Cui J. 2007. Mg2+ mediates interaction between the voltage sensor and cytosolic domain to activate BK channels. *Proc Natl Acad Sci USA* **104**:18270–5. DOI:10.1073/pnas.0705873104

Yang H, Shi J, Zhang G, Yang J, Delaloye K, Cui J. 2008a. Activation of Slo1 BK channels by Mg2+ coordinated between the voltage sensor and RCK1 domains. *Nat Struct Mol Biol* **15**:1152–1159. DOI:10.1038/nsmb.1507

Yang H, Zhang G, Shi J, Lee US, Delaloye K, Cui J. 2008b. Subunit-specific effect of the voltage sensor domain on Ca2+ sensitivity of BK channels. *Biophys J* **94**:4678–87. DOI:10.1529/biophysj.107.121590

Yang H, Cui J. 2015. BK channels In: Zheng J, Trudeau MC, editors. Handbook of Ion Channels. Taylor & Francis Group, LLC. pp. 227–235.

Yang H, Zhang G, Cui J. 2015. BK channels: multiple sensors, one activation gate. *Front Physiol* **6**:1–16. DOI:10.3389/fphys.2015.00029

Yang J, Krishnamoorthy G, Saxena A, Zhang G, Shi J, Yang H, Delaloye K, Sept D, Cui J. 2010. An Epilepsy/Dyskinesia-Associated Mutation Enhances BK Channel Activation by Potentiating Ca2+ Sensing. *Neuron* **66**:871–883. DOI:10.1016/j.neuron.2010.05.009

Ye S, Li Y, Chen L, Jiang Y. 2006. Crystal Structures of a Ligand-free MthK Gating Ring: Insights into the Ligand Gating Mechanism of K+ Channels. *Cell* **126**:1161–1173. DOI:10.1016/j.cell.2006.08.029

Yellen G. 1984. Ionic permeation and blockade in Ca2+-activated K+ channels of bovine chromaffin cells. *J Gen Physiol* **84**:157–186. DOI:10.1085/jgp.84.2.157

Yuan P, Leonetti D, Pico AR, Hsiung Y, MacKinnon R. 2010. Structure of the Human BK Channel Ca2+ -Activation Apparatus at 3.0 Angstrom Resolution. *Science (80-)* **329**:182–186.

Yuan P, Leonetti MD, Hsiung Y, MacKinnon R. 2012. Open structure of the Ca2+ gating ring in the high-conductance Ca2+-activated K+ channel. *Nature* **481**:94–97. DOI:10.1038/nature10670

Yusifov T, Savalli N, Gandhi CS, Ottolia M, Olcese R. 2008. The RCK2 domain of the human BKCa channel is a calcium sensor. *Proc Natl Acad Sci USA* **105**:376–381. DOI:10.1073/pnas.0705261105

Yusifov T, Javaherian AD, Pantazis A, Gandhi CS, Olcese R. 2010. The RCK1 domain of the human BKCa channel transduces Ca2+ binding into structural rearrangements. *J Gen Physiol* **136**:189–202. DOI:10.1085/jgp.200910374

Zeng X-H, Xia X-M, Lingle CJ. 2005. Divalent Cation Sensitivity of BK Channel Activation Supports the Existence of Three Distinct Binding Sites. *J Gen Physiol* **125**:273–286. DOI:10.1085/jgp.200409239

Zhang G, Huang S-Y, Yang J, Shi J, Yang X, Moller A, Zou X, Cui J. 2010. Ion sensing in the RCK1 domain of BK channels. *Proc Natl Acad Sci* **107**:18700–18705. DOI:10.1073/pnas.1010124107

Zhang G, Yang H, Liang H, Yang J, Shi J, McFarland K, Chen Y, Cui J. 2014. A Charged Residue in S4 Regulates Coupling among the Activation Gate, Voltage, and Ca2+ Sensors in BK Channels. *J Neurosci* **34**:12280–12288. DOI:10.1523/JNEUROSCI.1174-14.2014

Zhang G, Geng Y, Jin Y, Shi J, McFarland K, Magleby KL, Salkoff L, Cui J. 2017. Deletion of cytosolic gating ring decreases gate and voltage sensor coupling in BK channels. *J Gen Physiol* **149**:373–387. DOI:10.1085/jgp.201611646

Zhang X, Solaro CR, Lingle CJ. 2001. Allosteric Regulation of BK Channel Gating by Ca2+ and Mg2+ through a Nonselective, Low Affinity Divalent Cation Site. *J Gen Physiol* **118**:607–636. DOI:10.1085/jgp.118.5.607

Zhou Y, Xia X-M, Lingle CJ. 2011. Cysteine scanning and modification reveal major differences between BK channels and Kv channels in the inner pore region. *Proc Natl Acad Sci* **108**:12161–12166. DOI:10.1073/pnas.1104150108

Zhou Y, Zeng X-H, Lingle CJ. 2012. Barium ions selectively activate BK channels via the Ca2+-bowl site. *Proc Natl Acad Sci USA* **109**:11413–11418. DOI:10.1073/pnas.1204444109

Zhou Y, Yang H, Cui J, Lingle CJ. 2017. Threading the biophysics of mammalian Slo1 channels onto structures of an invertebrate Slo1 channel. *J Gen Physiol* **149**:985–1007. DOI:10.1085/jgp.201711845